UNIVERSITÀ DEGLI STUDI DI PADOVA

Dipartimento di Tecnica e Gestione dei Sistemi Industriali

Corso di Laurea Magistrale in
Ingegneria dell'Innovazione del Prodotto

Development of a sensorized physical model of the human head for the innovation of helmet safety tests

Laureando: Federico Uriati

1131023

Relatore:

Prof. Nicola Petrone

Supervisors:

Prof. Andrey Koptyug; MIUN Östersund (SWE)

Prof. Mikael Bäckström; MIUN Östersund (SWE)

Anno Accademico 2017/2018

“We don’t need any more luck, but only more receptors”

Acknowledgements

First and foremost, thank to my family, which always sustained me through all the difficult moments and shared with me the satisfaction of every single reached goal.

Thanks to the friends always by my side, for the fun time and the deep speeches, always available despite distance and problems; thanks to the friend in Vicenza for making University years easier.

I would like to thank all the people that made this thesis work possible:

Professor Nicola Petrone, for giving me the chance to work on this project, for his helpful attitude and for giving me the opportunity of living a lifetime experience.

Professor Andrey Koptyug, for his hospitality, patience and tutoring attention.

Professor Mikael Bäckström, Kajsa, Per, Rebecca, Carlos, David and all the Sport Tech team for the friendliness and for everything they taught me, among the workshop and the textile lab.

I desire to thank the “Akvariet” colleagues Johnny and Simon, the best mates I could desire, thanks to Edoardo for the intense work we share in the last months, and last but not least thanks to all new international friends met in Östersund, you all made my Swedish life.

This thesis has been conceived and developed under a formal Erasmus Programme collaboration between the University of Padua, Italy, and the Mittuniversitetet (Mid Sweden University) of Östersund, Sweden. The Erasmus grant was funded by the European Union. The research groups involved in this project are the *Department of Industrial Engineering* of the University of Padua and the *Sports Tech Research Centre* of the Mid Sweden University.

Table of Contents

Introduction

Head Impact and head related injuries are the most critical and most dangerous type of accidents that can occur to the human body, head traumas and related brain damages, caught the attention of many research teams and sport industries, either for prevent this type of accident and design and improve new protection systems. Even though traumatic brain injury (TBI) has long been acknowledged to be cause of injury-related death and disability, the exact physical parameters which best represent the TBI mechanism and their mutual relationships are still unclear.

The lack of an appropriate physical head surrogate capable of providing researchers with the necessary instrument to systematically test head injury phenomena is a problem to solve.

Mid Sweden University of Östersund (SWE) and the University of Padua (IT) have undertook a long-term collaboration aim to taking a first and consistent step towards the realization of a new sensorized prototype of a human head, meant to provide future researchers a real appropriate tool to investigate Head Related injuries.

The modern Anthropometric Testing Devices, used for the collection of data during crash tests and catastrophic events, are mainly designed for the analysis of the overall body behaviour, without a specific attention to the head. This research collaboration is working to create a new test device, focusing the attention to brain behaviour during impacts, which is the main problem for head injuries and concussions.

Mid Sweden University and University of Padova's aim is to obtain an innovative instrumented human head surrogate, composed by a sensorized brain and a skull, to collect many data about the behaviour of the brain and head system.

Accelerometers, gyroscopes and Pressure Sensors are used and implemented for collecting more information as possible, and with this innovative point of view, it will be possibly creating more advanced protection system.

A first prototype of Instrumented Human Head has been developed during different research works [1]–[3]. Accelerometers and gyroscope are positioned into the brain and pressure sensors inside the skull; the evaluation of acceleration in the different point of the grey matter is important for the analysis of impacts and the conditions of brain after a trauma, for the same reason evaluate the difference in pressure inside the cranium and in different position would be important for the comprehension of TBI mechanism.

This thesis work is based on the development of a second head prototype to be potentially used for the collection and comparison of accurate data from inside and outside the human head.

The Human head surrogate is composed from a Polyamide 3D printed Skull, Silicon rubber brain, a silicon rubber skin and Synthetic oil used as Cerebral Spinal Fluid substitute; this assembly is then coupled with a standard dummy neck and wore with a professional ski helmet.

Seven accelerometers and two gyroscopes are located into the brain in specific position for the collection of linear and rotational acceleration and ten pressure sensors are embedded inside the skull for the analysis of the inner pression.

Chapter 1

State of the Art

1.1 Traumatic Brain Injury

The human brain commonly experiences injury due to trauma and despite extensive research studies, the injury mechanisms of the brain are not completely understood.

Sports organizations and research teams are starting to understand the harm that can be inflicted by high-contact activities to athletes' body and on the head.

Sports institutions have started to acknowledge the problem, authorities have addressed their educational efforts and change rules to make games safer.

The most frequent form of head injury is the Traumatic Brain Injury (TBI), it occurs when the brain is severely damaged by an external force that could be a direct contact or non-contact.

Traumatic Brain Injury (TBI) is one of the most serious result of game accidents in sports, crashes in motor vehicles or blast exposition[4], [5] and is a major cause of death and disability in the USA, contributing to about 30% of all injury death.[6]. The intensity of a TBI may range from "mild" (mTBI or "concussion") to "severe" (extended period of unconsciousness or memory loss). Any injury that results in trauma to the skull or brain is classified as a head injury.

Most of the tests and studies are Motor Vehicle crash related, those are the leading cause of severe head injuries in the United States and has been estimated that automotive head injury accounts for nearly thirty percent of the total harm of car occupants. This type of

injuries is more connected with unexpected events, but the head health is also related with the long-term distribution.

Neurodegenerative brain diseases can be found in individuals who have been exposed to repeated head trauma. Chronic Traumatic Encephalopathy (CTE) is one of the most early discovered disease relate with brain trauma. In general, post-concussion syndrome (PCS) effects can include reduced cognitive, motor and sensation functioning, emotional disorders or other neurodegenerative diseases, mostly: Motor Neuron Disease, Alzheimer's Disease (AD) and Parkinson's Disease (PD).

Sports are the leading cause of TBI, second only to motor vehicle crashes. In winter sport, injuries occurring to the head show a high degree of severity, despite their relatively lower incidence with respect to knee and wrist injuries[7].

Many different authors state that a deeper knowledge of head impact biomechanics/kinematics can and must be achieved since there are still formal studies proving that most of current protections are not designed either tested for every possible impact condition that could occur in a real-life scenario.

Despite the advancements in helmets in reducing head accelerations, there has not been a similar reduction in the incidence of concussion. This suggests that other factors contribute to the incidence of reported injuries. Studies have shown that although wearing traditional EPS (Expanded polyester) helmets decrease the risk of severe head injury by approximately 75%, the reduction in mild traumatic brain injury (mTBI) rates it statistically insignificant[8][9].

Research and performance standards to assess the effectiveness of Football helmets traditionally focus on head form response and do not consider the other reaction force. Helmet manufacturers, regulatory institutions and scientists have been working since decades towards the improvement of protective devices and surveillance methods to reduce the incidence of TBI. Compact lightweight recording systems help to analyse the collisions in active sports, supporting the improvements into injury prevention technologies and equipment [10]–[12] and the use of wearable technologies [13] or video analysis: a typical issue is how to link the external sensor data to actual brain injury mechanisms.

On the other hand, laboratory testing of helmets, despite established in several international standards, is still evolving towards the implementation of multidirectional impacts and considering instrumented dummy heads able to evaluate the degree of protection against these complex cases[14].

Monitored cadaveric brain response to impact in helmeted and helmeted conditions and reported that helmet use reduced linear and angular accelerations; however helmet use resulted in increased strain in increased brain strain in the cerebrum[15].

It has long been recognized that angular acceleration (together with peak linear acceleration) plays a non-negligible role as a biomechanical mechanism for TBI and particularly for DAI (Diffuse Axonal Injury), despite this, the specific relationships between linear, angular acceleration and resultant injuries, have not been thoroughly linked together yet.

The current helmets are primarily designed to reduce the linear acceleration component of the shock, but cannot completely eliminate the angular acceleration response; the NOCSAE (National Operational Committee on Standards for Athletic Equipment) testing only simulate a purely linear acceleration, that means prevent main skull fracture, but this kind of test doesn't give any guarantee about rotational acceleration [16].

Research Centre and scientists are working constantly in the development of protective devices and the reduction of TBI incidence. Advanced sensors analyse the collisions in active sports, but the question is about the link data to actual brain injury mechanisms.

1.2 Human Body Surrogate

A dummy is a device that represents the human body by mimicking the geometry, weight, inertia, joint stiffens and energy absorption characteristics of humans, ATDs are expected to simulate human response when exposed to a crash environment.

An Anthropomorphic Test Device (ATD) is a dummy that simulates the anatomical characteristic of a real human body. The Crash Test Dummy is widely used by researchers

and companies to predict the biomechanics, force, impact and injury of a human being after different type of crash.

Dummy specifications are public and official, this means that every improvement in each dummy as to be approved from the government; the Standard (Federal Motor Vehicle Safety Standard No.208, Occupant, Car, Protection) was promulgated in 1972 and hasn't change substantially since then.

There are different testing procedures for ensure that the dummies obtain a correct human like response and they would react to a crash in a similar way that a human body would.

Using a cadaver or animals for these topics of research is more realistic than using a dummy for physiologic reasons; the first tests subject were human cadavers fitted with accelerometers and strapped into cars; but it raised many moral doubts and it risks to across a moral ethic line.

The automotive sector raised a high number of dummies: the now retired Sierra and the more recent Hybrid Family.

The Hybrid III 50th Percentile Male Crash Test Dummy is the one of the last and most widely used crash test dummy in the world; it is developed Humanetics ATD (Humanetics Innovative Solutions, Farmington Hills, MI USA). It is considered to have excellent bio fidelity and instrumentation capability[17]

Figure 1.1 - Anthropometric Testing Device "Human Hybrid III"

. Head forms as used in international standards are typically hollow aluminium shells with standardized shape and dimensions. An increasing number of works utilize the Hybrid III dummy head for helmet evaluation, mostly due to the connection to the Hybrid neck that presents a differential flexibility in flexion and extension. The primary benefit provided by the Hybrid III is improved neck response that better simulate the humans.

Another advanced dummy is the World SID (Worldwide harmonized Side Impact Dummy), designed from a worldwide consortium of experts and industries; it can record 258 different measurement in a single crash. The project that is going on at Humanetics is related with FOCUS[1] (facial and ocular countermeasure for safety head form), it consists of a dummy face, with synthetic eyeballs made of silicon like material to register penetrating injuries and load cells at the back of each eye socket to measure non-penetrating impacts; it was developed to evaluate helmets, goggles and protective features.

Figure 1.2 - a) World SID stands for Worldwide harmonized Side Impact Dummy

b) Facial and Ocular Countermeasure for Safety Head form (FOCUS)

THOR (Test device for Human Occupant Restraint) is an Advanced 50th percentile male Dummy. The successor of Hybrid III, THOR has a more human-like anatomy and its face contains several sensors which allow analysis of facial impacts to an accuracy currently unobtainable with other dummies.

The development of a physical model is helpful to achieve repeatability and keep the attention on the right parameters during different type of test and trial. Those replicas used currently for crash tests and experimentation are generally basic, they don't have a

[1] Developed by Denton with the U.S. Army Aeromedical Research Laboratory and the Centre of Injury Biomechanics, run jointly by Virginia Tech College of Engineering (Blacksburg) and Wake Forest University School of Medicine (Winston-Salem)

proper representation of the human head and features (eyes, ears, skin, hair) and completely lacking elements to reflect its inner anatomy.

Bio fidelity is a description of the extent to which passive human-like mechanical behaviour is simulated in a mechanical surrogate. Bio fidelity can be assessed through comparison of the kinematic and mechanical responses of a mechanical surrogate to a human volunteer or cadaver.

Some studies are made for the evaluation of the bio fidelity of the human dummies and the mechanical behaviour in general resulted different between dummy and cadaver[18]. Out of all the possible data channels provided by a fully instrumented dummy, just few of them are dedicated to the head-only motion and all of them relate to the hollow-aluminium head, considering it as a rigid body neglecting all the relative brain-head movement.

The sensors used are Triaxial accelerometers and Gyroscopes, and in the case of the FOCUS, also 8 Load Cells are implemented for the evaluation of the load acting on the skull.

The hollow ATD skull and absence of a deformable brain might influence the inertial loading parameters of the head -neck spine complex [19]. Those ATD can collect a lot of information about the load and global acceleration to which the complete head is subjected, anyone of those dummies can display reliable information about the brain movement and stress.

The lack of bio fidelity of the recent Anthropomorphic test devices is the main reason why the Project is going on, the state-of-the-art of crash dummies completely lack a brain and does present instead a hollo cavity inside a skull-like aluminium shell.

Very few literature sources can be found regarding the development of biofidelic human head surrogate for use in the field of helmet development.

A research by Zhang et al. [20] create a gel-filled ellipsoidal-shaped physical model, the shell cavity was filled with gel, four pressure transducers were attached outside the shell and other four were symmetrically distributed about the longitudinal axis of the model in the mid-coronal plane, 35 mm deep into the brain surrogate. The transducers managed to catch the intracranial pressure response, but the bio fidelity of the model was not correct, the replication of head anatomy, skull material properties and meninge, was too simple.

Zhu et al. [21], used the same kind of silicone gel (Sylgard® 527 AB) and an egg-shaped skull/brain surrogate was exposed to blast over pressure in a shock tube environment but also in this case there was any intention to recreate an anatomically correct surrogate and the anatomical details of the human head were admittedly neglected. A third study was carried out by Taha et al. [22], investigating the effects of soccer heading on the brain structure. A head surrogate was created with a hollow plastic skull and filled with ultrasound gel12. This solution not only is anatomically inaccurate but also ignores the relative movement between the brain and the skull as well as the influence of the intermediate tissues between them. In 2015, Awad et al. [23] developed a more sophisticated head model while investigating blast-induced mild traumatic brain injuries. In this case four pressure transducers (one in the frontal lobe, one in the occipital lobe, one in the temporal lobe and one between the two hemispheres towards the right side) were embedded in the surrogate brain, while one accelerometer (only) was attached to the brain surface. The main focus of the work was nevertheless the design of a reliable air driven shock tube rather than the design of the brain-skull complex itself, exactly as it was by Zhu et al. [21]. In addition, the standardization process for the brain molding or the consistency of the used geometries was not explicitly mentioned (no information about separation between lobes, cerebellum presence, etc.).

The most advanced Human Head surrogate is the one developed by Freitas et al. [24] for use in military helmets blast investigations. This human head surrogate is based on refreshed human craniums and surrogate materials representing human head soft tissues such as the skin dura, and brain. Sensors embedded in the human head surrogates allow for direct measurement of intracranial pressure (four pressure sensors in the brain), cranial strain (12 strain rosettes), and skull (triaxial accelerometer at the hard palate) and helmet acceleration.

Concussion, traumatic Brain injury (TBI) and Spine Injuries continue to pose a threat to athletes engaged in contact sport. The head itself, as an important part of the human body, deserves a more accurate analysis eventually a complete data collection. The biggest aim

is to build a reliable Dummy Head which can allow the collection of most data as possible about the movement, forces and stress on the brain.

1.3 FEM Models

The human brain commonly experiences injury due to trauma and despite extensive research efforts over the past several decades the injury mechanism of the brain is not entirely understood.

The attention nowadays is addressed on the development of mathematical model that could represent a real exemplary in a virtual environment. The main part of studies about the brain behaviour during impact and trauma is made with Finite Element Analysis (FEM) [25], [26].

The combined finite element models are validated against selected tests then used as a research tool to study parameters affecting injuries in a wide variety of hits and crashes and against cadaver brain deformation experiments and are then used to predict brain injury based on strain metrics. Skull Vibration, Pressure Waves, Cavitation, Brain Rotation and Shear Deformation have been deeply investigated as explanation of Brain Injuries but most of them are not been confirmed because of the practical difficulty of measuring brain deformation in human subject. FEM simulations have a fundamental role in the study of brain injury mechanisms, especially considering the intrinsic difficulty of performing repeatable and accurate tests on human cadavers or scaling the results of animal testing to humans.

This kind of approach is an important tool to predict head acceleration responses or intra cranial pressure variations and stress on the brain, but only few of the studies have been validated for different kind of experimental data such as brain motion kinematics and brain intra cranial pressure values. There are, for example, several FEM studies that achieved a good or even very good correlation between human cadaver experimentation data and FE simulations in terms of intracranial pressures [27] but it has been shown that a correct pressure response in the brain does not necessarily mean that other predictions regarding strains and accelerations are correct.

The selection is a determination of all the variables and parameters have a significant effect on the correctness and accuracy of simulation results.

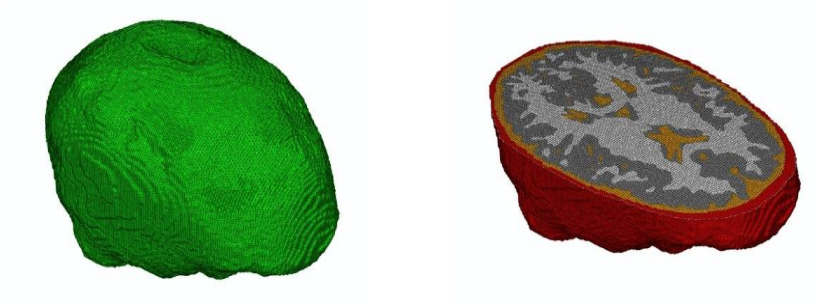

Figure 1.3 - Finite Element model of the Human Head from Chen et al.[26], [28]

There are some older studies though that managed to carry out experimental characterizations of head tissues and analyses of impact kinematics using either human data (mostly from cadavers [29] and MRIs [30], [31] or animal tests (swine, bovines and rats [32], [33]) but it's difficult to obtain certain results from this type of evaluation that could be spendable in a proper FEM reproduction and can explain the real head movement and reaction.

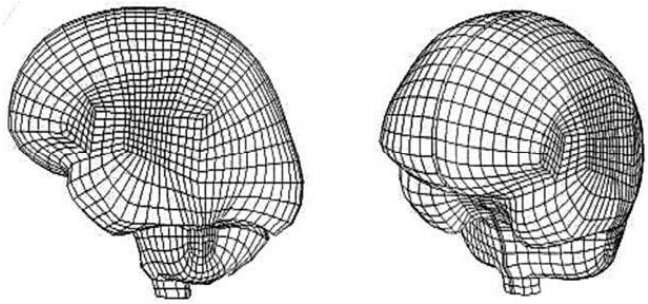

Figure 1.4 - Side and perspective view of the meshed brain[25]

Besides displacements, strain fields are also obtained by FE simulation, which provides a better measure of brain deformation. Brain tissue is most vulnerable to shear strains due to its high bulk modulus and low shear modulus. In addition, tensile strains are believed to be more dangerous than compressive strains. Rapid Deformation of brain matter caused

by skull acceleration is most likely the cause of concussion as well as more severe traumatic brain injury (TBI)[26], [34]

Many researchers postulate that these shape changes or deformations of the brain are the primary cause of the TBI. A common theory is that deformation of the brain is caused by shear strains that develop due to rotational kinematics of the skull and the brain [35].

Despite this recognition, it is not clear which acceleration is the major cause of TBI, FEM is a powerful tool to study tissue level brain strain under global head acceleration.

The general interest of investigation is to determine which acceleration is the major contributor to brain strain and should to be measured during crash tests to provide better evaluation of brain injury potential. One of the most advanced mathematical models is the Simulated Injury Monitor (SIMon) Finite Element Head Model (FEHM), it was developed by the National Highway Traffic Safety Administration (NHTSA) with the aim to relate three-dimensional skull kinematics to brain injury prediction metrics.

It is very accurate from the anatomical point of view and reproduce all the inner layer of the head.

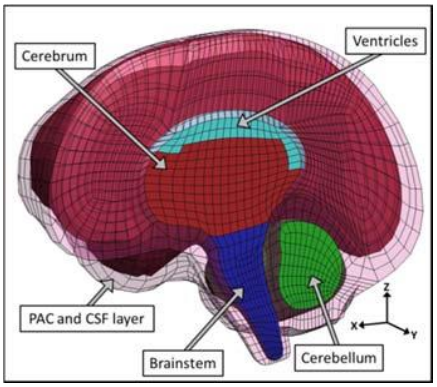

Figure 1.5 - Component of SIMon FEHM

The simulations conducted assume that rigid body kinematics of the skull are adequate to describe how impact forces are transmitted to the brain. Different metrics could be calculate in particular related with the brain strain: Maximum principal strain (MPS) and Cumulative Strain Damage Measure(CSDM) both calculated for all the brain part[35].

Those FEM model with detailed brain structure are very useful for the analysis of the brain response but they have some limitation in relation with the validation and the correct reproduction of every movement of the brain in every direction.

1.4 Injury Criterion

After the collection of multiple data and obtained results from tests and computer simulations, is necessary trying to correlate the values for describing the head and brain behaviour under different testing evaluation.

Over the past years, a remarkable effort has been learned regarding head injury mechanism and injury criteria.

1.4.1 Head Injury Criterion

The only injury criteria in wide usage is the Head Injury Criterion (HIC), adopted over twenty-five years ago. First introduced as a curve fit to the Wayne State Tolerance Curve(WSTC), it provides a relationship between peak acceleration, pulse duration and concussion onset [36].

With respect to overall head kinematics, the Head Injury Criterion (HIC) is the most widely used method to estimate the head injury and appears in many product specifications and automotive regulations[37]. The HIC considers the time integral (typically on an interval of 15 ms) of the resultant translational acceleration recorded at the head CoM.

$$HIC = \left\{ \left[\frac{1}{t_2 - t_1} \int a(t)dt \right]^{2.5} (t_2 - t_1) \right\}_{\max}$$

Those injury metrics were Primary developed to predict skull fracture, although they were thought to likely correlate with severe parenchymal brain injury as well. Only Linear acceleration is considered in these injury metric, and all current safety standards for head injury are based on these works.

The HIC limit value of 1000 is fixed by standards as the threshold that is supposed to not be crossed, and a time duration of 15ms as the duration of the interval on which the values

as to be calculated , no brain damage or skull fracture data exist where the HIC durations are greater than 15ms [38].

It is important to consider the bio fidelity of the human surrogate in establishing critical levels of the injury criteria.

Despite is method is highly used for the crash damage evaluation, it has some serious limitation for the evaluation of brain damage.

Researches have revealed that the risk of the occupant of a car crash who sustained a brain injury without skull fracture would be greater than the ones who sustained a skull fracture without a brain injury [39].

Previous studies have shown that a HIC of 1000 corresponds to 50% risk of skull fracture[40], a HIC of 700 is estimated to represent a 50% risk of concussion in athletes[41] but recent studies suggest that a HIC value of 250 represented approximately a 1% risk of concussion [42] .

The evaluation of the brain trauma was only confirmed by the recognition of physical ruptures, but an absence of skull damage does not signify an absence of a brain injury.

1.4.2 Brain Injury Criteria

Despite the wide use of HIC in crash tests, it is a measure of the linear impulse of the head's motion and is not a comprehensive predictor of all head injuries. As a further step a has been developed a Brain Injury Criterion (BrIC) based on head rotational velocity that could be used in conjunction with HIC for a more complete evaluation of TBI risk. The basis for BrIC is its correlation with measurements of strain in finite element (FE) brain model, for example Maximum Principal Strain of the brain MPS and Cumulative Strain Damage Measure CSDM.

$$BrIC = \sqrt{\left(\frac{\omega_x}{66.25\ \frac{rad}{s}}\right)^2 + \left(\frac{\omega_y}{56.45\ \frac{rad}{s}}\right)^2 + \left(\frac{\omega_z}{42.87\ \frac{rad}{s}}\right)^2}$$

Where the ω_i is the single absolute value of the maximum magnitude velocity measurement about the i axis (x, y,z with respect to the anatomical reference system) and

ω_{iC} are the critical angular velocities in their respective directions ($\omega_{xC} = 66.25$ rad ; $\omega_{yC} = 56.45$ rad ; $\omega_{zC} = 42{,}87rad$)

The equation considers a combination of angular velocities each normalized with respect to a critical value obtained considering a case of $\mathrm{CSDM}_{\epsilon=0.25} = 49\,\%$ and a $\mathrm{MPS}_{\mathrm{threshold}} = 0.87$. The maximal value that BrIC can assume is 1 and it corresponds to a probability of 50% of AIS 4[2]. Angular velocity, correlated to two physical parameters: CSDM (cumulative strain damage measure) and MPS(maximum principal strain), is the only component of BrIC. Angular accelerations were excluded from BrIC as they did not correlate well to any physical parameter; recent studies are reporting consistently the angular acceleration values [43].

The BrIC is a complement to the existing HIC, which is based on translational acceleration. Together, the two criteria may be able to capture most brain injuries and skull fractures occurring in automotive or any other impact environment [44].

However, both HIC and BrIC consider the human head solid entity and assume that referring to the head CoM linear acceleration and angular velocities is enough to evaluate fracture and brain injury risk. Nonetheless, despite their diffusion, this assumption has proven to be weak in real-life scenarios as repeatedly expressed by different authors [45]. The reliability of this metric as an indicator of TBI it depends on the scaling method and the head motion, so it's again not a completely full valid method.

[2] The Abbreviated Injury Scale (AIS) is an anatomical-based coding system created by the Association for the Advancement of Automotive Medicine to classify and describe the severity of injuries.[1][2][3] It represents the threat to life associated with the injury rather than the comprehensive assessment of the severity of the injury.

Chapter 2
Instrumented Human Head Surrogate Development

The main purpose of this long-term project is to create a biofidelic human head, reliable from the anatomical point of view and capable of reproduce the real human head behaviour under impact or traumatic event[46], [47].

The anatomy of Human Head is very complicate to reproduce accurately and achieve a reliable result is very difficult and almost impossible, after a wide anatomical study and shared decision with the researchers involved in the study a global simplification of the Dummy head has been accepted and only the main parts of the Head were reproduced artificially.

Substantial simplifications are made in the design and choice of the parts to include in the physical model. The study is focused on skull, brain, Cerebral Spinal Fluid (CSF), Dura Mater, Subarachnoid Space and skin; this choice has been made because those parts are

the most important and have a big influence in the protection of the Head, and relative movement of the inner part. The mechanical properties of each part are investigated and in the following sections the discussion on them is displayed.

1.5 Human Head Anatomy

Analysis and comprehension of the Human Head Anatomy and structure for the proper reproduction of an accurate Dummy Head is fundamental. The Human head is the most complex and probably important organ in the human body.

Its anatomy is very difficult to reproduce, and each component has a specific physiological role and mechanical characteristics

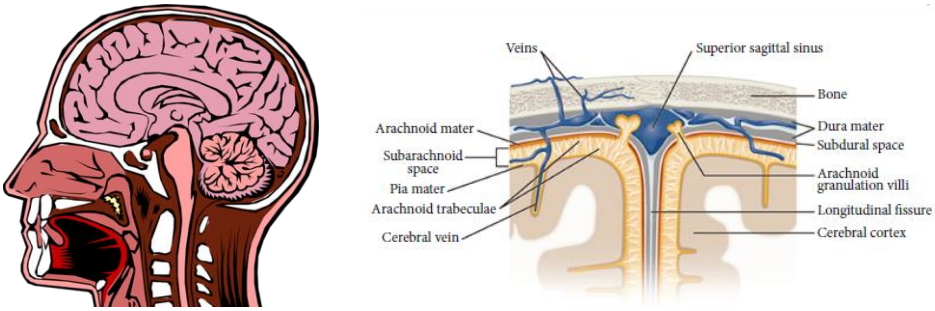

Figure 2.1 Human Head Anatomy and main physiological parts

Data from direct experimentation or FE models were collected and selected, obtaining a big database of mechanical value and characteristic and try to reproduce them with other materials.

The extreme simplification of the Human Head would allow to reproduce and design the human head also with a FEM software and being able to have a comparison between the physical and mathematical results.

The physical properties of the biological tissue of each component are collected from multiple and different studies. Once completed the study of brain injury mechanisms, has been decided to focus and the properties and characteristics of the main parts.

The final aim of the thesis is to realize a simplified prototype, easy to reproduce also from a mathematical point of view rather than a perfectly reproduced human head, mostly because it is not possible to find and apply material that have the same physical properties of the human tissue, so it is not possible to achieve the desired outcomes with the available technologies.

The knowledge of this value is anyway a starting point for the development of the prototypes and as a valuable milestone for deeper researches.

1.5.1 Skull

The skull is composed of two parts that are the cranium and the mandible, is a bones structure that support the face and guarantees a protection of the brain, it fixes the distance between the eyes and the position of the ears to enable sound localisation.

Except for the mandible, all the bones of the skull are joined together by fixed joints formed by bony ossification but fibres permitting some flexibility.

The skull protects the brain from damage through its high stiffness; the skull is one of the least deformable structures found in nature with it needing the force of about 1 ton to reduce the diameter of the skull by 1 cm [48].

The mechanical properties of the Skull's bones are not uniform, the resistance of the cranium depends from the thickness of each part and the specific bone took in consideration.

Since he mechanical properties of the cranium bones are not uniform all around the skull, their characteristics are difficult to identify due to complex geometry and differences in shape and thickness of every part of the skull. Different study is conducted for the analysis and the comprehension of the cranium bones mechanical properties. Different literature studies are used as reference for the identification of the skull bone properties and the average values are displayed in the following chart.

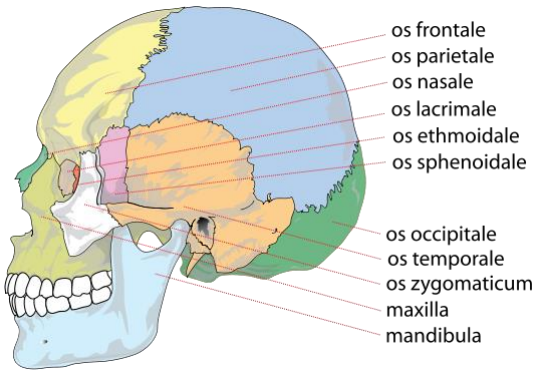

Figure 2.2 Skull Anatomy Side View

The date are collected from different studies, mainly acted to obtain the skull properties and apply the results in FEM simulations. [49], [58]–[61], [50]–[57]

Table 1 - Skull Bones Mechanical Properties

	Density $[\frac{km}{m^3}]$	E [Mpa]	Poisson Ratio
Skull	$1410 - 3000$	$4460 - 15000$	0.2
Cortical Bone	$1900 - 3000$	$1790 - 15000$	0.21
Diploe Bone	$1300 - 2100$	$730 - 4665$	0.5
Facial	$2500 - 8000$	$5000 - 6500$	0.2

As is possible to observe the physical characteristics are not easy to identify uniquely and since the biological structure of the bones is very particular it would be almost impossible to reproduce it artificially and obtain the same physical appearance.

The mechanical properties of the real bones structure are difficult to reproduce and as previously displayed the characteristics of every part are slightly different.

The use of a polymeric material is a choice necessary to produce a complex 3D printed shape, the mechanical properties are in the same range of values but it's impossible naturally the complex biologic structure of the bone.

1.5.2 Dura Mater and Subarachnoid Space

The human brain is encased in the skull and is suspended and supported by a series of fibrous tissue layers, dura mater, arachnoid, trabeculae and pia mater, known as the meninges. In addition, cerebrospinal fluid (CSF), located in the space between the arachnoid and the pia mater which is known as the subarachnoid space (SAS), stabilizes the shape and the position of the brain during head movements [61].

Human dura mater is a protective membrane surrounding the brain. It has a fibrous structure. Typically, with age, the dura mater thickness changes from 0.3 to 0.8 mm. As an object for light propagation, this is a turbid, low transparent medium in the visible and near-infrared spectral ranges [62]. The data about the mechanical roperties of the Dura are collect along numerous test performed by other research [63] made on numerous and different aged people between male and female.

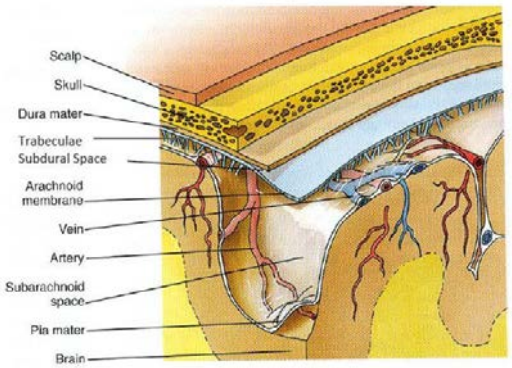

Figure 2.3 – Subarachnoid and Intercranial Space

Subarachnoid Space identifies the internal volume between the skull and the dura mater and the external part of the brain. It is composed from Arachnoid, Arachnoid trabeculae, Pia Mater, different membrane and ligaments that act as support for the brain. It is a structure that allows the flooding of the CSF around the brain, this structure works as a protection from the impact and damp the effect of an impact on the brain.

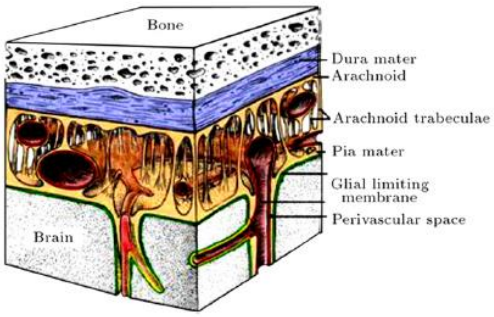

Figure 2.4 - Schematic diagram of the SAS space, trabeculae, the pia mater and the arachnoid

he hollow parr of the Arachnoid is called Arachnoid trabeculae, and it's the part where the CSF flows completely

1.5.3 Cerebral Spinal Fluid

Cerebrospinal fluid (CSF) is body fluid found in the brain and spinal cord. CSF acts as a cushion or buffer for the brain, providing basic mechanical and immunological protection to the brain inside the skull. The CSF occupies the subarachnoid space (between the arachnoid mater and the pia mater) and the ventricular system around and inside the brain and spinal cord. It's important to insert a substitute of the CSF into the Head Surrogate because it has a very important role in the absorption of the hit and the distribution of the pression all around the Brain. The fluid has also the role to reduce the friction between the layer and sustain the brain in his normal activity. A big research work was make from Lui et al.[64] and during this investigation a lot of data were collected from patients , with the aim to determine the densities of cerebrospinal fluid(CSF) under different conditions. The CSF in the end of the study results has a Newtonian fluid with viscosity like water: and its at 37 degrees is in the range of 0.7-1 mPa(cSt). The CSF surrounds the human brain and allows it to slide around inside the skull upon head impact and protect it from direct hits. The brain "floats" in this fluid inside the head and in this way is protected from rotational stress. The modern Helmets developed by MIPS (MIPS AB, Källtorpsvägen 2, Täby Sweden) are based on the same principal: a sandwich layer of low-friction material is inserted between the outer shell and the inner shell reducing the oblique impact and rotational acceleration [65].

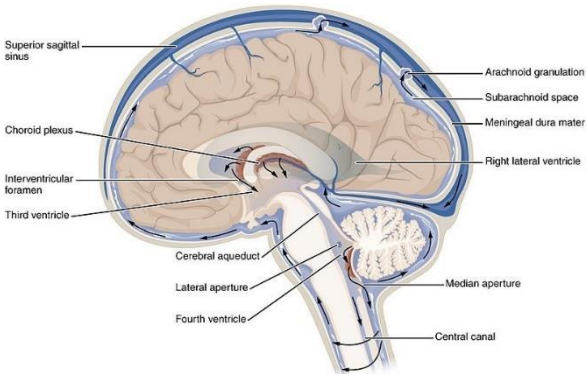

Figure 2.5 - Cerebral Spinal Fluid position and flowing

1.5.4 Brain

The human brain is the command centre for the human nervous system. It receives input from the sensory organs and sends output to the muscles.

The largest part of the human brain is the cerebrum, which is divided into two hemispheres. Underneath lies the brainstem, and behind that sits the cerebellum. The outermost layer of the cerebrum is the cerebral cortex, which consists of four lobes: the frontal lobe, the parietal lobe, the temporal lobe and the occipital lobe.

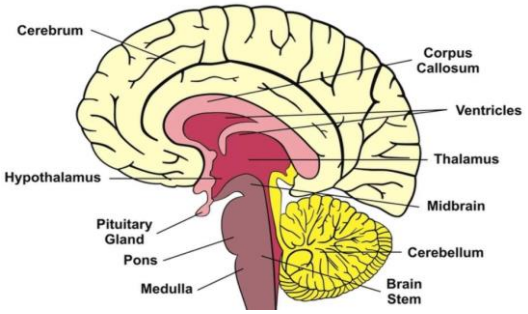

Figure 2.6 - Brain Anatomy

The human brain is divided into two hemispheres, the left and right, connected by a bundle of nerve fibres called the corpus callosum. The hemispheres are strongly, though not entirely, symmetrical. The left brain controls all the muscles on the right-hand side of the body; and the right brain controls the left side. One hemisphere may be slightly dominant, as with left- or right-handedness. The mechanical properties of the grey matter are investigated during different studies [34], [60], [66]; the aim is to know the characteristics of the brain structure and being able to reproduce it into FEM software and recreate the behaviour of the total human head under impact or head injury.

The brain matter can be considered as an elastic material, characterized physical properties summarized in the following chart.

Table 2- Brain Material Mechanical Properties

	Density $[\frac{km}{m^3}]$	E [Mpa]	Poisson Ratio
Range Values	1040	$0.05 - 66.7$	$0.48 - 0.4999$

1.5.5 Skin

The human skin is the outer covering of the body and it is the largest organ of the integumentary system. The skin has up to seven layers of ectodermal tissue and guards the underlying muscles, bones, ligaments and internal organs. Because it interfaces with the environment, skin plays an important immunity role in protecting the body against pathogens and excessive water loss. Skin has an important role in protection of the lower

layer of the body, it acts as a physical barrier against external attack and works as the first obstacle to hits and strikes.

All the literature about the Thickness's tissue give different and incomparable results because every single human analysed is different; from some studies about facial reconstruction and FBI recognizant with different approximation, has been possible obtain a technique for developing a representation of the face from the skull of an unknown individual.

For more than a century, researchers have employed a broad array of tissue depth collection methodologies, a practice which has resulted in a lack of standardization in craniofacial soft tissue depth research.

To combat such methodological inconsistencies, researcher [67] examined and synthesized a large number of previously published soft tissue depth studies. The authors collected craniofacial soft tissue depths using three-dimensional models generated from computed tomography scans of living males and females of four self-identified ancestry groups from the United States ranging in age from 18 to 62 years.

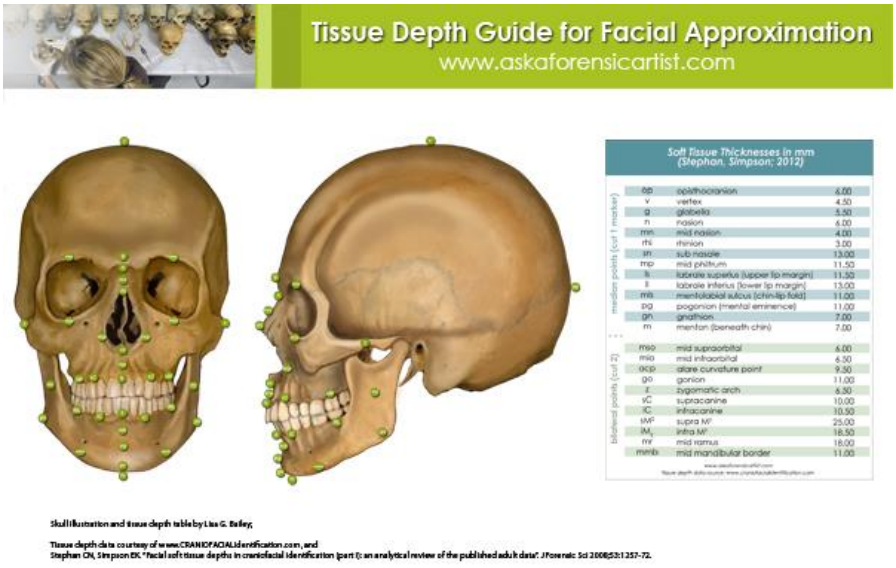

Figure 2.7 - Tissue Depth Guide for facial Approximation

The skin mechanical properties are different when measured using in vivo and vitro methods. In vivo methods for testing mechanical properties can be generally divided into two categories: imaging techniques and mechanical testing methods. Imaging techniques

have mainly been used to observe deformation and calculate mechanical properties of skin.

Chapter 3

Instrumented Human Head Surrogate 1.0

The first dummy head was developed by Mid Sweden University and University of Padova. The first dummy head has been developed during a previous research work [1]–[3]} and this part will illustrate only briefly the properties of each part.

In this chapter the first prototype is described, preliminary test discussed, discovered problem explained and restored.

The first dummy head was composed by an ABS 3D printed Skull, silicon Rubber Brain and silicon Rubber Skin, the dura mater and the arachnoid were reproducing with other materials.

The bio fidelity of those material is not reliable but as a first result it was supposed to be good. Some trial tests were performed, and initial results collected.

Some problems related with the leakage of the CSF, the reliability of the accelerometers and pressure sensors were observed and for this reason was desired to redesign and optimize a second Prototype.

1.6 IHHS 1.0 Structure

1.6.1 Skull

The skull geometry was obtained from human body data obtained from MRI scans. Original complex geometries were simplified, and a smoothing process was carried out: in addition, a bottom part of the skull flattened to accommodate the connection with H-III neck.

The MRI image is obtained and converted in a STL file and optimized using the software Meshmixer (Autodesk, San Rafael, California, USA) a basic free ware software useful for working on and modelling 3D Modelled part. It evaluates the mesh structure and allows to modify it, changing the shape, the orientation and the position of the triangular elements.

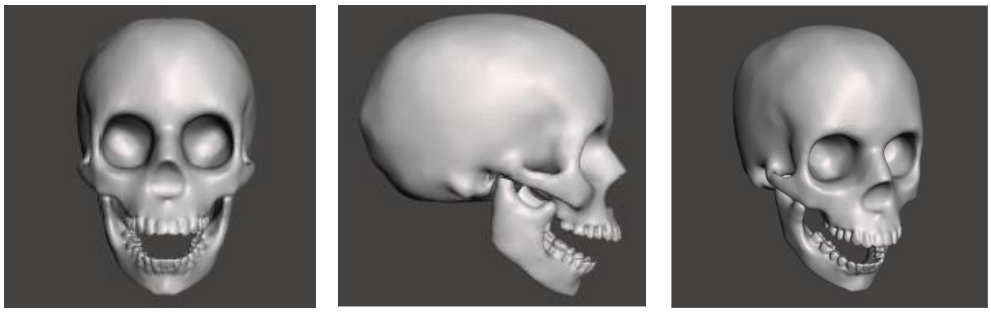

Figure 3.1 3D representation of Human Head skull obtained from MRI

The skull is designed and modified with this CAD software and then exported again in the STL format for the uploading in the machine with the specific printer software called CatalystEX 4.5 (Alphacam GmbH, Schorndorf, Germany), this program inspects the model file and convert it in the work-path that the nozzle must follow, and where automatically put the support or the model material.

First Skull prototype was 3D printed in ABS plus-P430 by FDM technology using the uPrint SE Plus 3D printer (Stratasys Ltd., Eden Prairie, MN, USA), mechanical properties analysed at page 123.

The uPrint SE Plus 3D printer, uses the technology of Fused Deposition Modeling (FDM) . This machine works with the ABSplus thermoplastic, creating models and parts that are durable and stable.

This technology is commonly used for prototyping: the machine lays down material in layer following the correspondent position read from the CAD file previously loaded.

The process is fast and allows to have in few hours the final object, this printer has an accuracy of 0.25[mm] and the size limit is related with the dimension of the printing base [203x203x152mm (WxDxH)].

A sawtooth suture was introduced to separate the two portions of the skull, with capacity of sustaining shear loads between the two skull portions and sealing to contain cerebrospinal fluid (Figure 1.a).

The skull is composed by three parts: upper part, lower part and jaw.

,

Figure 3.2 IHHS 1.0 3D Printed Skull
a) Top Part b) Bottom Part c) Jaw

1.6.2 Brain

The brain geometry was simplified to respect the anatomical separation between the hemispheres and with cerebellum: representation of brain sulci was ignored to allow a simpler and more robust demoulding phase. The silicone rubber used for the molding of the brain is Platsil Gel 01-30 (Polytek Development Corp., Easton, Pennsylvania, United States of America) (mechanical properties page 128), the process of moulding and curing requires some time because of the time necessary for the positioning of the sensors inside the uncured rubber.

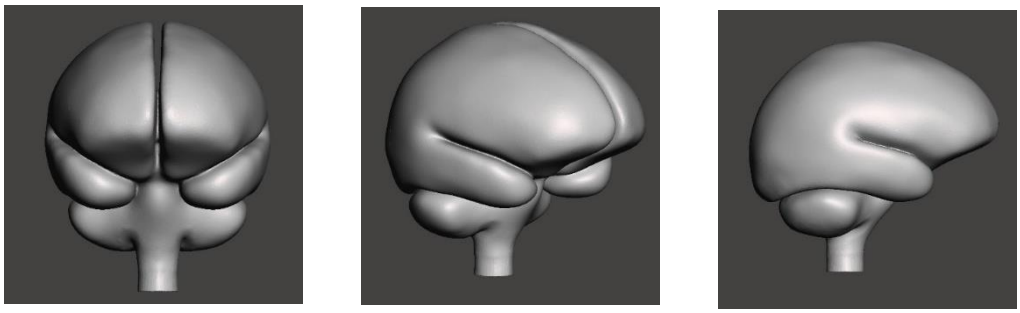

Figure 3.3 3D Representation of Human Brain obtained from MRI and with smoothed surfaced a)Front View b)Front/Side View c)Side View

The brain was moulded pouring the rubber on the moulds in three different stages corresponding to the layers of application of accelerometers in the brain, with moulds placed upside down, starting from the brain top. The result was a complete brain with separation of hemispheres and cerebellum having the sensors cables coming out via the brain stem. The accurate description of this procedure will be described in the following chapter.

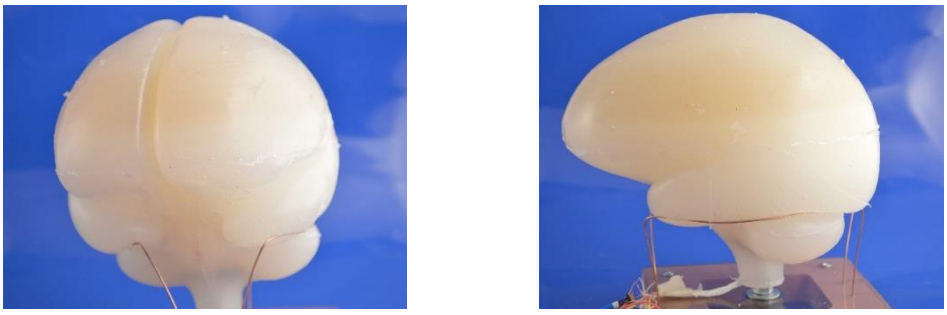

Figure 3.4 Silicon Rubber Brain after demoulding and with imbedded sensors

1.6.3 Dura Mater and Subarachnoid space

Starting from the brain geometry, a series of templates were shaped to facilitate the brain wrapping of the most curved parts. Using these templates, the fabric, Silicone coated Nylon Denier 31, used to simulate the dura mater and the arachnoid trabeculae, nonwoven polyester, were cut, weighted, stitched together and finally attached to the brain.

Figure 3.5 Wrapping of the brain with nylon sheet to mimic the SAS

1.6.4 Cerebral Spinal Fluid

The fluid chosen to simulate CSF had to display the lowest possible friction. In addition to this it was important to select an oil that would have not reacted with the silicone-rubber or the electronics. The chosen fluid was the low-viscosity silicone oil SilOil M4.165/220.10, commercialized by Huber (Huber USA, Inc.Centrewest Ct., NC)

.

1.6.5 Skin

The skin was made by a casting process into a specific mould. The moulds have been designed starting from an X-ray scan of a real human head, after 3D printing the moulds. Silicone rubber Platsil-Gel 01-30 was used to mimic the skin properties as found from literature. The skin is composed by only one piece that must be put on the front part of the head and then pulled back until it is worn properly, it has a small cut, not more than 5cm, on back part of the neck, so the head can get inside.

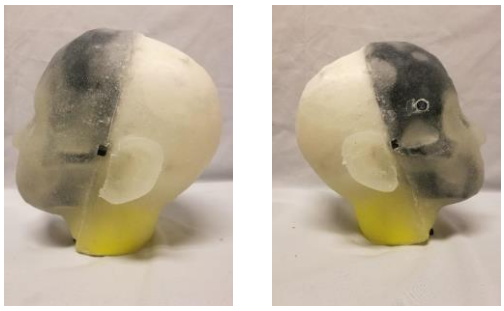

Figure 3.6 Rubber Skin on the Surrogate

1.7 Sensors

1.7.1 Accelerometers and Gyroscopes

Accelerometers

The location of the sensors in specific point with the aim of collect data from position interest. Most peak accelerations related with head trauma are consistently lower than 200 g/s. It was decided to set the accelerometers range at +-200 g.

The chosen model was the ADXL377 3-Axis accelerometer, manufactured by Analog Devices Inc (data sheet page 147). Those sensors are very small (3x3x1.45mm), they are of the right dimension for being embedded inside the rubber brain.

As described in Analog Devices datasheet they are designed for concussion, head trauma and high force detection. Then gyroscopes are necessary to embed for evaluation of the angular velocity and the angular acceleration of the brain.

Gyroscopes

The interest of the research was to collect the information about the rotation of the head around the three main axes, collecting information about Roll. Pitch and Yaw of the instrumented human head. It was decided to couple two 2-axes gyroscopes one (LPY4150AL) able to collect pitch and yaw rotation and another (LPR4150AL) for pitch and roll (datasheet page 152). The sensors of choice are manufactured by STMicroelectronics.

These sensors present very small dimensions (4x5x1 mm) and can collect data in range of angular velocities spanning from 1500 dps (26.2 rad/s, with amplification) to 6000 dps (104.7 rad/s, without amplification), those values are enough for the value of the velocities described in literature.

Nine triaxial accelerometers (ADXL377, Analog Devices, +/- 200g) were placed on the brain to explore its local behaviour during impacts. A stack of two biaxial gyro chips (LPY4150AL- pitch &yaw, and LPR4150AL- pitch &roll, both +/- 1500 deg/s, ST Microelectronics) and one accelerometer were placed on the centre of mass of the brain (BCOM).

Two accelerometers (ML-MidLeft and MR-MidRight) were put on the side of the CG-CentreOfGravity); two accelerometers (TL-TopLeft and TR-TopRight) were positioned

on the same coronal plane of CG; finally, three accelerometers (CL-CerebellumLeft, CM-CerebellumMid and CR-CerebellumRight) were put roughly on the barycentric line of the cerebellum to track its motion separately from the rest of the brain.

Two biaxial gyroscopes are set in the CG for collecting the angular acceleration in all three rotational direction.

Table 3 Accelerometers coordinate with respect to the brain Com

Accelerometer	x [mm]	y [mm]	z [mm]
Top − Left (TL)	0	+26	+43.6
Top Right (TR)	0	−26	+43.6
Mid Left (ML)	0	+40	0
CenterOf Gravity (CG)	0	0	0
Mid Right(MR)	0	−40	0
Cerebellum Left (CL)	−23.4	+35	−44.4
Cerebellum Mid(CM)	−23.4	0	−44.4
Cerebellum Right (CR)	−23.4	−35	−44.4

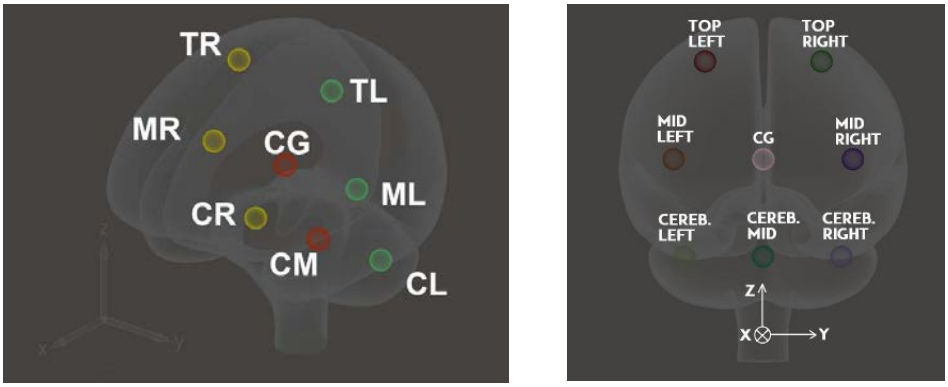

Figure 3.7 Position of Accelerometers and Gyroscopes in IHHS1.0

1.7.2 Pressure Sensors

Ten pressure sensors are settled on the skull, the position of them is symmetric to the sagittal plane. Eight out of ten are in the mid plane at the same height of the CG, then two mounted in top position of the skull above the higher points of the two brain's lobes.

The pressure sensor used are Solid State Pressure Sensor STD Series (Sencer Co. Ltd., Jen Ai Road, Taipei, Taiwan).

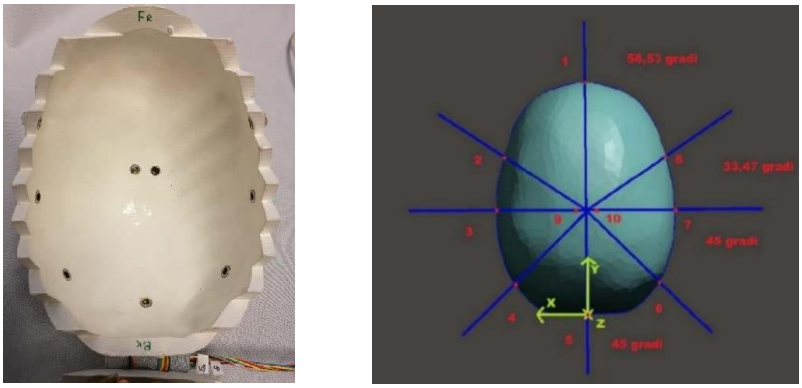

Figure 3.8 Position of the Pressure Sensors in the IHHS1.0 a) inside picture from the decoupled skull b) 3D representation of the position of the sensors

1.8 Problems and Restoring

A deep analysis and preliminary set of tests was performed from Luca Broggio [3] in a previous work but during those test several problems showed up that put doubt on the acceptability of the obtained results and their reliability.

Head Size

The final size of the complete dummy head revealed bigger than the average, the circumference is of 64cm. This problem is related with the necessity of find a proper helmet the could fit it.

The helmet used for the first set of tests was too small (Size M, 58cm of circumference), and probably this inaccuracy gave incorrect results.

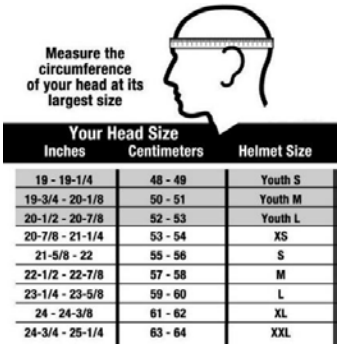

Figure 3.9 Size of the IHHS1.0 and wearing of the helmet

Oil Leakage

One of the problems that showed up during the first check of the dummy was the leakage of oil from the skull. The connection between the parts of the skull was designed without an accurate shape and the tightness was not guaranteed, the lower connection with the metal adaptor wasn't sealed enough and the plenty of holes for the position of the pressure sensors was a chance for the liquid to go away.

Another hypothesis is that the honeycomb structure of the 3D printed ABS allows the diffusion of the liquid through the structure itself, causing the outflow.

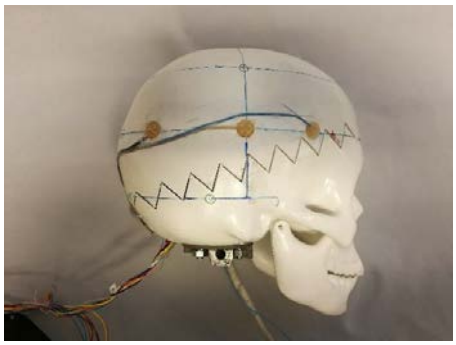

Figure 3.10 Skull connection and pressure sensors holes (left); Adaptor lower connection (right)}

The outcome of the oil was a problem because it does not allow to reproduce a correct space between brain and skull, the impact transference and energy transmission is different and not accurate ad in a real-life scenario.

Brain Swelling

Interaction problems are noticed between the silicon rubber and the silicon Oil. The fluid showed a tendency to soak into the rubber and make it increase in volume.

Since the Brain was moulded with Plastigel 01-30 and then the head filled with silicon oil, there is the suspect that this interaction made the brain increase in size and keep it stuck into the cranium, avoiding some of its relative movement.

Some trial test of interaction between Silicon Oil and Silicon Rubber are performed.

Silicon Oil - Silicon Rubber Interaction

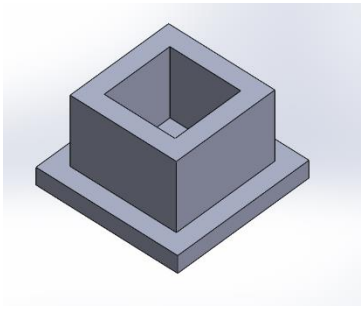

Figure 3.11 Mould for rubber square sample preparation

For the evaluation of the behaviour of the silicon Rubber in the Silicon Oil four specimens have been tested. Fours sample of Silicon Rubber (00-20) are prepared with a specific mould.

Table 4 Initial volume and weight of the samples

Sample	Volume [mm^3]	Weight [g]
1	20x20x20 (8000 mm^3)	8.58
2	20x20x20 (8000 mm^3)	8.74
3	20x20x20 (8000 mm^3)	8.55
4	20x20x20 (8000 mm^3)	8.36

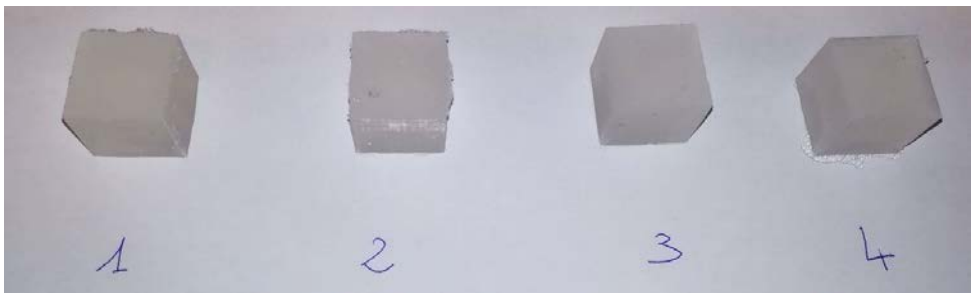

Figure 3.12 - Silicon rubber samples and identification number

All the sample are drowned in the silicon oil for 72 hours and after this time they are measured and weighted again for the evaluation of the differences there are some.

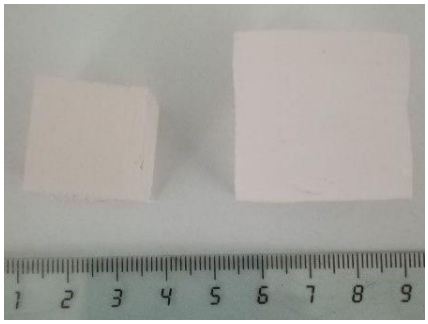

Figure 3.13 Size comparison between on sample before (left) and after(right) the drowning in the Silicon Oil

Table 5 Samples size and weight and percental increasing after drowning period

Sample	Volume [mm^3]	Weight [g]	Increase in Volume	Increase in Weight [%]
1	28x28x30 (23520)	20.44	294[%]	238[%]
2	30x29x28 (24360)	21.12	304,5[%]	241[%]
3	29x30x29 (25230)	21.23	315,3[%]	248[%]
4	30x31x29 (26970)	21.28	337[%]	254[%]

The rubber shows a huge increase in his volume and weight, the chemical composition of the silicon oil and the rubber are very similar and for this reason the two material are

strongly compatible, and the fluid and the molecular chain of the silicon Oil makes the rubber swollen.

For this reason, has been deciding to change it and select another type of fluid that would allow to reach the low viscosity of the Physiological CSF.

The choice is on different type of synthetic oil, but the only type that could allow the low viscosity behaviour and in the same time doesn't give problem of interaction with the Silicon rubber of the brain is the dielectric oil used for capacitors.

Sensors Problems

Due to the compression of the rubber on the skull walls the pressure sensors stopped working and they were not finally available for the test and collection of data; another suspect is that they were not developed for working in contact with fluid.

Some general problems with accelerometers and gyros showed up during the test but is not possible to define a precise reason of this imprecision.

All the efforts invested in the preparation and study of this innovative prototype are anyway worth a functional dummy head from which is possible obtain some results and collect more data as possible.

1) Is task of interest to restore the first prototype as well as possible and try to collect data to analyse and compare with the following results and project.
2)

1.8.1 Head configuration

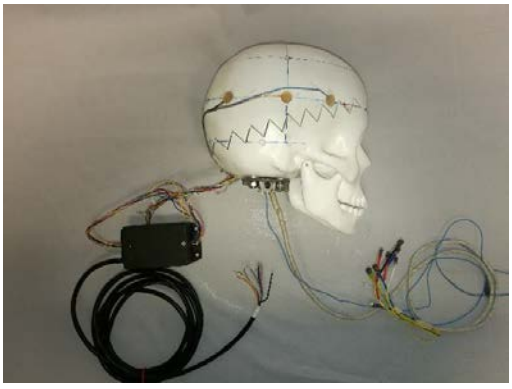

Figure 3.14 IHHS1 wiring and final configuration

The head is connected to the board platform, checked the functionality of the sensors and the connection to the acquisition system through LabView software (National

Instruments, Austin, Texas, USA). Every sensor and its functionality were controlled, figuring out the correct axis orientation and relative position with the reference system.

Name	Label	Position	Channel	Acc_Axes	Brain_Axes
Accelerometer 1	ACC1	Top Left	A0 (X)	x1	-xb
			A1(Y)	y1	+yb
			A2(Z)	z1	+zb
Accelerometer 2	ACC2	Top Right	A3(X)	x2	-xb
			A4(Y)	y2	+yb
			A5(Z)	z2	+zb
Accelerometer 3	ACC3	Mid Left	A6(X)	x3	-xb
			A7(Y)	y3	+yb
			A8(Z)	z3	+zb
Accelerometer 4	ACC4	Mid Right	A9(X)	x4	-xb
			A10(Y)	y4	+yb
			A11(Z)	z4	+zb
Accelerometer 5	ACC5	Cereb Left	A12(X)	x5	+xb
			A13(Y)	y5	-yb
			A14(Z)	z5	+zb
Accellerometer6	ACC6	Cereb Right	A15(X)	x6	+xb
			A16(Y)	y6	-yb
			A17(Z)	z6	+zb
Accelerometer 7	ACC7	Mid COM	A18(X)	x7	-xb
			A19(Y)	y7	+yb
			A20(Z)	z7	+zb
Accelerometer 8	ACC8	Cereb Mid	A21(X)	x8	+xb
			A22(Y)	y8	
			A23(Z)	z8	+zb
Gyroscope1 X-Z	GYR1	COM	A24(X)	Vref	
			A25(Y)	ωx	-wxb
			A26(Z)	ωz	-wyb
Gyroscope2 X-Y	GYR2	COM	A27(X)	Vref	

			A28(Y)	ωy	wxb
			A29(Z)	ωx	wzb

1.8.2 Experimental Set-Up

Test Frame

To validate the Instrumented Human Head Surrogate a test system frame has been used which allowed to perform impacts tests under different energy condition.

Figure 3.15 Impact Frame structure and impact point

The system is a structure composed by aluminium profiles and a pendulum with a mass at the end of the profile. The system can be adjusted choosing the preferred direction and position. The impactor is a metal cylinder: 60mm diameter, 255 mm long, made from steel ρ = 7749.5 kg/m3. The impactor was padded with foam to reduce the sharpness of the edges and introduce a damping. The pendulum is armed with a rope and pulley system until the correct angle is reached and then the correspondent potential Energy value.

Laser Trigger and Acquisition board

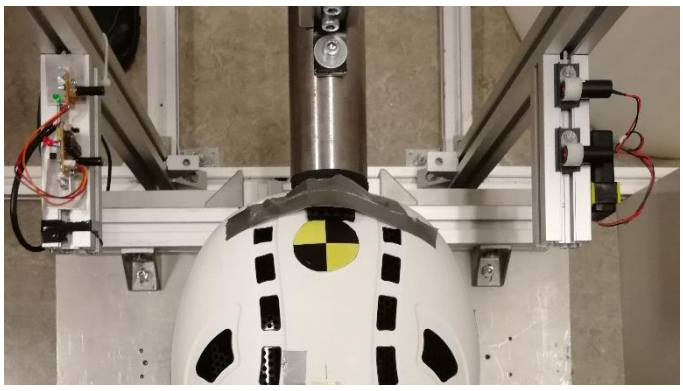

Figure 3.16 - Laser triggering System: the crossing of the pendulum through the laser beam, the computer starts the acquisition

A manual trigger is used to drop the pendulum and start the acquisition of data. The falling pendulum pass through a double laser beam, this light system optical sensors give the signal to the recording board and makes the sensors data acquisition start. The acquisition time is long enough to guarantee the collection of the data relative to the main head impact and the following head rebounded reaction.

The signal is collected with a Data acquisition Board NI USB-6343(National Instruments): and elaborated using LabView software (National Instruments, Austin, Texas, USA).

Force Platform

The Head is coupled to a standard dummy neck from Jasti (JASTI CO., LTD Miyoshi, Koto-ku, Tokyo, Japan); it is part of the Human Dummy Hybrid III 50th-percentile male, and this head neck structure is mounted on a Kistler 9281 EA (Kistler Group, Eulachstrasse 22, 8408 Winterthur, Switzerland, datasheet in appendix page. 147) force platform from which it would be possible also to collect data related with the forces applied to the neck. It is composed of a 600x400 mm aluminium sandwich top plate of lightweight construction and four piezoelectric 3-component force sensors. Measurements are allowed over a very wide frequency range. The measuring range can go from –10 to 20 kN [47].

Cameras

The impacts tests are always record with two cameras GoPro Hero 5 Black. The impact recording as obtained from a lateral point of view and from the top. The settings used for the test are 1920x1080pp, 120 fps of recording speed and a reduced fish eye effect. The videos were also used to verify approximately the concordance between the real displacement of the head and the displacement calculated by time integrating two times the acceleration.

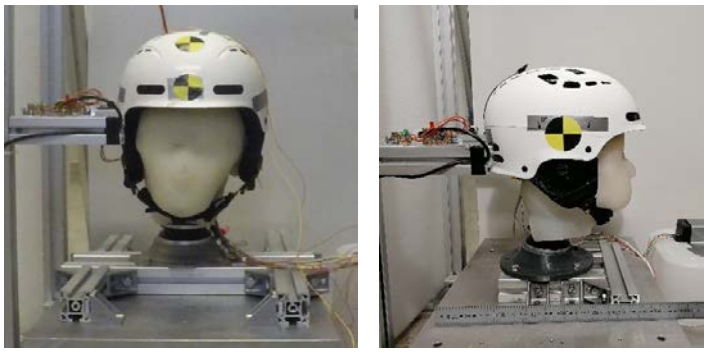

Figure 3.17 - GoPro Hero Black 5 side point of view

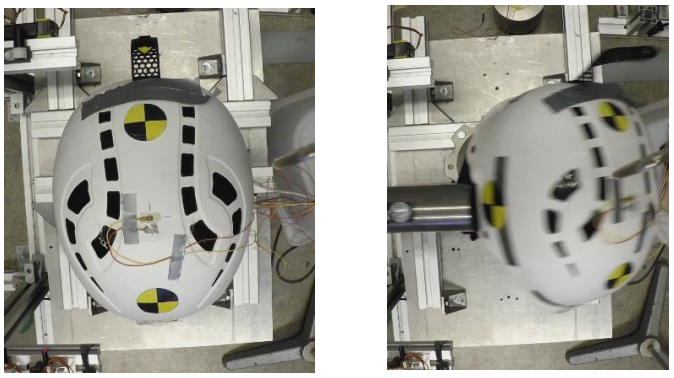

Figure 3.18 - GoPro Hero Black 5 top point of view

1.8.3 Test Method

The setup of the head was studied with respect to anatomical position of the human head. Correlation with physiological reference points was needed to correlate the orientation of the brain using marker during in vivo experiment. A customized base was designed for obtaining the correct planarity of every anatomical correspondence

The line which connects the eternal acoustic meatus, situated on the temporal bone, with the root of the nose has been taken as the reference anatomical line, this line is inclined of *17° degrees* with respect of the horizontal plane in the posterior-anterior direction. This is the desired position to reproduce on the experiments setup, it represent the anatomical position and orientation of a human head in the standing straight position.

For the evaluation of the angles during the configuration was used the internal Girometer of a Smartphone (Huawei P10 Lite 2017) using a digital goniometer.

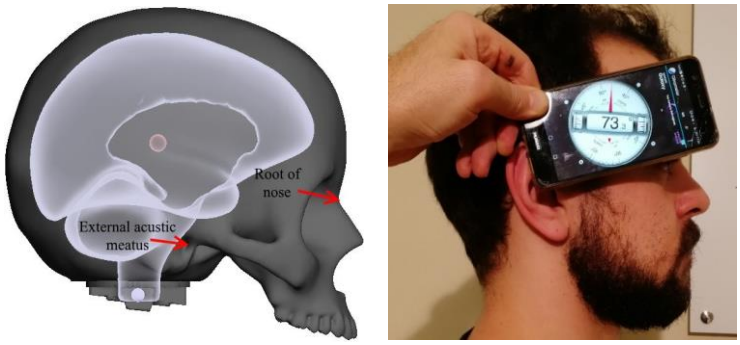

Figure 3.19 - Evidence of the physiological angle between the nose root and acoustic meatus with respect to the horizontal plane, the obtained value is 17degrees

The skull's reference system has been defined as well. The reference system has been positioned in the centre of the head-neck joint, its axes are parallel with the brain's reference system and they have the same convention.

The centre of skull's reference system is lying on the sagittal plane.

The Head Neck system is respecting the anatomical orientation mounted on a base inclined of 7° degrees for obtaining the correspondent inclination of every plane and line of reference.

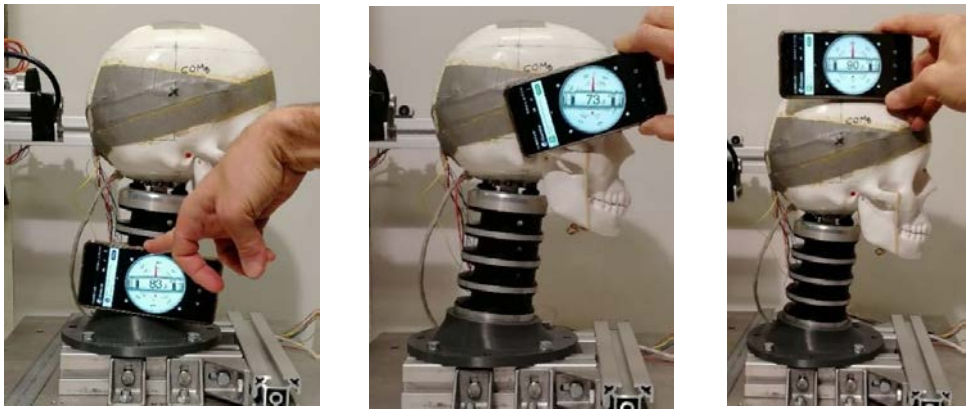

Figure 3.20 - Position of the Skull on the setup platform and checking of the respect of physiological angles a) angle orientation of the base adaptor connection of 7 degrees b) acoustic meatus-nose root and horizontal plane angle of 17 degrees c) the transversal plane of the brain is parallel with the horizontal plane

Skull Acceleration

An improvement is the embedding of an accelerometer directly on the skull, the triaxial accelerometer(ADXL377, Analog Devices, +/- 200g), the same used in the brain, is placed on the palate ceiling [24]. This sensor is placed for the collection of the real acceleration of the skull, analysed as a rigid body, and compare the results with the others acceleration values.

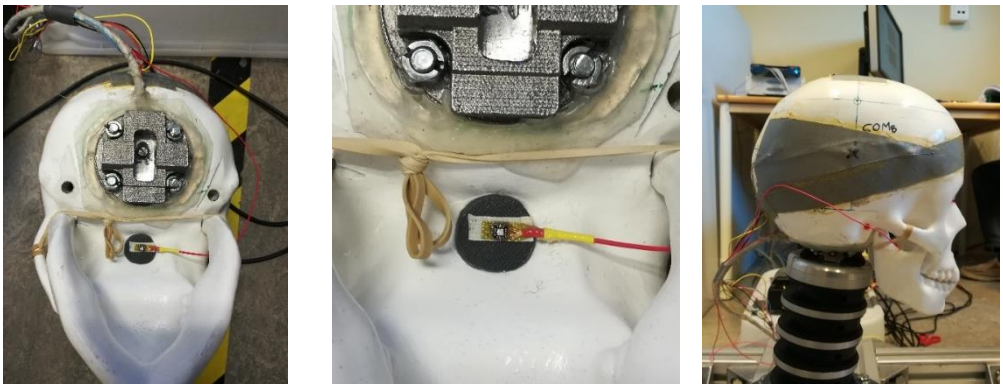

Figure 3.21 - Embedding of the accelerometer on the IHHS1 gluing it on the palate ceiling

The skull is covered with its rubber skin previously prepared, a polyester under helmet cuff was applied on the head. This hat is applied to reproduce the sliding relation between inner helmet part and head/hair friction.

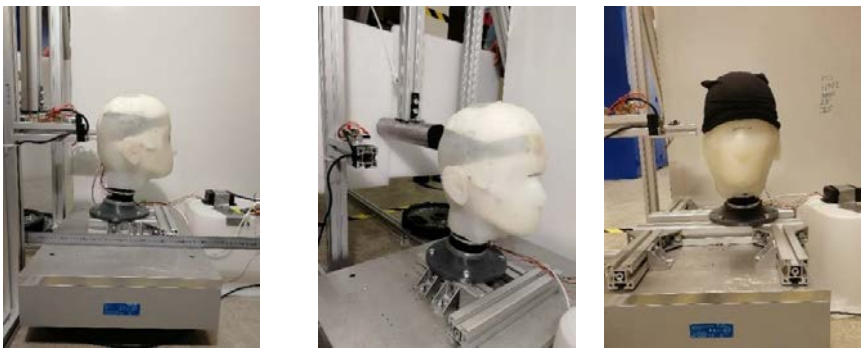

Figure 3.22 - Head covering with moulded silicon rubber skin and under helmet cuff covering

A modern ski Helmet produced by Sweet Protection (Igniter Mips Helmet) is fitted on the Head (size XXL), this time it is properly measured and chose in relation with the circumferential size of the dummy. It is previously marked with positioning marker and placing it on the system correctly.

This type of Helmet technology was chosen on purpose, due to the desire of compare the results obtained with the MIPS system activated or not.

MIPS

This Helmet is a Performance Helmet characterized by a high protection level, it is manufactured including the innovative MIPS system, a protective mechanism aim to reduce the strain on the brain reducing the rotational acceleration on the head during an impact [65]

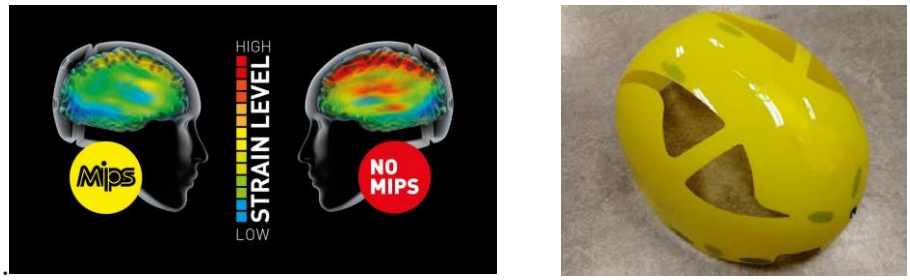

Figure 3.23 - MIPS is a protective mechanism aim to reduce the strain on the brain reducing the rotational acceleration on the head during an impact

MIPS system is an innovative protection system developed for reduce head injury related with high impact and fast rotational stress.

Traditional helmets have an energy-absorbing polymer inner foam liner and an external stiff shell. In an oblique impact, the helmet shell will transfer the tangential force component to the foam liner and that one can partly transfer it to the head. Researchers working on this project believe that head protections can be improved by interposing a low friction layer between the shell and the liner[14], [68].

MIPS helmet are thought to mimic the natural protection of the brain inside the skull, permitting to the head to slide inside the helmet in the same way the brain floating in the cerebrospinal fluid can slide inside the skull.

During the testing procedure the Helmet will be put on and off the helmet, and this is for both validate the correct working of the dummy head and either for checking the correct working of the MIPS protection system.

Helmet

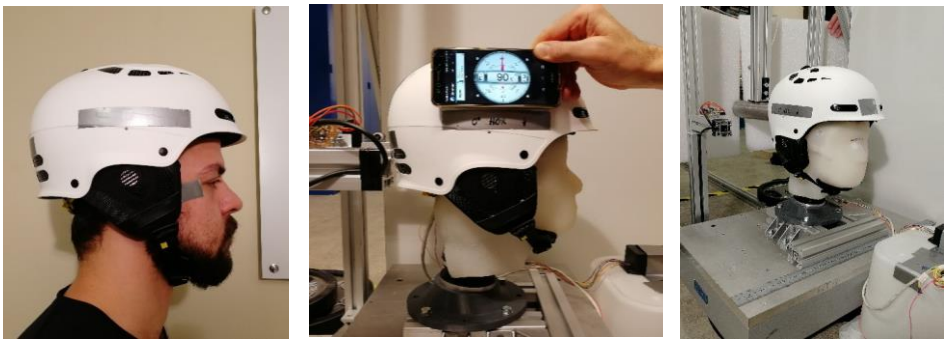

Figure 3.24 - Helmet wearing on the dummy head respecting the anatomical configuration checked on a real human configuration

A further accelerometer is applied on the Helmet to complete the global instrumentation of the Instrumented Human Head, this last outer sensor allows to obtain the value of the acceleration and the energy acting directly on the dummy head itself.

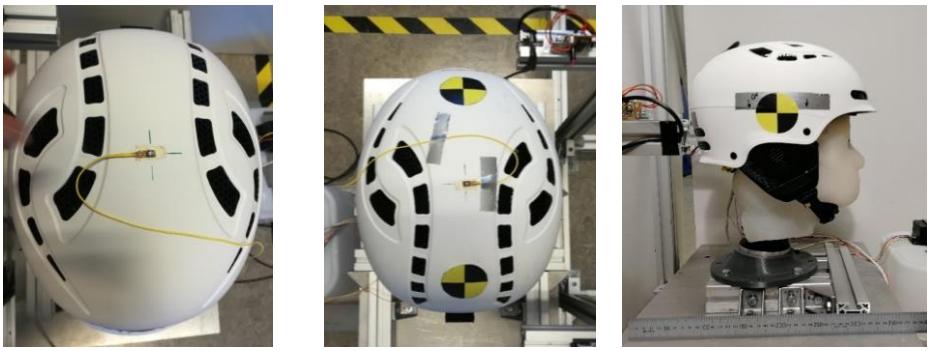

Figure 3.25 - Helmet configuration with the apex accelerometer glued on the top part, this sensor will collect the energy reached directly from the pendulum

A short table resuming all the main coordinate:

High COM Brain (from bottom)	312 mm
High Neck Base (from bottom)	45mm (Profile Side) + Neck and inclination
Neck Support Inclination	7°
Inclination anatomical axe between ear and nose root	73°
High of accelerometer on the helmet apex	431mm

1.9 Test Protocol

After the positioning of the Head on the base system, a test protocol is established for collect data from different impact position of the head and different energy values.
The Pendulum system can be armed at different position and obtaining different values of potential energy.
The head/neck system can be rotate and positioned differently, this disposition allows to recreate different impact positions and collect data under different effect and compare the results.

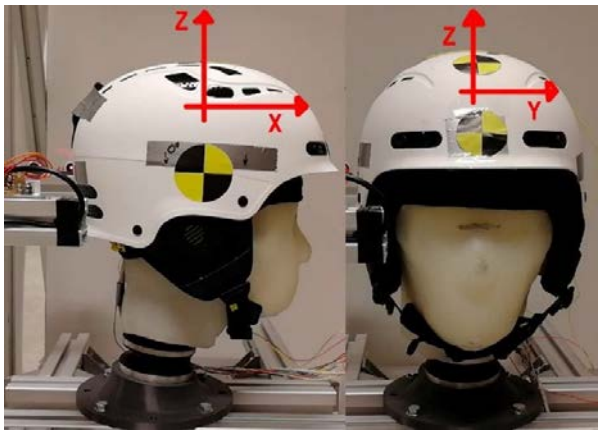

Figure 3.26 - Anatomical Reference system and axes orientation correspondent with the sensors data collection direction

After the setup of the Head on the force platform and the positioning at the correct high, different test on different orientation of the dummy head are performed.
To obtain different data and comparison options, the head has been impacted under four different orientation in different impact point: Back, Right, Front Right and Back Right, a deeper description of the test is discussed further. For each orientation, 4 different Energy level are reached to hit the target. The heights have been calculated in function of how much potential energy the impactor should have at the starting position.

Head configuration and orientation

The head is orientable moving the base support custom designed to obtain the 45 degrees step of rotation.

The hammer is always settled to hit the dummy in correspondence of the Head Centre of mass.

The helmet is prepared with special labels necessary for the video analysis and recognize the point to follow during the movement, this would be use for the analysis of the movement, range of motion and speed.

The systems are connected to a pc and the collected data are analysed and displayed with the software LabView.

The software allows to observe immediately the response and the correct working process of the signals, aft wards all the information are saved and analysed Using MATLAB software, for cut, filtering and study every signal individually and compare the interesting data.

The Potential Energy chosen for the impacts are originally selected by preceding researcher [3] on the base of earlier studies [69] and personal opinion based on the materials knowledge and design.

The principal interest of this project is to obtain useful data from the prototypal dummy head and analyse the information coming from it. The aim of the first thesis work was to compare the data of the IHHS1.0 against the data of a Hybrid III tested in the same conditions, to observe if the design of the IHHS was coherent and comparable with the standardized model.

For this set of tests, the same energy is imposed for the protocol, initially has been decided to not reach high values because the main point is to try the dummy head without stress it until his limit.

Table 6 - Experiments protocol and explanation of dummy orientation

Legend	
Date	02/03/2018
HS1	Human Surrogate 1 2017
HM1	Helmet with Mips
B/F/BR/FR	Back – Front – BackRight – FrontRight

Pendulum Angle	$29° - 41° - 51° - 72°$
Potential Energy	$8J - 16J - 24J - 44J$
Test	Test1

The estimation of the energy of impacts was calculated starting from the potential energy of the hammer coupled with the pendulum in the testing frame.
Moment of inertia of the moving part (aluminium profile 1 m long and a cylindrical steel with a mass of 5.6 kg) was calculated and the total inertial moment is formed by the two contributions.

Table 7 - Pendulum characteristics and potential energy calculation

Aluminium profile		2	kg/m
Length Aluminium profile		2	m
Total Moment of Inertia	$I_t = I_R + I_m$	6.607	$kg * m^2$
Moment of Inertia Rotating Beam	$I_R = m_r * \frac{L^2}{3}$	0.666	$kg * m^2$
Moment of Inerzia rotating weight At one end (cilinder)	$I_m = m_i * r^2$	5.94104	$kg * m^2$
Equivalent Mass	$m_{eq} = \frac{I_t}{r^2}$	6.607	kg
Potential Energy	$m_{eq} * g * h$	16	J
g		9.822	m/s^2
h	$\frac{E_p}{m_{eq}} * g$	0.246	m
angle rad		0.706	rad
Angle grad		40.4989	deg

The correspondent configuration pendulum angle to reach for every energy is:

Table 8 - Potential Energy and initial pendulum angle position with respect to the vertical plane

8 J	29 deg
16 J	41 deg
24 J	51 deg
44 J	72 deg

The different energy level test is performed for every head orientation, every set of tests is composed of a hit of the target 3 times for each configuration.

1.9.1 Tests

With IHHS1 has been performed 48 tests (4 position of the head tested at 4 different energy levels of the impact with 3 repetitions) for the head wearing a normal sky helmet and 48 tests for the head wearing the same helmet with multi-direction impact protection system (MIPS) activated, that means a total of 96 tests performed.

In the following table will be shown the test program. The tests about the IHHS1 test are deeply discussed by Edoardo Marzella[70], the obtained results are displayed in the following charts and some estimation are done about that.

Table 9 – Description and total number of tests performed on the IHHS1

Position	Impact
Name	Energy [J]
Back	8 16 24 44
Back-Right	8 16 24 44
Right	8 16 24 44
Front-Right	8 16 24

44

A test protocol is fixed to guarantee the repeatability of the tests e for every energy level three test are performed and discussed.

The pendulum impact location is always at the height of the brain centre of mass; during the impact tests when the head is rotated, for instance Front Right and Back right impact, the interest is to hit the target at the same height and then the impact direction is radial with respect to the brain centre of mass.

In the following pages summary charts are displayed and discussed for the analysis of the global behaviour of the dummy head, comparing the effect of the activation of MIPS system.

Back Impact

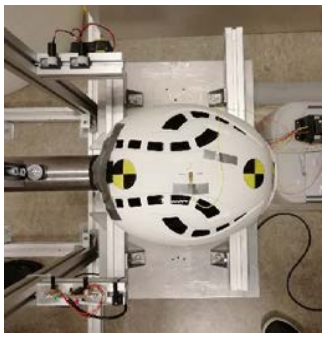

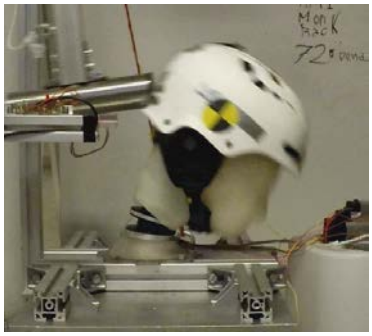

Back Right Impact


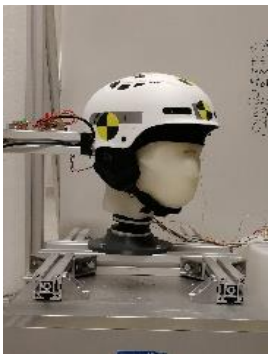
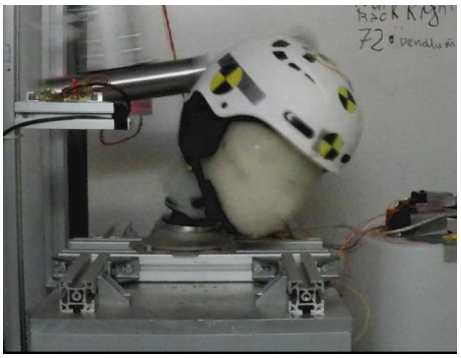

Right Impact

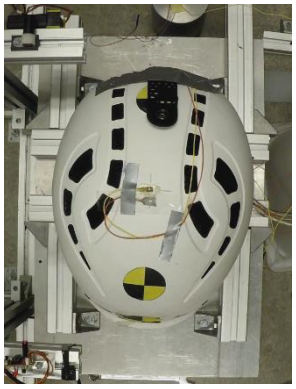

Front Right Impact

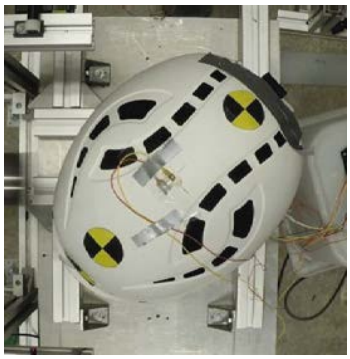
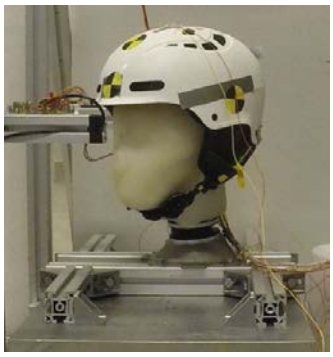
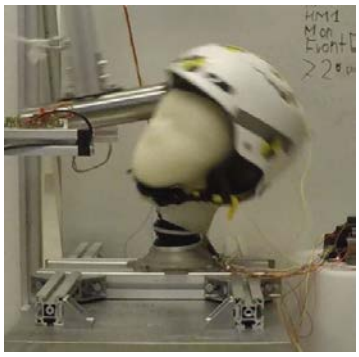

Tests Results Comparison and analysis

To explain the main results and comment the differences, histograms are used.

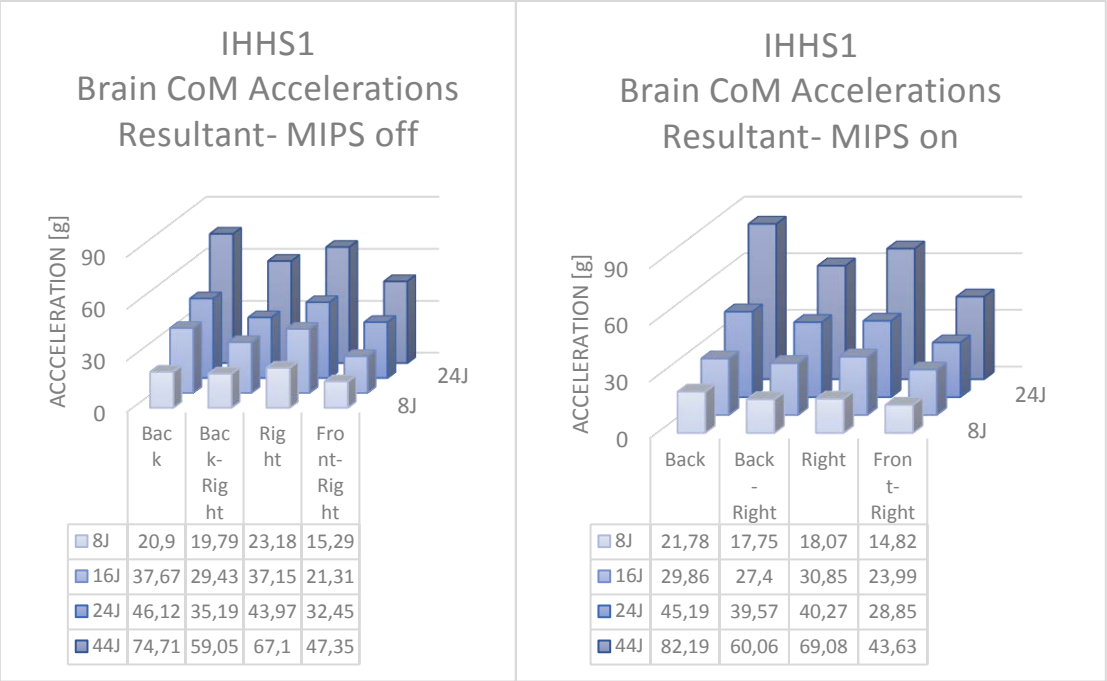

Figure 3.27 – Brain centre of mass accelerations resultant: Comparison 8J, 16J, 24J and 44J and Impact position Back. Back-Right, Right, Front-Right. a) MIPS off b) MIPS on

The first comparison is between the resultant acceleration of the Brain CoM for every impact position and each energy level with MIPS off (Figure 3.27-a) and then with MIPS on (Figure 3.27-b).

From both previous graphs is visible that the increase in the energy level means a rise of the resultant acceleration as could be predictable, and the behaviour is the same for both MIPS conditions. The peak value obtained on every condition don't change in a remarkable way between the two graphs, this means that MIPS layer does not influence linear accelerations. In general, is possible to observe that the higher value of the results is on the impacts performed from the back and from the right, those to impact have only one principal direction of acceleration.

From the resultant acceleration is possible to evaluate the HIC, then the same trend of the values is showed in the HIC plot (Figure 3.28); Back and Right impacts have higher HIC values than Back-Right and Front-Right position. The HIC results with the MIPSon are

not displayed since the global trend is the same already discussed for the resultant acceleration.

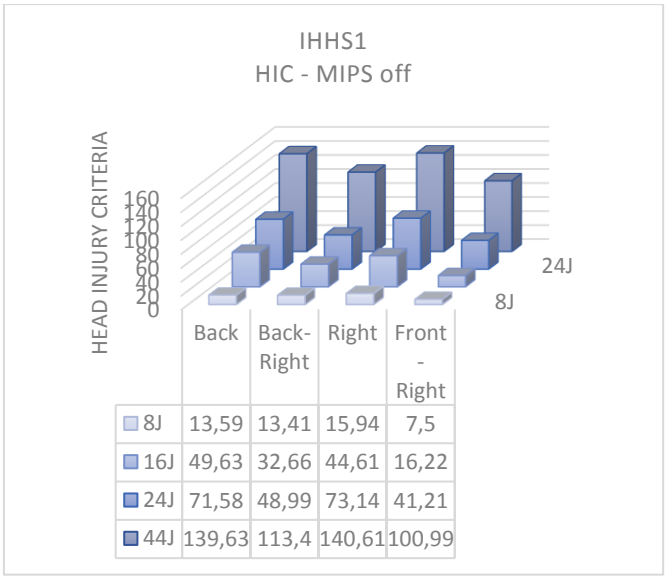

Figure 3.28 - Brain centre of mass HIC; Comparison 8J, 16J, 24J and 44J and Impact position Back. Back-Right, Right, Front-Right

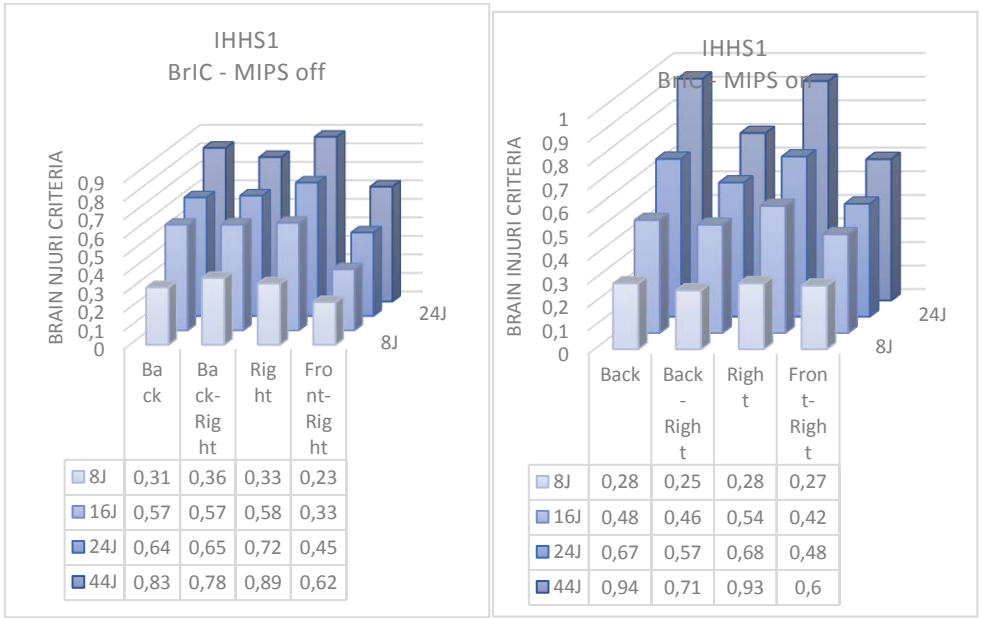

Figure 3.29 - BrIC; Comparison 8J, 16J, 24J and 44J and Impact position Back. Back-Right, Right, Front-Right a) MIPS on b) MIPS off

An important value to compare is the one related with the BrIC, the two previous graphs (Figure 3.29) plot the differences of the value between the MIPS on and MIPS off condition. BrIC is calculated using the angular velocity maximum values and any

remarkable differences are visible from this comparison, but since MIPS is designed to reduce angular accelerations it could be correct to not directly obtain difference in the angular velocity; Back and Right impacts show higher values than Back-Right and front-Right.

To observe if the MIPS system is efficient is necessary to analyse and compare the angular acceleration values; those results are obtained deriving the angular velocity value collected by the gyroscopes in the brain centre of mass. A single test comparison between MIPS off and MIPS on for far 24J Energy level impact is displayed (Figure 3.30) and the differences discussed.

Is visible that a decrease is always found, for every impact type the activation of the protection system help to reduce the angular acceleration. This result could useful for two reasons: to test the MIPS technology and to validate the correct operative of the dummy head.

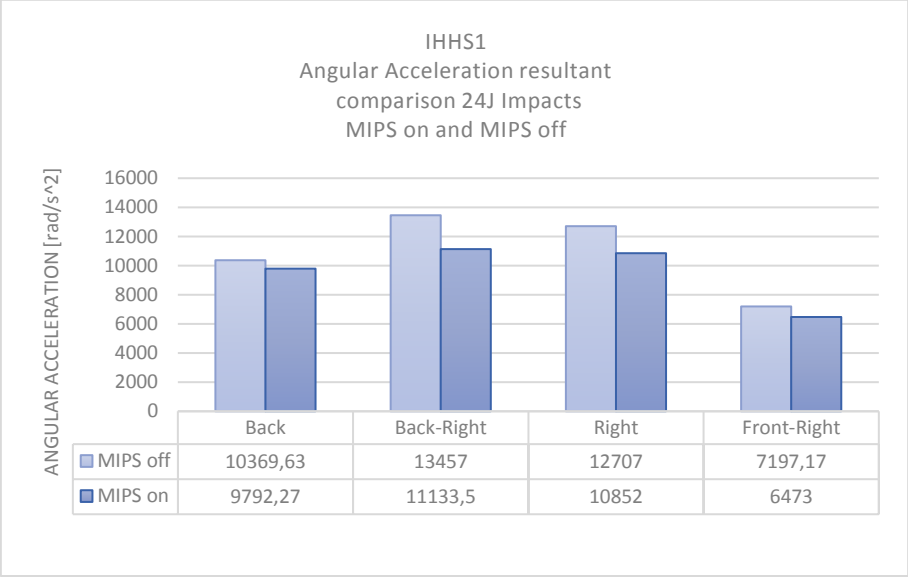

Figure 3.30 – IHHS1 MIPS On and Mips Off Comparison for a 24J test, on Impact position Back. Back-Right, Right, Front-Right

One more graph is added as an explanation of the dummy head behaviour and impact tests response. The acceleration transferred from the hammer to the dummy head follow

an order that is predictable, from the helmet, to the skull and finally to the brain (the order of the peak during the time is displayed in the analogue test performed for the IHHS2 Figure 4.59), the energy through the head components has to show a reduction related with the damping effect introduced from the helmet.

Chapter 4

Instrumented Human Head Surrogate 2.0

1.10 Head design

The first human head prototype, as discussed, showed many problems. The second study was started to introduce substantial changes and obtain a more reliable physical model. The tests results reached with the first dummy head are matter of study for the comprehension of the traumatic injury and they would be used for the comparison with the new prototype.

1.10.1 Skull

The first problem to fix was related with the global size of the head. The circumference was too big and did not allow the proper wearing of an average helmet.

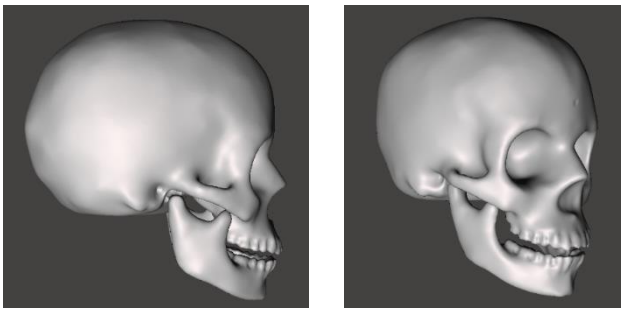

Figure 4.1 - 3D representation of the reduced skull for the realisation of the IHHS2

The first correction was to rescale the 3D model of the cranium, obtaining a 10% smaller skull, the software used for the redesign is MeshMixer.

During the redesign phase was introduced another improvement in the connection between the two parts of the skull. The saw junction present in the first head was not accurate and did not guarantees the proper sealing.

The contact part between the top and the bottom part in the second prototype was changed with different connection geometry, easier to assemble and more reliable also for stress distribution and tightness of the skull itself.

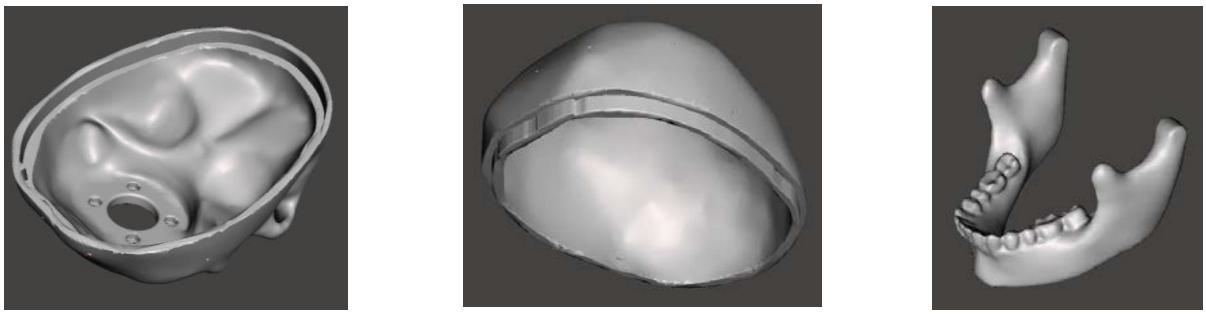

Figure 4.2 - Separaed parts of the IHHS2 skull a) Low Part b) Top Part c) Jaw

The head is composed of three parts: Upper Skull, Lower Skull and jaw.

The Skull is 3D printed with FORMIGA P110 (EOS, Krailling, Germany) and the Selective Laser Sintering (SLS) technology, the material used is Polyamide (PA2200) (Datasheet page 149) some test are performed for the evaluation of the mechanical properties of this material and investigate the differences in relation of the Printing orientation and direction (results showed in next section)

This machine works with different type of Polyamide, can reach a thickness accuracy of 0.06 mm and the effective dimension of the printing base is 200 mm x 250 mm x 330 mm.

SLS is an additive manufacturing procedure that uses a laser as the power source to sinter powdered material, aiming the laser automatically at points in space defined by a 3D model, binding the material together to create a solid structure.

SLS is an AM technology that so far has mainly been used for rapid prototyping and for low-volume production of component parts. SLS involves the use of a high-power laser to fuse small particles of plastic or other materials powders into a mass that has a desired three-dimensional shape. The laser fuses powdered material by scanning cross-sections

generated from a 3D digital model. After each cross-section is scanned, the powder bed is lowered by one-layer thickness, a new layer of material is applied on top, and the process is repeated until the part is completed.

Figure 4.3- Top view of IHHS2 3D polyamide printed parts with FORMIGA P110

This printing technology guarantees a bulks structure geometry of the printed object, this choice is made avoiding the possible leakage of the liquid inside the skull through the plastic itself, problem that showed up with the first prototype.

Figure 4.4 - Side view of IHHS2 3D polyamide printed parts with FORMIGA P110

The Weight of this Skull is 867 grams.

1.10.2 Brain

The Size of the Brain was rescaled of 10% with respect to the first prototype.

The geometry is the same with the same separation between the lobes and the cerebellum giving the possibilities of evaluating and collect the linear and rotational acceleration for every part.

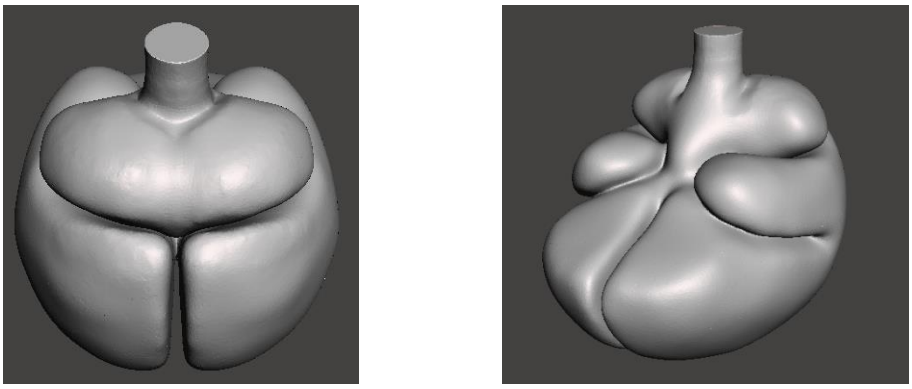

Figure 4.5 - 3D Model of the size reduced Brain of IHHS 2.0

The decision for the second prototype is to choose a softer rubber and define the correct parameter that fit with the mechanical behaviour of the brain.

The Moulding of the brain has been started with the use of the softest rubber available and already in stock Plastigel 00-20.

Brain Sensors

Accelerometers are positioned as far as possible from the centre of gravity of the brain mostly to get a grasp of the macroscopic movements of the brain.

Since the geometries were completely known from the simplification phase, it was possible to locate the sensors with great precision. One choice is to set the gyroscopes and one accelerometer in the centre of gravity of the brain. This point was exactly defined by a specific tool in Meshmixer (*Analysis* - *Stability*).

The chosen accelerometers are the ADXL377 3-Axis accelerometer, manufactured by Analog Devices Inc (data sheet page 147).

Two accelerometers (ML and MR) were put on the side of the CG guaranteeing 15 mm of rubber protection; two accelerometers (TL and TR) were positioned on the same coronal plane of CG, 10 mm from the rubber surface; finally, two accelerometers (CL, and CR) were put roughly on the barycentric line of the cerebellum to track its motion separately from the rest of the brain; each sensor is positioned with a 15mm of guaranteed rubber protection.

Differently from the Previous surrogate, only two accelerometers instead of 3 are put into the cerebellum, this because as observed in the first impact test, the data collected by the MidCerebellum accelerometer don't give any more information that the later ones.
Instead of this Accelerometers, has been decides to collocate one gyroscope in the Middle of the cerebellum, with the aim of observe the relative rotation and eventually the differences of angular velocity relative to the brain sensors, the gyroscope embedded in this position is a single biaxial sensor from which are going to be evaluated only the signal around x and y axes. Another gyroscope is still positioned in the brain COM. The gyroscopes LPY4150AL and LPR4150AL manufactured by STMicroelectronics are used for the dummy brain instrumentation.

Accelerometers

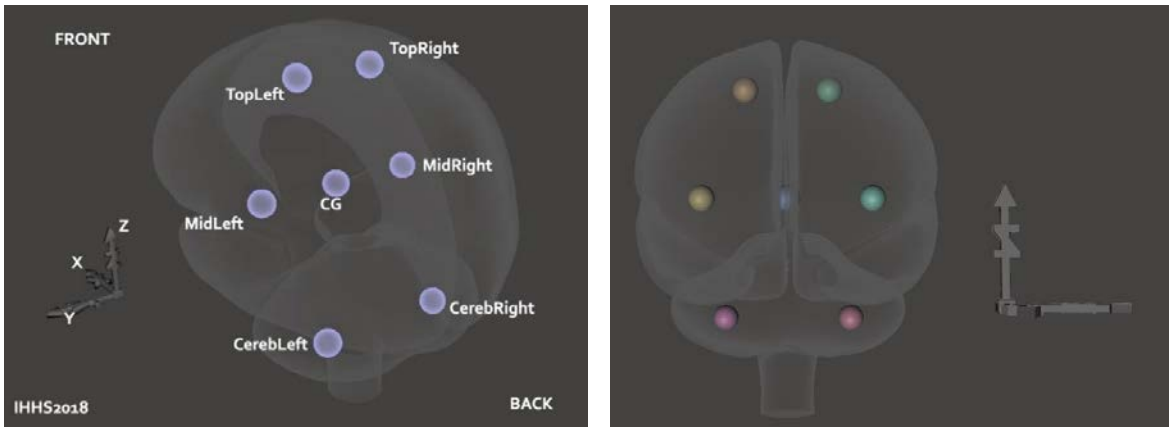

Figure 4.6 - Position of brain accelerometers IHHS2

Table 10-Coordinates of the Accelerometers with respect to the Centre of Gravity

Accelerometers	X [mm]	y[mm]	z[mm]
CG	0	0	0
MidRight	0	−37	0
MidLeft	0	+37	0

TopRight	0	+20	42
TopLeft	0	−20	42
CerebRight	−26	−32	−45
CerebLeft	−26	+32	−45

Gyroscopes

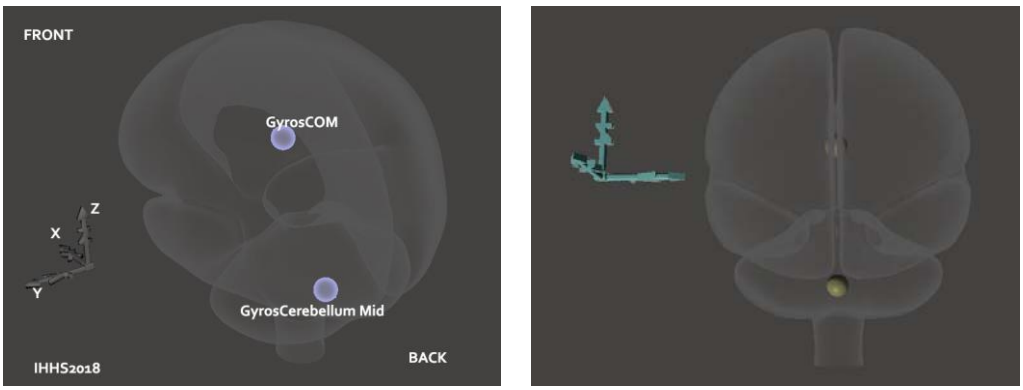

Figure 4.7 -Position of brain gyroscopes of IHHS2

Table 11 - Coordinates of the Gyroscopes with respect to the Centre of Gravity

Gyroscopes	X [mm]	Y [mm]	Z [mm]
Gyros CG	0	0	0
Gyros midCerebellum	−26	0	−45

Brain Molding and Sensors Placements

The process of brain moulding is divided in more step, allowing to define different layer and the positioning of every sensors in the correct position, already decided and defined by technical and research reason.

Figure 4.8 - 3D printed mould designed for Brain casting and sensors positioning of IHHS 2.0

The moulding of the brain is operated Layer by layer with a 3D printed Mould, during every step the accelerometers and gyroscope are positioned and moulded inside the rubber. The lower part is ended with a threaded bolt, that would be connected to the lower base and is supposed to work as the brain stem.

TOP LAYER

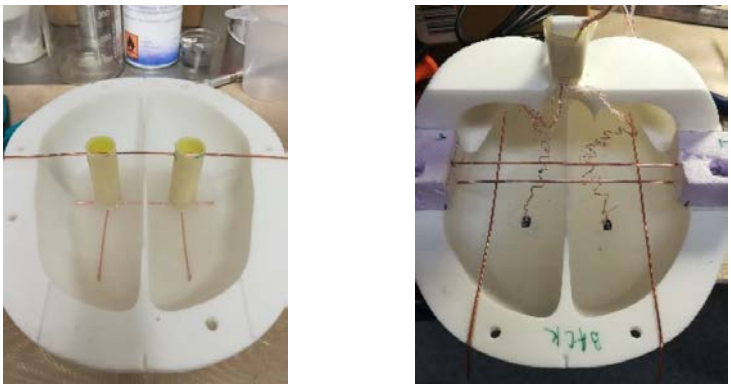

Figure 4.9 – Brain casting procedure: a) Top Part of the brain with cylinders for sensors spots localization b) Embedding of sensors in the correspondent position in the top layer

The first Layer is prepared, with the help of some copper wires is defined the position of sensors, using 2 cylinders is possible to obtain the flat surface on which the sensors will be positioned.

The first layer has been prepared and after the gluing it would be possible to connect the sensors.

After the deposition of the first layer of rubber and let everything curing overnight the first two accelerometers are positioned and glued on the flat surface. This two first accelerometers are in the upper part of the brain and will show the data relative to the up part of the brain lobes.

The Sensors are glued with normal glue, just to keep them in position and recognize the orientation in the three reference axes. The wires connected with the sensors are bended because of during the curing of the rubber the shrinkage of it could create some stress and distortion near the connectors and break the connection.

MID LAYER

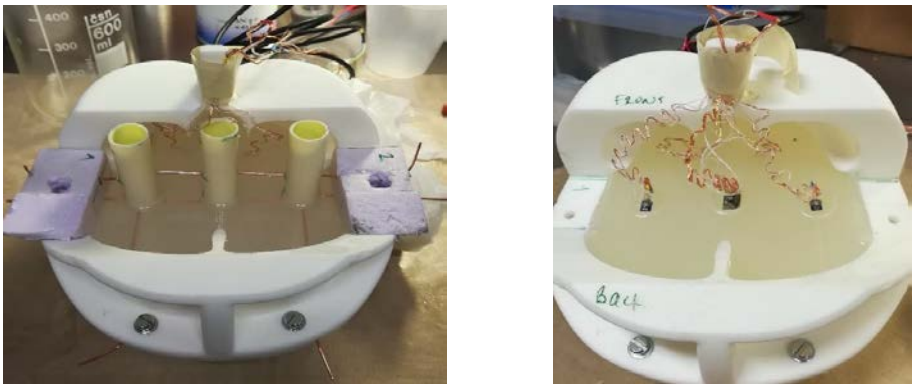

Figure 4.10 - Brain casting procedure: a) Mid layer of the brain with cylinders for sensors spots localization b) Embedding of sensors in the correspondent position in the middle layer

After the position of the sensors, the following layer has been prepared and the localization of the position for the sensors in the middle plan: 3 accelerometers and 1 gyroscope in the COM and After the wait for the curing of the rubber the following sensors are positioned in the midplane. Two accelerometers on the sides and one accelerometer and gyrometer in the correspondent point of the COM.

CEREBELLUM

Figure 4.11- Brain casting procedure: a) Cerebellum casting with cylinders for sensors spots localization b) Embedding of sensors in the correspondent position of cerebellum

The following step is Molding of the lowest part of cerebellum and preparation for the positioning of the accelerometers and gyroscopes.

Two accelerometers on the sides and one gyroscope in the centre is glued and the covered with silicon Rubber.

BRAIN STEM

The last step is the position and inclusion of the brain stem, substituted with a threaded bolt, that will connect with the base of the skull and is aim to sustain the brain from the bottom and avoid unreal movement and rotation, From anatomical point of view the connection with the skull is recreated but this is not correct from a biomechanics point of view, but despite this the brain behaviour is the centre of the study this structure could be neglected,

The M6 Bolt has been positioned and the rubber of the upper part of the brain has been casted.

The bolt and the wires were prepared to stay in the right position and go out of the skull from the back part.

After the curing of the silicon rubber the brain has been demoulded and some holes are fixed and filled with other rubber.

Figure 4.12 - Brain casting procedure: a) The threaded stem is put in the rubber and cured together with the lower part b) Closure of the brain mould and curing time

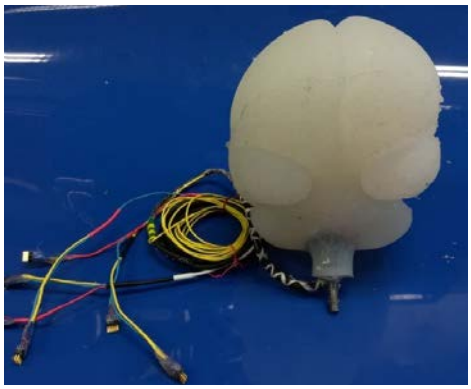

Figure 4.13 - Brain casting procedure: Brain demoulding and particular of the complete rubber component with the connection wires

The weight of the Brain in Silicon Rubber is 1075 grams

Dura Mater

The first idea was to model the 3D shape of the Dura Mater ad then unwrap it into a 2D surface for having the possibility to print it or cut it over a fabric or a thin sheet of desired Material.

Frome the 3D Model of the Brain it has been possible to obtain the easiest mesh and a very simple shape of the brain, this just for obtain the first overview about the dimension a characteristic of the Layer around the brain. After a discussion with the stakeholders has been decided to put only a very thin layer of Silicon Glue as a substitution of the Dura Mater connection directly on the skull.

The Silicon Glue that is used is Contractive Adhesive S9 Super, it will be spread around the internal part of the Skull with the aim to reproduce the Dura Mater thin Layer and properties.

This Material is very strong and very good for the coupling with other polymeric material. No other layer will be put inside the head because is not possible to obtain the proper thickness and every other option is difficult to guarantee the real stability and keep the position inside the brain.

Figure 4.14 - Dura Mater substitute in IHHS 2.0; thin layer of silicon glue is spread over the inner surface a) bottom skull part b) top skull part

The Silicon Glue Layer will reproduce the anatomical correspondence of the Dura Sticking directly on the Skull. The problem is that is not possible to obtain a very uniform layer of material because of the extremely high viscosity of it.

1.10.3 Subarachnoid Space

The SAS (Sub Arachnoid Space) is composed by thicker material that allows the flooding of the CSF around the brain, in our model this part is substituted with a NONWOVEN fabric, the Same already used in the first dummy head, but in this case, it will be arrange only in some spot in contact with the brain and below the Dura Mater.

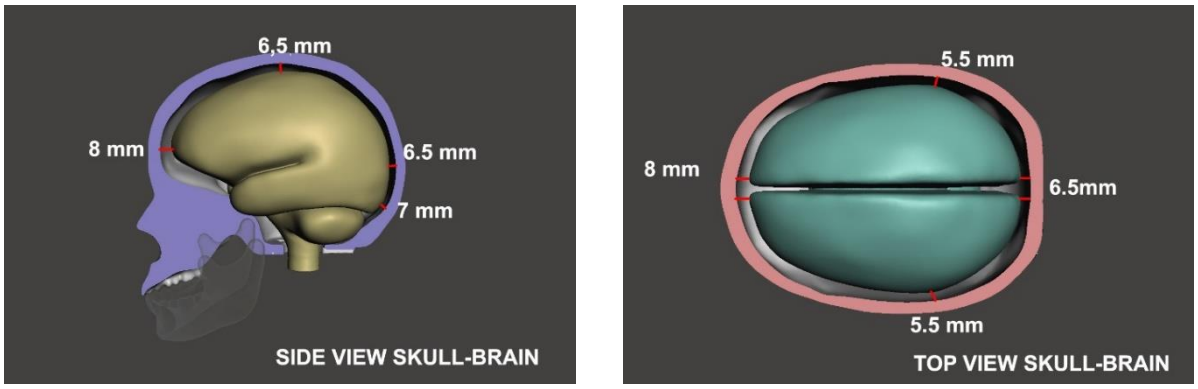

Figure 4.15 – Subarachnoid space with representation of intercranial distance between skull walls and brain surface:

The aim of this layer is to create a protection from the impact and damp the effect of an impact on the brain. The choice of Positioning the NW only in some spots is related with the necessity to model it from a mathematical point of view and analyse the physical model also in a FEM software.

Based on the anatomy of the human brain, in our 3D head model, the thickness of the SAS was assumed to be 3mmall around the brain[71], [72].

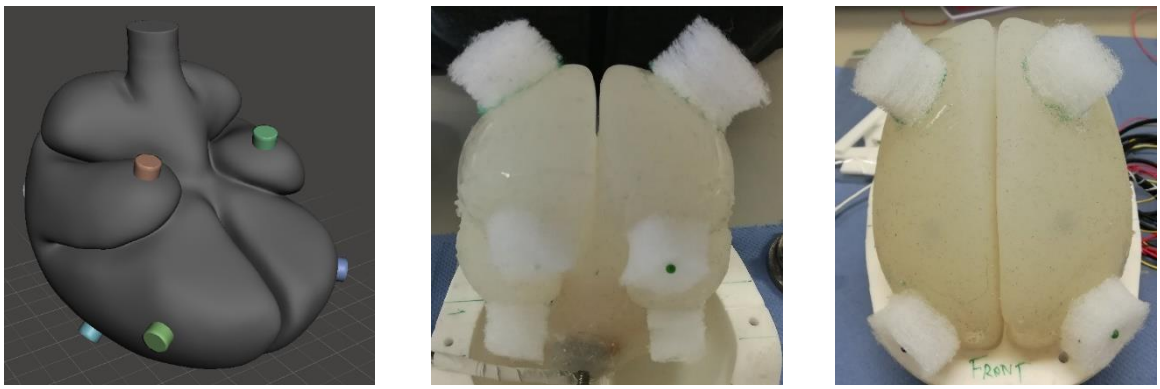

Figure 4.16 - Subarachnoid space substitute for IHHS 2.0 and position around the brain a)3Dmodel b) Nonwoven localization front view c) Nonwoven localization Top view

It's important to define and have a knowledge of the right thickness of this layer.

The hollow part of the Arachnoid is called Arachnoid trabeculae, and it's the part where the CSF flows completely

1.10.4 Cerebral Spinal Fluid

The fluid chosen to simulate CSF must display the lowest possible friction. In addition to this it was important to select a liquid that would have not reacted with the silicone-rubber

or the electronics, for the sake of the durability of the model, it is not possible to use simply water because of the presence of the wires inside the skull, and so for avoid any interaction between the electric contact has been choosing to use a liquid that doesn't give problem from this point of view.

The chosen fluid for the first prototype was the low-viscosity silicone oil SilOil M4.165/220.10, commercialized by Huber.

As a substitute of the CSF has been used a synthetic motor oil Q8 Formula Ultra V 0W-20, the viscosity of this liquid is displayed in the following chart. The characteristics of this oil are far away from the ones of the real CSF, but no other synthetic oil has been found with similar properties and every type of Silicon oil has been avoided for the negative interaction with silicone rubber (page 42).

Table 12 - Cerebral spinal fluid and substitute fluids properties comparison

Name	*Type*	*Density [g/(cm^3))*	*Dynamic Viscosity [mPa]*	*Kinematic Viscosity [cSt]*	*Temperature*
Cerebral Spinal Fluid		*1.0006-1.008*	*0.65-0.88 (0.7-1 37°)*	*0.69582505*	*36°*
Silicone Oil (1st Prototype)	*Silicon Oil*			*10*	*40°*
Q8 Formula Ultra V 0W-20		*0.845*	*41.1515*	*48.7*	*40°*

1.10.5 Pressure Sensors Position

After the observation of the precedent position of the pressure sensors in the first head has been decided to change the position of the sensors in the skull. The reason is for analyse different data and try to collect the pression value in more interesting point. The chosen pressure sensors are more reliable and certified for the use into oil for brake pressure evaluation and they should guarantee any problem with the interaction of synthetic oil. The sensors used for the second prototype are MS5401-AM Miniature SMD Pressure Sensor Surface mount, with a full-scale range of 1 bar; the type of sensors was changed and selected a smaller type and more reliable for the interaction with oil and synthetic fluid.

The small dimension moreover allows to put the pressure sensors inside the skull, without the need to drill the skull from the outside and reducing the leaking probability.
The diameter of the sensors is around 6mm, so with a flat drill bit is possible to obtain the surface for the positioning of sensors.
Before gluing the pressure sensors in the skull, they have been calibrated.
The sensors were calibrated by customized calibration system, the pression sensor was embedded in a thigh glass bottle and then connected with the voltmeter. The calibration procedure requires to register the volts value during a gradual increasing of the inner pressure of the bottle using a pump. The pressure sensors have a linear response then the regressions lines are found for each sensor. The slope value of the regression line represents the coefficient necessary to calibrate the sensors and convert the volts value read on the instrument into a pressure value to collect.

Table 13- Pressure sensors calibration chart: the values obtained from the experiments are used on MATLAB software for correlation between voltage and pressure

Pressure mmHg	0	20	40	60	80	100	120	140	160		
Pressure Pa	0	2666.44	5332.88	7999.32	10665.76	13332.2	15998.64	18665.08	21331.52	V/mmHg	Correlation Coefficient
LTT	-0.013	0.6	1.4	2.3	3.2	3.9	4.8	5.9	6.2	0.04096	0.994687
RTT	-0.119	0.5	1.25	2.1	2.9	3.7	4.5	5.9	6.2	0.041313	0.992529
RBT	-0.148	0.5	1.3	2.2	3	3.8	4.8	5.8	6.2	0.041577	0.996214
RMT	-0.129	0.45	1.3	2.15	3	3.9	4.7	5.5	6.3	0.04118	0.999698
LMT	-0.086	0.42	1.3	2.1	3	3.9	4.6	5.5	6.4	0.04132	0.999529
LBT	-0.169	0.3	1.2	1.9	2.9	3.6	4.52	5.3	6	0.040013	0.998795
RMM	-0.129	0.4	1.3	2.15	3	3.9	4.9	5.6	6.4	0.042222	0.999034
LM	-0.162	0.4	1.3	2.1	2.9	3.7	4.6	5.52	6.3	0.041173	0.999549
RM	-0.143	0.3	1.3	2.05	2.85	3.6	4.45	5.3	6.2	0.040185	0.999049
LMM	-0.202	0.3	1.3	2	2.9	3.7	4.5	5.5	6.3	0.041423	0.999053

Some trials were made on the skull to have the wire tight attached to the skull and don't have any flying wire, the Position and the total number of Sensors in the IHHS 2.0 is the same, with 8 of them in the midplane and two of them in apex above each lobe.

The midplane position of the Pressure sensor is at the same high of the Centre of Mass of the brain.

This position has been chosen for evaluate the pressure all around the centre of mass plane of the brain and see the differences in the pressure between the skull and the inner organs.

10 Sensors are going to be used.

2 Sensors are in the frontal lobe, instead of only one two are put in front of each lobe.

The same has been done in the back part and on the top, all of them are on the same plane of the COM of brain. It's more interesting in the evaluation of the different distribution of pression observing the difference between the two lobes. Other two sensors are position on the two side, on the same plane of the COM of the brain.

The first series showed up functionality problems and because of their dimension they gave problem in relation of the necessity of drill holes in the skull for their positioning.

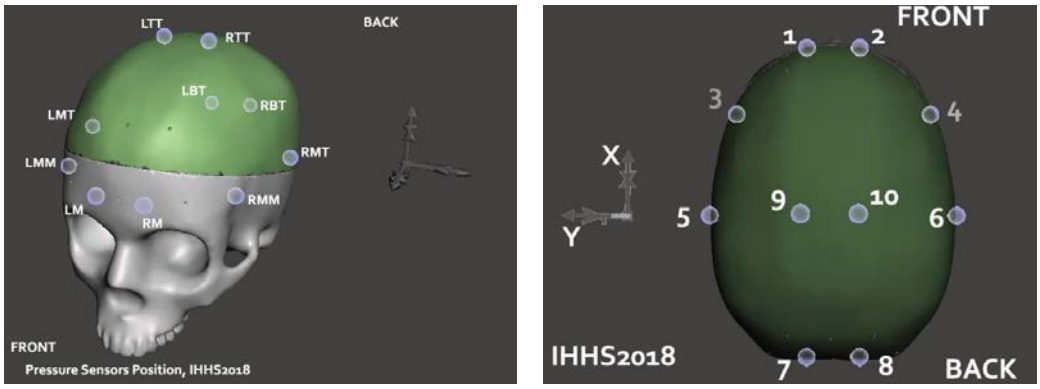

Figure 4.17 - Pressure sensors position in IHHS2

Table 14- Coordinates of pressure sensors in IHHS2 with respect to the brain centre of mass

Pressure Sensors			X [mm]	Y[mm]	Z[mm]
CG			0	0	0
RM	1	Frontal Left	95	+15	0
LM	2	Frontal Right	95	-15	0
RMM	3	Sphenoid Left	57.5	+55	-4.5
LMM	4	Sphenoid Right	57.5	-55	-4.5
RMT	5	Temporal Left	0	+70	0

LMT	6	Temporal Right	0	-70	0
RBT	7	Occipital Left	-80	+15	0
LBT	8	Occipital Right	-80	-15	0
RTT	9	Parietal Left	0	+15	68.5
LTT	10	Parietal Right	0	-15	68.5

Following the preparation of the inner surface of the skull the location of the pressure sensors was prepared milling the correspondent point previously designed.

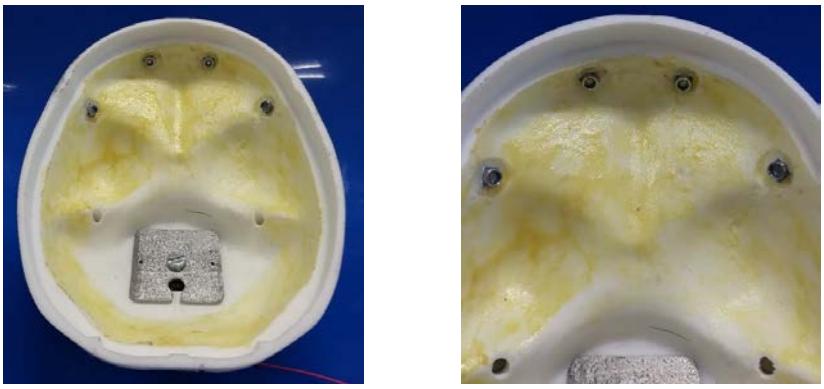

Figure 4.18 - Pressure sensors location in the lower part of the skull on IHHS2

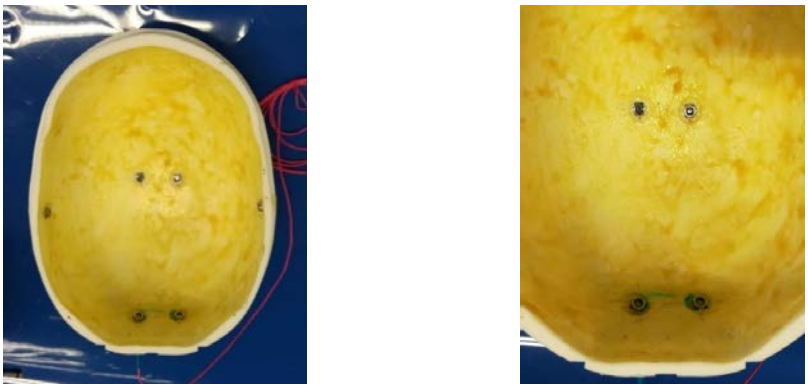

Figure 4.19 - Pressure sensors location in the top part of the skull on IHHS2

1.10.6 Head closure

Skull sealing

The last step in the assembly of the dummy skull is the closing and sealing of the two parts of the cranium. The low and top part are connected and glued using Casco Rubber Fix, a rubber glue compatible with the polymeric material used in the project and chose for its waterproof and chemical resistance.

Figure 4.20 - The connection between the upper part and the lower part of the skull are connected using the silicon Rubber glue

Skull Filling

After the coupling of the two skull parts the cranium is filled with the CSF substitute. The selected oil is inserted from the bottom trying to remove all the air in the volume.

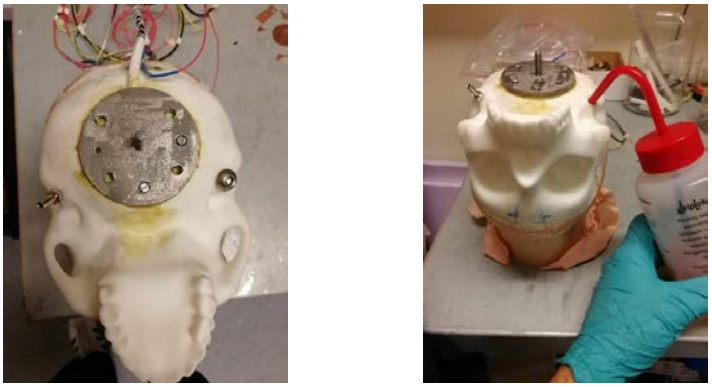

Figure 4.21 - The Skull is filled with CSF substitute using the prepared holes in the base; two holes are necessary to avoid air bubble and a proper filling

1.10.7 Skin

The Skin as all the rest of the dummy head model, has been scaled to the 90 percent of the original one to reducing the total dimension of the head and achieve a more realistic size of the surrogate.

The optimization of the STL file was made using the MeshMixer Software and Materialise Magic (Materialise Magics, Technologielaan 15, 3001 Leuven Belgium) an

advanced software for data preparation and STL editor for 3D Printing and Additive Manufacturing machine.

Is a professional software that allows to go through every step of the file preparation and AM process; from the import of the Solid Part File to problem correction and STL preparation.

The reproduction of the skin requires the use of a specific mould the could allow the preparation of a "mask" which has been wrapped around the skull and would reproduce the skin anatomy and physical and mechanical behaviour.

It's important from the anatomical point of view to add also the skin layer to the Surrogate head because the presence of this layer helps the distribution of the impact energy and it's a first dumper. The male and female part of the mould for the skin molding has been modelled and scaled for obtaining the best fitting around the new skull; every part has been 3D printed in different round and secondly assembled obtaining the result.

The material used for the mould is ABS plus-P430 and the printer is the uPrint SE Plus.

The Skill has been moulded with a softer rubber respect the one used in the first surrogate.

The Skin mould is formed from 3 main part:

- 2 Female parts that represent the frontal and back part of the human face
- 1 Male part representative of the Head itself and necessary to leave the hollow part inside the skin volume.

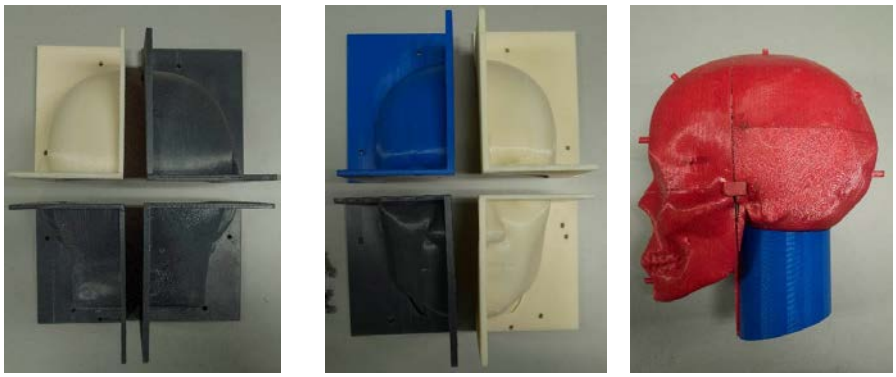

Figure 4.22 - ABS 3D printed Skin Mould used for the casting of the external part of IHHS2 a)BackFemale part of the skin mould b)Front Female part of the skin mould c) Male Part of the skin mould

The Rubber used for the second reproduction is the Plastsigel 01-30 (Datasheet page 148) the mechanical characteristics of the rubber are investigated with compression test performed with the Instron Machine (Test page 128)

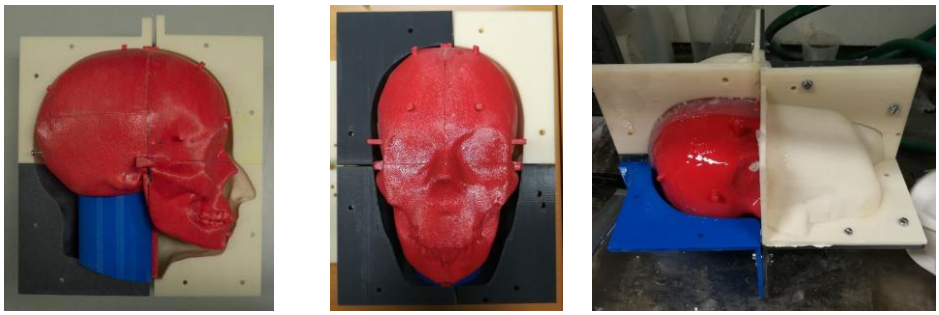

Figure 4.23 - Casting procedure for skin preparation; every part is casted step by step starting from the back part of the skin

The Rubber 01-30 has been used for the molding of the skin, the skin was prepared in different step, for being sure to avoid air bubble and gap.

Figure 4.24 - Silicon Rubber Skin Demoulding and final appearance

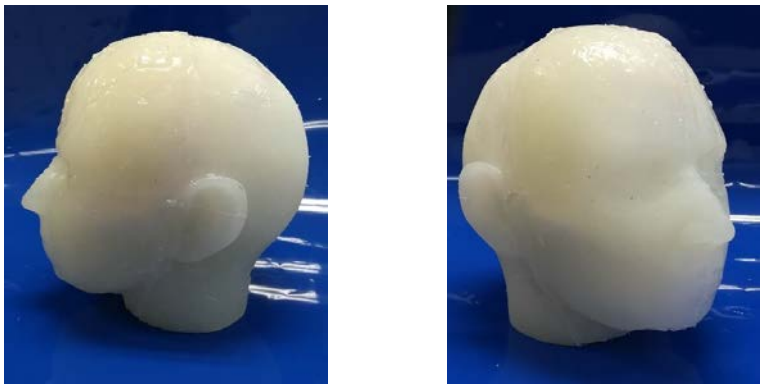

Figure 4.25 - IHHS2 Silicon Rubber Skin; the external surface is cleaned and fixed for the presence of imperfection

The surface of the mould was mirrored with a release agent to facilitate the demoulding of the rubber after the proper curing time.

The weight of the Rubber reproducing the Skin is 1727 grams, the weight is quite high also because it reproduces some others part as fat and facial muscle.

1.10.8 Neck-Head Connection

The Dummy head is supposed to be used for impact tests and the use of a dummy neck and a proper connection between the part is required.

Head - Neck connection adaptors

The resizing of the skull and the different geometry of the Dummy Head requires the modelling of a different connection between the skull base and the Hybrid Neck.

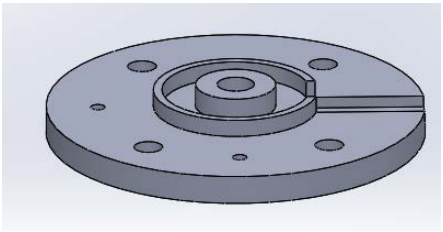

Figure 4.26 - Lower external part of the neck- skull connection parts

The CAD Model of the connection Joint between head and neck has already been used for the first prototype and a new version is modelled using the Modelling Software Solidworks (Dassault Systèmes SolidWorks Corporation 175 Wyman Street Waltham, MA, USA). A different connection in the skull side has been thought with the aim of fix the leaking problem and not allows the fluid to go out from the skull.

The stem used for the stability of the brain will be threaded in the base part in the extern of the brain, this method will avoid the necessity of holes in the lower joint and for the same reason the cable will be lead out from the back of the skull and not from the bottom as in the first dummy head.

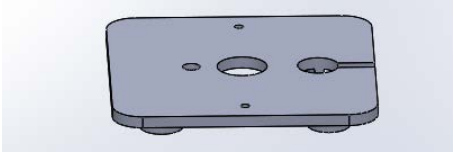

Figure 4.27 - Lower inner part of the neck- skull connection parts

The CAD model has been designed and fixed for obtaining the best result. This Part is inside the Skull and is the internal plate that must allow the passage of the Brain stem trough the skull and the cable coming from the brain accelerometers and gyroscopes

This is the lower plate of connection between the inner plate and the Joint Neck-Head Connection, the central hole is threaded for the screwing of the brain stem and is working as a connection and sustain of the brain with the neck.

And two small 3mm Holes for the positioning of a small centring screw. For avoiding any leakage of CSF through this connection plates, they have glued with skull with a silicon glue, that is very strong and guarantees a good tightness of the head neck system.

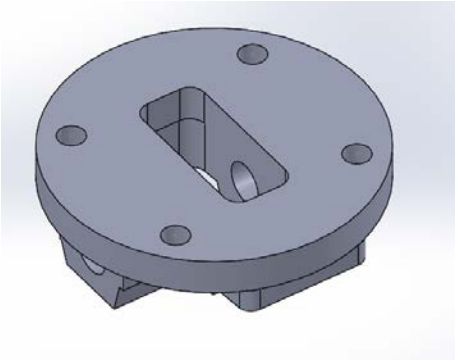

Figure 4.28 - Customized Skull-Neck Adaptor for the connection of the head with the standard dummy Neck; Top View

The adaptor is designed following the standards dimension for the coupling with the Hybrid Neck.

The CAD file is modified obtaining the proper characteristic and dimensions. The Joint is increased in the thickness of the upper plate and in the middle part the material has been removed for allowing some more space for the brain stem coming out from the upper threaded plate (fig

It is connected and fixed to the neck with a block pin.

All this part after the preparation are printed out of Titanium, Ti6Al4V (datasheet page 155) using Arcam EBM Q10plus (Arcam AB, Mölndal, Sweden).

The most advance type of 3D printer is the EBM machine, a specific printer that can work with specific type of metal.

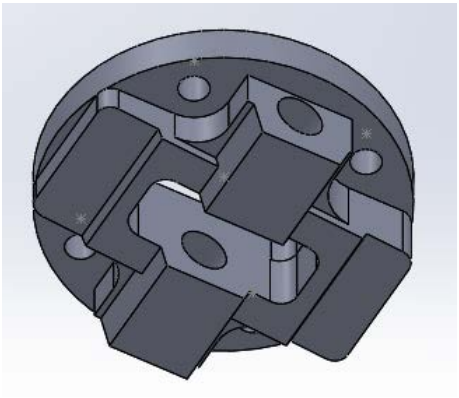

Figure 4.29 - Customized Skull-Neck Adaptor for the connection of the head with the standard dummy Neck; Bottom View

Electron-beam additive manufacturing, or electron-beam melting (EBM) is a type of additive manufacturing, or 3D printing, for metal parts. The raw material, usually metal powder, is placed under a vacuum and fused together from heating by an electron beam.

Parts are manufactured by melting metal powder, consolidated into a solid mass layer by layer using an electron beam as the heat source. The volume of the chamber where is possible to print is 200x200x180 mm (W x D x H), and this technology allows to achieve a layer Thickness of 0,05 mm.

This procedure allows to obtain the final parts fastly and being sure that the mechanical properties are extremely high.

Figure 4.30 - Customized Neck Adaptor parts printed with EBM machine. Left) Skull-Neck Adaptor; centre) External part; right) inner part

Finally, the Metal part are glued to the base of the skull with Silicon glued, this type of connection helps to avoid leakage and non-necessary holes for bolt connection.

Dummy Neck

The dummy neck is purchased from Jasti (JASTI CO., LTD Miyoshi, Koto-ku, Tokyo, Japan), it is part of the Human Dummy Hybrid III 50th-percentile male.

JASTI manufactures Hybrid-50th dummy in according to US Standard of NHTSA (National Highway Traffic Administration) and is calibrated following the same standards.

The neck for ATD consists of aluminium disk plate moulded with rubber and wire cable.

The neck behaviour is controlled and regulated at some extent by tight/loosen the cable torque.

Figure 4.31 Neck Assembly Hybrid III 50th-percentile

1.11 Test Method

After the closure of skull, the dummy head is ready for the mounting on the neck and its position on the platform.

The set up followed for the test is the same already described in the chapter about IHH1(page 53).

During this work only, some preliminary trial tests are performed, aim to check the correct functionality of every sensor, the deeper research and complete test evaluation is finished from another Master student.

Head Preparation

The skull is connected to the dummy Neck with the titanium customized adaptor.

On the skull are glued and connected two more sensors, the purpose is to collect data related with the movement of the skull as a rigid body.

One external accelerometer is connected in the outer part of the skull in the correspondence of the frontal bone and on the same plane of the brain COM, to being able to compare the acceleration values.

Two biaxial gyroscopes are embedded in the apex of the skull to collect the rotation around the three main axes, this sensor is important to being able to compare the relative rotation of the brain with respect to the skull during impacts.

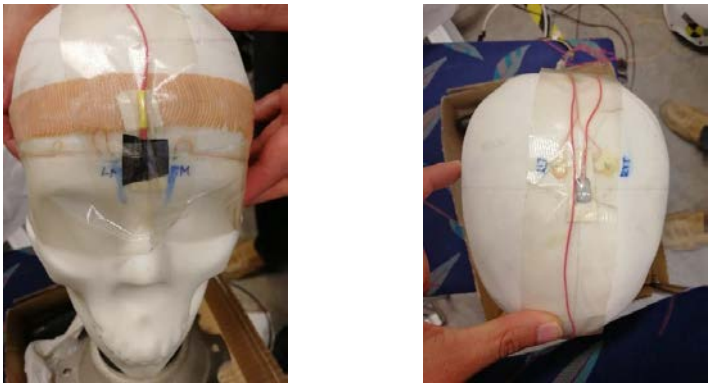

Figure 4.32 - IHHS2 Skull sensors; a) One accelerometer is embedded on the surrogate frontal bone b) one gyroscope is embedded on the skull apex

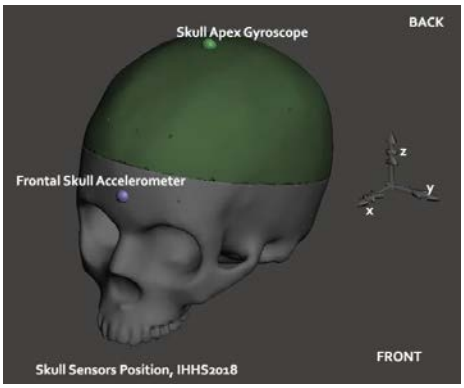

Figure 4.33- IHHS2 Skull sensors position 3D representation

Table 15- The position of the sensors with respect to the Brain Centre of gravity

Skull Sensors Position	X [mm]	Y[mm]	Z[mm]
Brain CG	0	0	0
Frontal Accelerometer	95	0	0
Apex Gyroscope	0	0	68.5

The cranium is carefully covered with the silicon skin and prepared on the platform with the fitting Helmet, the same model as the one used for the first dummy head but smaller in size (size L/XL), Sweet Protection Igniter MIPS Helmet.
One more accelerometer is applied externally on the apex of the Helmet, the helmet is the first layer receiving the impact energy then will show the higher values of acceleration and before every other part.

Figure 4.34 - Accelerometer applied externally on the apex of the Helmet.

The Impact Tests performed on the Instrumented Head Human Surrogate 2 follow the same protocol described and respected for the Head 1 Tests.
For the second dummy head the tests are performed at two different energy level, 16J and 24J.
The tests were completed from Edoardo Marzella during a corresponding research study.

Table 16 - Description and total number of tests performed on the IHHS2

Position	Impact
Name	Energy [J]
Back	16
	24
Back-Right	16
	24
Right	16

	24
Front-Right	16
	24

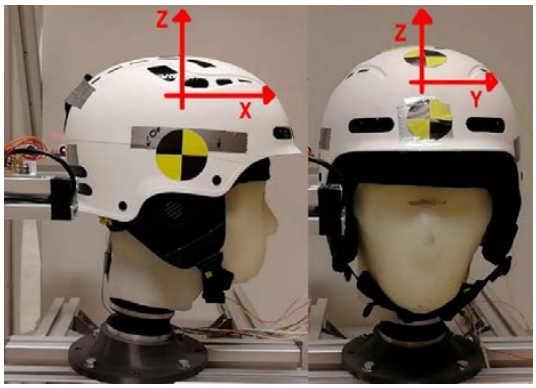

Figure 4.35 – Test orientation correspondent with the anatomical reference system

The following charts will display the value of the data collected from the sensors in every direction of motion and a short explanation will be written

The results of the test for the two different energy level have basically the same response and behaviour with a different magnitude.

In the following pages there will be described a 24J impact test on the four different orientation with an explanation.

The comparison between the energy level is displayed in the end of the chapter.

1.12 Back Impact on IHHS2, Energy 24J

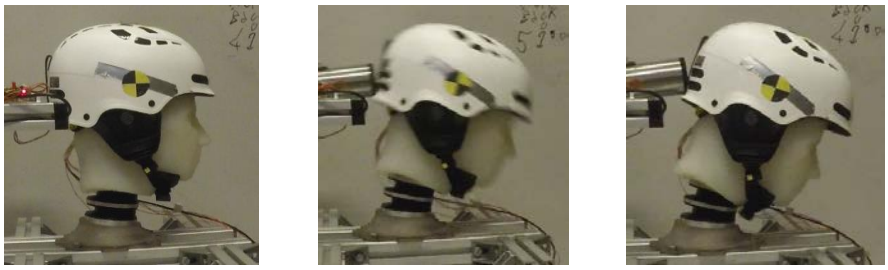

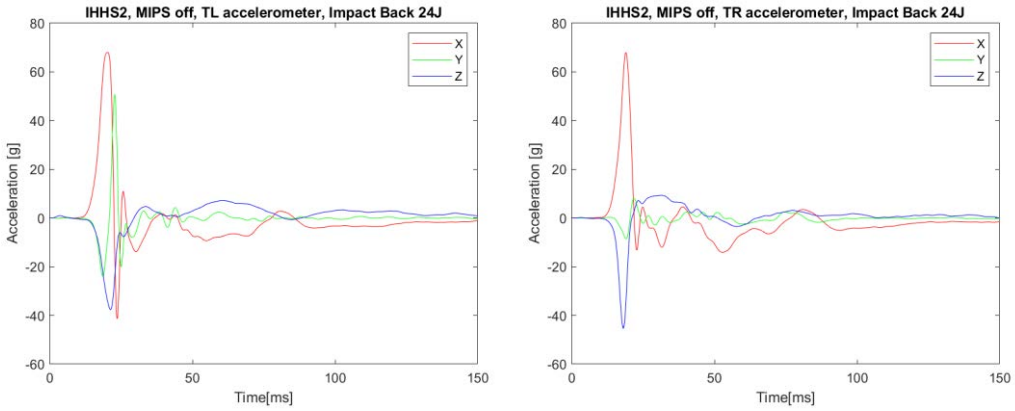

Figure 4.36 - Acceleration collected from sensors during a 24J Back Impact a) TopLeft b) TopRight

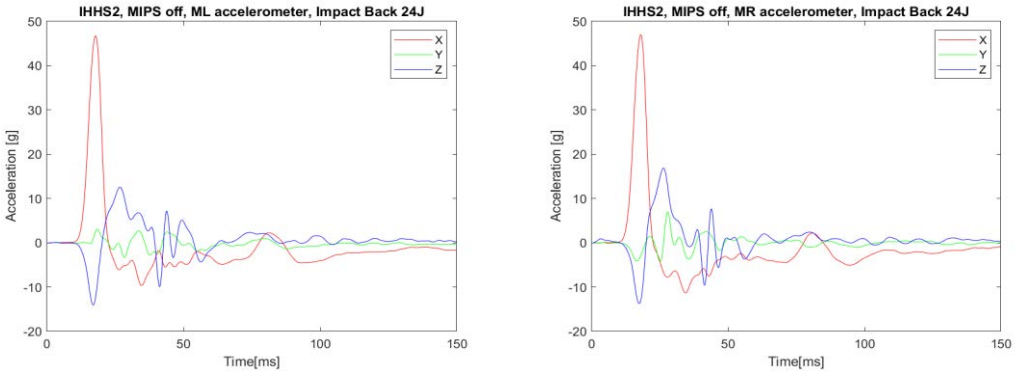

Figure 4.37 - Acceleration collected from sensors during a 24J Back Impact a) MidLeft b) MidRight

The previous plots show the responses of respectively TopLeft-TopRight (Figure 4.36) and MidLeft-MidRight (Figure 4.37) accelerometers in all the 3 axes directions. Since the impact is from the back the principal direction is along the X axe and this easy prediction corresponds to the results obtained in the charts.

The principal direction X is the same for each sensor, the sensors on the top layer TL and TR reach a higher value of acceleration around 65g and the two in the mid layer ML and MR have lower values around 45g. After the peak values that correspond to the hit moment of the dummy head, is possible to observe a big negative acceleration along the x direction probably due to the rebounding of the brain. Along the Z axe is possible to observe for each sensor a negative peak of acceleration, this behaviour is related with the movement of the head that after the impact moves to the ground rotating around the neck

joint; this movement pushes the sensors above and create the negative acceleration values. On the Top Left Sensor, a strange behaviour on the Y direction is evident, this conduct could be probably related with sensibility problems, but the global trend is still coherent.

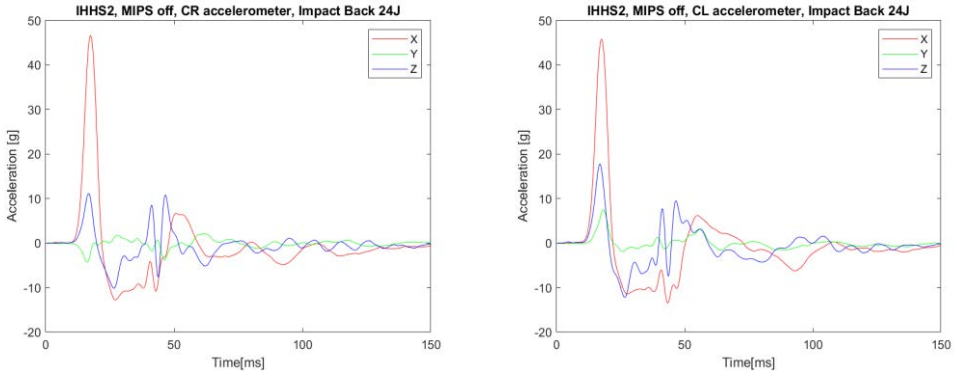

Figure 4.38 - Acceleration collected from sensors during a 24J Back Impact a)CerebellumLeft b)CerebellumRight

The plots related with CL and CR (Figure 4.38) are very similar to the previous ones, but for those two accelerometers is possible to notice that the Z acceleration is firstly in a positive direction, that confirm that it represents the rotation around the neck joint because those sensors are in a back position with respect to the rotational point and they tend to go up.

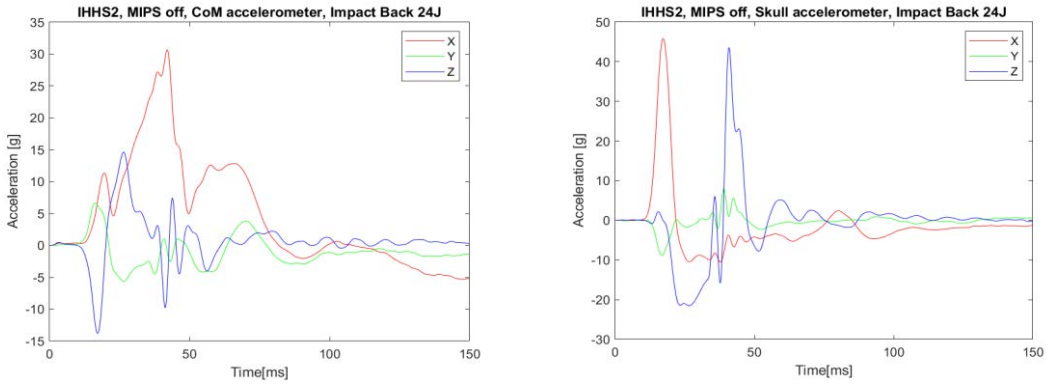

Figure 4.39 - Acceleration collected from sensors during a 24J Back Impact a) Brain Centre of mass b) Skull accelerometer

The accelerometer in the brain centre of mass display a behaviour like the one observed for the more external sensors, a small peak appears in the beginning of the test and then a bigger value is reached with a longer delay with respect the peak of the other sensors,

the delay this is probably related with the damping effect of rubber and oil into the skull. Is interesting to compare the value of the BCom accelerometer with the accelerometer coupled with the skull (Figure 4.39). The skull sensors display an early peak value along the X axe that is the principal direction, it happens before the brain peak value and as supposed it is correct because the first energy transmission is on the skull and then the damped impact arrives to the brain. The highest value is around 45g for the skull and around 30g for the brain, a remarkable reduction in energy transmission

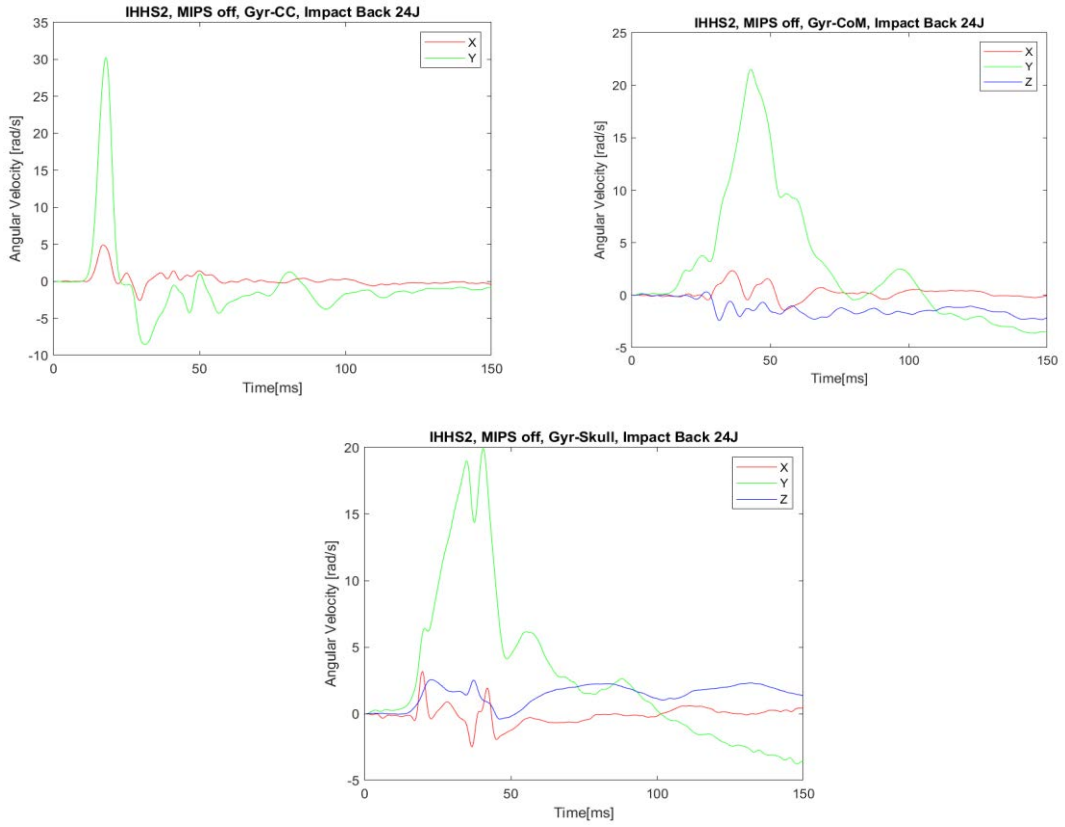

Figure 4.40 – Angular velocity collected from gyroscopes during a 24J Back Impact a) Cerebellum centre b) Brain Centre of mass c) Skull

The Three gyroscopes are embedded on the head and the global response is coincident (Figure 4.40).

The main rotation is the around Y axe and each sensor shows a single peak values of angular velocity that correspond to a pitch. The higher value of angular velocity is into

the CC sensor and is also early in time respect the other two, the cerebellum is free to move in the skull because is connected with the brain main portion only through a small fragment and basically it flows by itself, the oscillation is coherent with the main behaviour but it rotate more until 30 rad/s and then show an smaller counter rotation respect.

The angular velocity of the BCom is around 20 rad/sec as the skull but it returns in position without rebounding otherwise the skull shows a couple of counter movements. The behaviour of the Bcom is interesting and it could confirm that the liquid and the layer around the brain helps to keep it in position without dangerous counter movement and rebounding inside the skull.

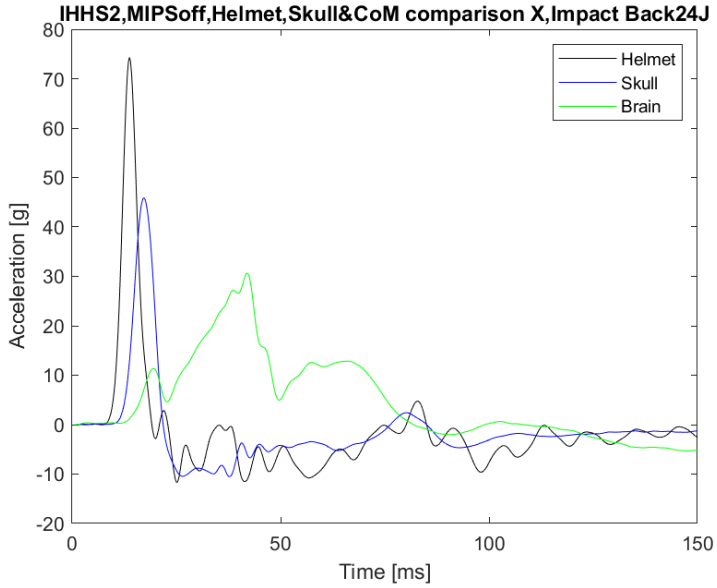

Figure 4.41 – Acceleration comparison between Helmet, Skull Brain; collected from sensors during a 24J Back Impact

In the previous image (Figure 4.41) it is possible to notice that the first peak to appear is the Helmet acceleration, the second peak from Skull and the last peak is from the brain more delayed in time. This temporal delay respect and confirm the impact timing and energy transmission; the helmet receives the highest energy and reaches a 70g acceleration then the movement is transmitted to the skull that has almost an halved value of acceleration of 40g and finally the brain that receive a softer hit, the acceleration of brain is 30g but displays a longer and less impulsive movement, the fluid and the inside layers work as damper from this point of view.

The same tests are performed with MIPS activated and not activated in the helmet, since the purpose of this technology is the reduction of rotational stress is necessary to make a comparison of the angular acceleration collected with the gyroscopes, obtained deriving the angular velocity recorded in CoM.

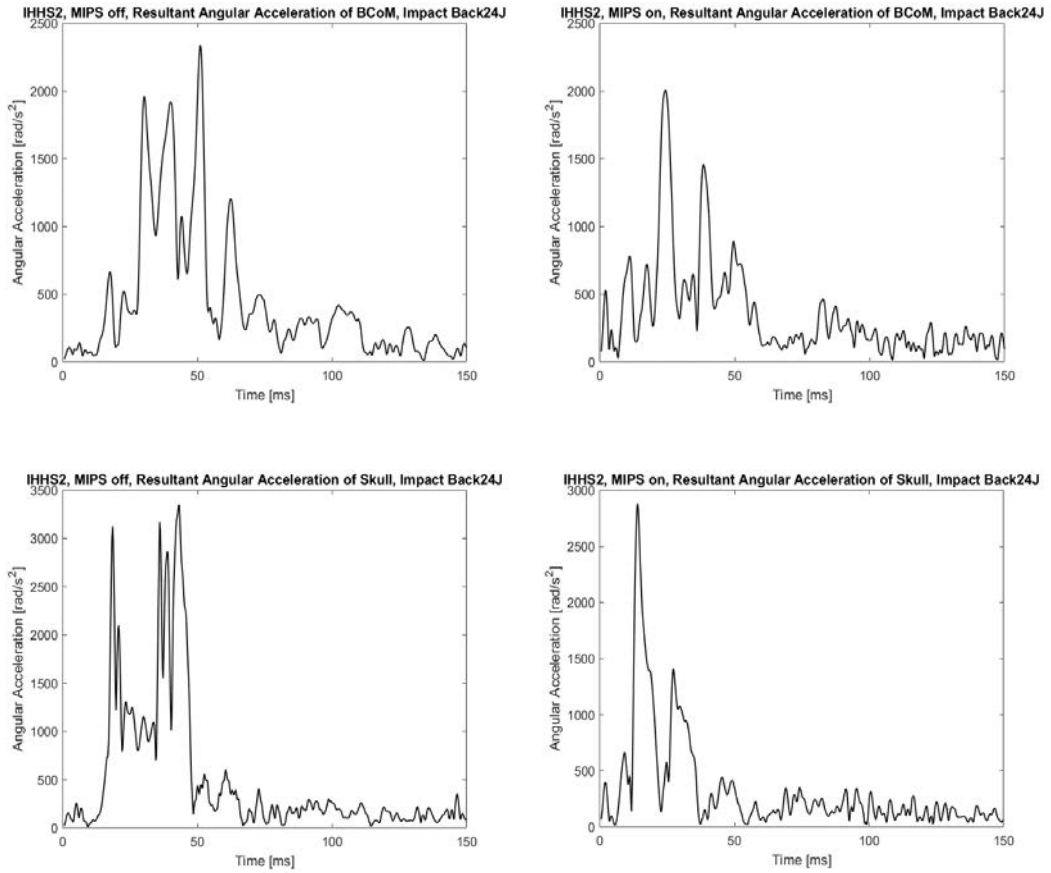

Figure 4.42 – Angular Acceleration resultant collected from sensors during a 24J Back Impact a)Brain Center of Mass angular acceleration MIPS off b) Brain Centre of Mass angular acceleration MIPS on c) Skull angular acceleration MIPS off d) Skull angular acceleration MIPS on

The previous pots show the angular acceleration collected during a Back impact performed with activated (Figure 4.42 b and d) and not activate (Figure 4.42 a and c) MIPS at the same energy level. The angular acceleration is higher on the skull around 3000 rad/s^2 and the value collected from the brain is 2000 rad/s^2 this reduction could be

related with the sliding reduction effect acted from the CSF on the rotational and external hits, the relative movement of the brain inside the skull helps to reduce rotational stress. The differences between the activated or not activated MIPS are however not so remarkable; the reason is related with the little rotational effect that the back impact apply to the head and since the MIPS works during tangential component for the reduction of rotational stress, these results are acceptable.

Pressure Sensors

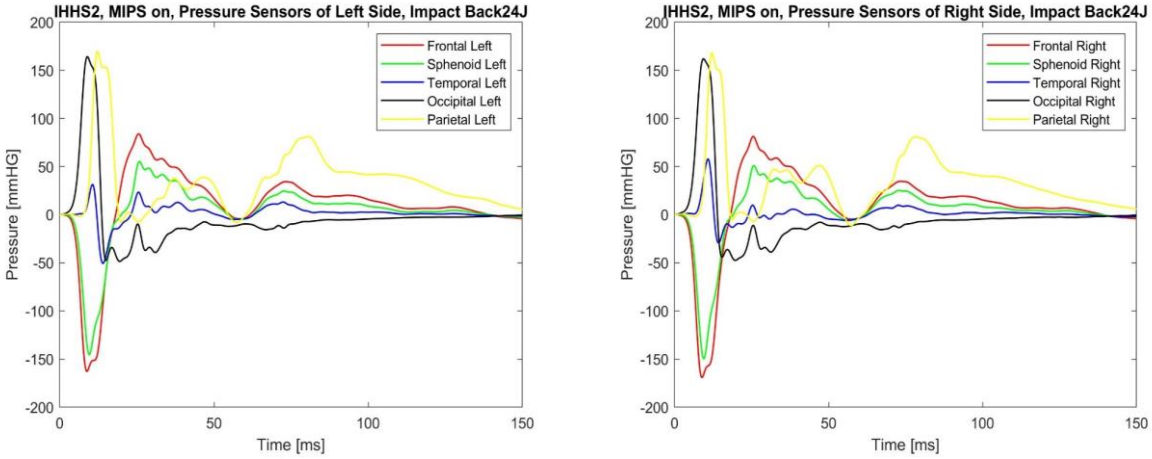

Figure 4.43 – Pression values collected from sensors during a 24J Back Impact a) Sensors on the Left Side of the skull b) Sensors on the right Side of the skull

IHHS2 has a distribution of pressure sensors located all around the brain, to comprehend the different activities of right and the left lobe during an impact two different plot are displayed. It's important to point out that the original not filtered signals collected during the test showed a saturation of the values for every signal bigger that 150 mmHg, so for each peak, was originally obtained a plateau region. This plateau region is not visible because of the 7th order low-pass filter at 200 Hz applied during the data analysis but the

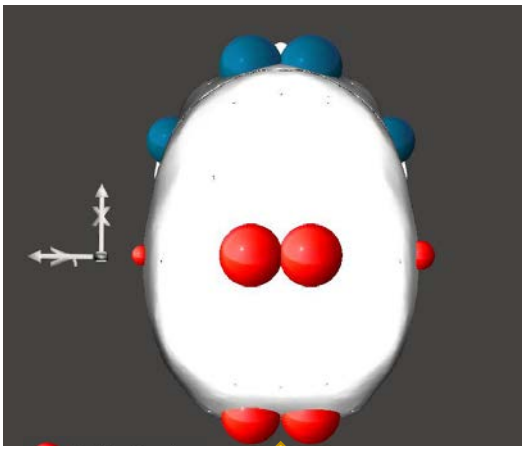

Figure 4.44 - Pression distribution representation around the skull; the diameter of the circle represents the scale, the colour represents the sign of the pression

represented values are not trustable as number but useful to describe the pressure overall timing and distribution. The signal saturates not because of the sensors, but because of the board used to record the signals.

The impact is hitting the head from the back and as first reaction is possible to observe a positive compression of the sensors located and the Occipital, Parietal and Temporal parts, the reaction is the same for both the lobe, since the impact is symmetrical. The Frontal and Temporal sensors display a depression. The compression is showed in the back and top area of the head(Figure 4.44), where the impact is located; the head moves in the positive X direction and since the brain is isolated inside the skull tents to follow the movement with a short delay, and the shortening of the distance between the skull and the brain creates a overpressure inside cerebral fluid. For the same reason on the opposite side the brain moves away from the frontal bones and generates a depression.

The positive pression on the parietal sensors, on the top of the skull could be caused from the rotation of the brain around the Y axis. After the first peaks of each sensors a positive increase in pressure is markable for everyone, maybe it could represent a global expansion in volume of the brain that increase the total inner pressure. The trend is not stable, and the overall state display compression and depression also after the main impact occurrence

The signal recorded by the pressure sensors can be used to understand the behaviour and movements of the brain, but no considerations on the value of the peaks can be done because the signals often saturate.

1.13 Back Right Impact 24J IHHS2

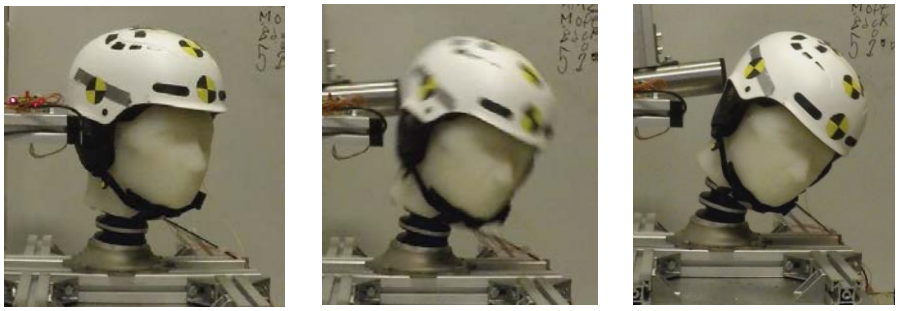

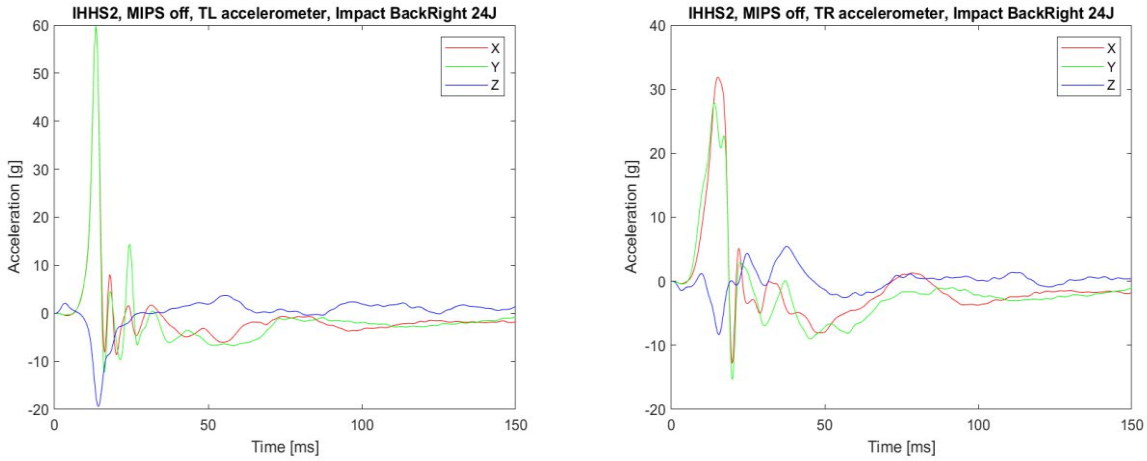

Figure 4.45 - Acceleration collected from sensors during a 24J Back Right Impact a) TopLeft b) TopRight

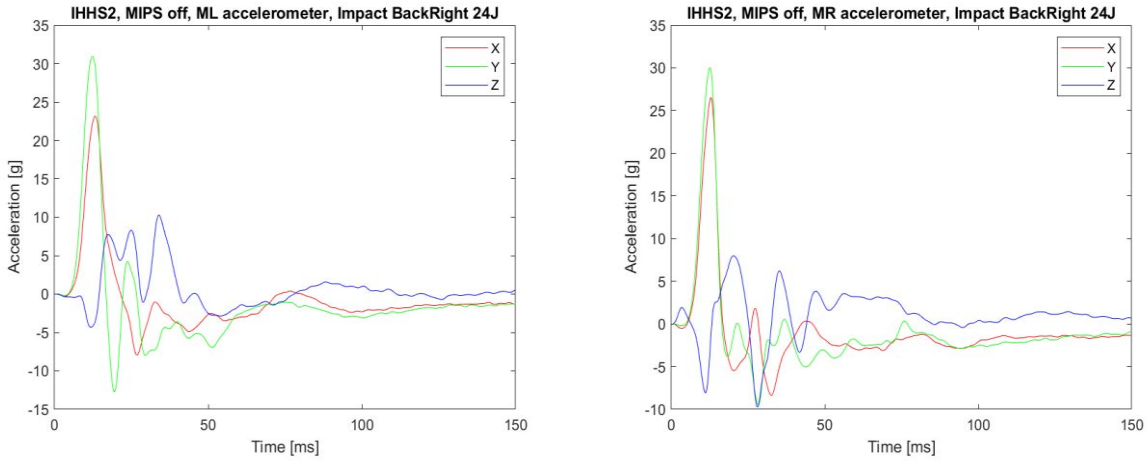

Figure 4.46 - Acceleration collected from sensors during a 24J Back Right Impact a) MidLeft b) MidRight

Previous plots display the responses of respectively TopLeft, TopRight, MidLeft and MidRight accelerometers in all the 3 axes directions for a Back-Right impact at a 24J energy level.

The principal directions for this configuration are along both X and Y, this conduct is visible on each accelerometer, in fact the overall trend of sensors TL, TR, ML and MR is with a peak in X and Y direction. The average value is the same around 30g for everyone, but the TL one shows a greater peak, probably related with calibration imprecision. After the main peaks there's a waving effect in all direction, difficult to describe the general trend, but the reason could be related with the stabilizing reaction of the brain inside the cranium. Along the Z axe is possible to observe that the trend is basically the same for the sensors in the top layer but seems to be inverted in the Mid Layer: since the two lobe are free to move with respect to each other, this impact is more effective to one side then the other and while one lobe is going up the other shows an acceleration in the other direction until the stabilization.

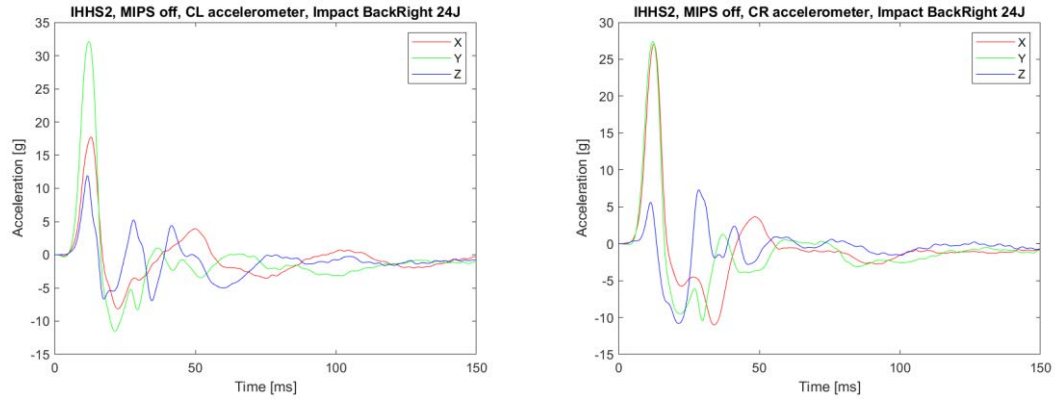

Figure 4.47 - Acceleration collected from sensors during a 24J Back Right Impact a) CerebellumLeft b) CerebellumRight

The sensors located in the cerebellum have the same behaviour of the ones in the higher layer, the main accelerations directions are along the main axes X and Y, the component along Y correspond in value and trend, is noticeable that the X component on the Left

side is shorter reaching a 18g acceleration against the 27g value of the right side. This is related with the impact position, since the CR sensor is closer to the impact point it receives most of the hitting energy and this is reflected in a higher acceleration, this difference is noticeable also in the other lateral sensors but less evidently.

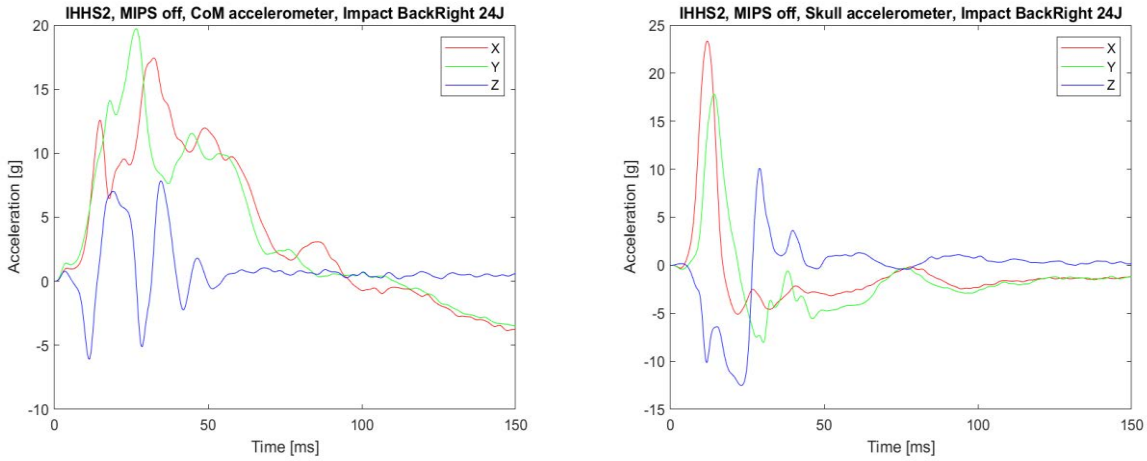

Figure 4.48 - Acceleration collected from sensors during a 24J Back Right Impact a) Brain Centre of mass b) Skull accelerometer

The sensor located in the brain centre of mass shows a trend analogue to the other sensors embedded in the brain: main acceleration along the X and Y axes and oscillation along Z. The comparison with the skull accelerometer confirms the delay that occur after the impact before the energy is transmitted into the brain. The plot displays a narrow peak along X and Y coherent with the impact direction but early in time with respect to the brain response. The peak displayed from the brain accelerometer is delayed and wider, that means a slower return to the stationary position.

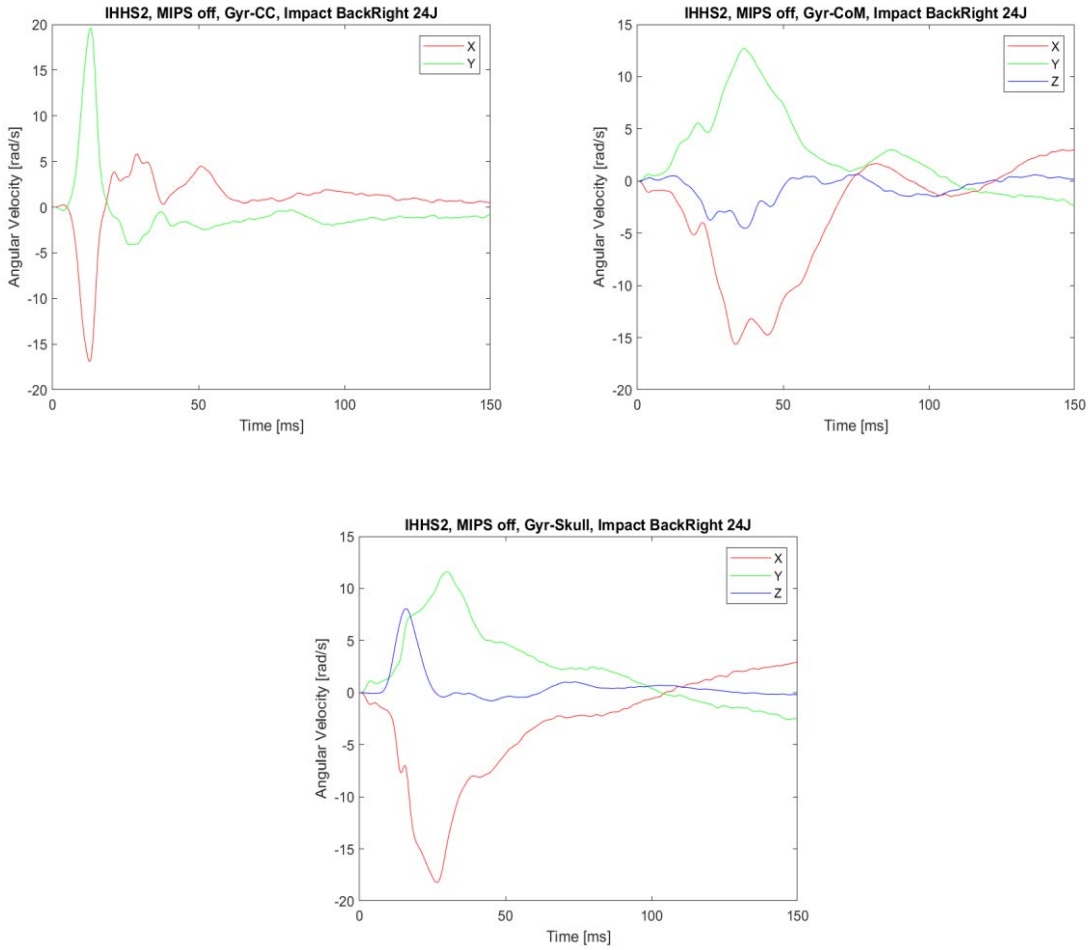

Figure 4.49 - Angular velocity collected from gyroscopes during a 24J Back Right Impact a) Cerebellum centre b) Brain Centre of mass c) Skull

Analysing the gyroscopes applied on the head is possible to describe the global dummy head rotational behaviour. The rotations happen around the Y axe, that represent a pitch oscillation and around the X which is a roll. The rotational velocity is higher in the cerebellum sensors and happen before the other gyroscope, the peaks on the skull and brain plots are similar in value but wider in the distribution.

A narrow peak around Z is displayed by the skull gyroscope, this value is representative of a fast-rotational movement impressed from the hammer and create a great acceleration around the neck axes.

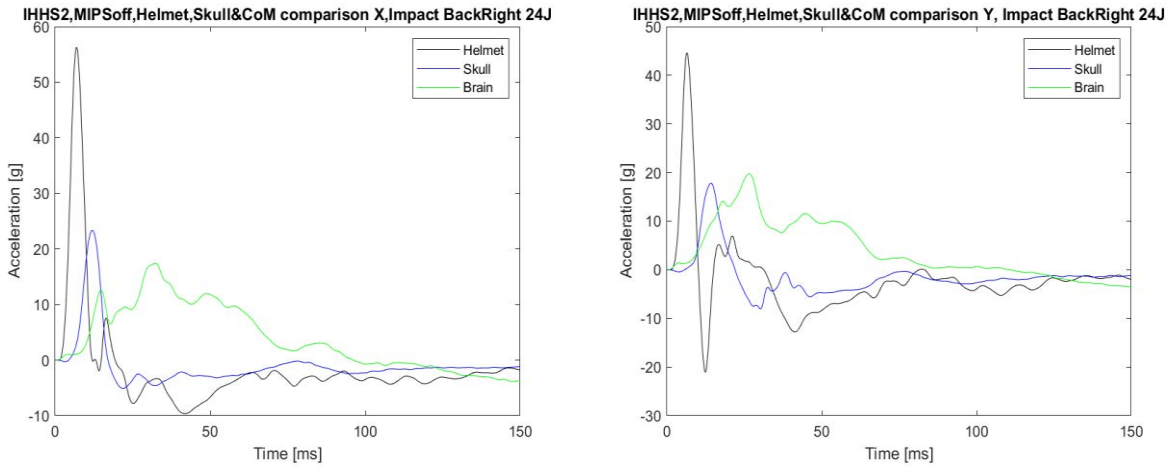

Figure 4.50 - Acceleration comparison between Helmet, Skull Brain; collected from sensors during a 24J Back Right Impact a) Acceleration comparison along X b) acceleration comparison along Y

The acceleration comparison within the Helmet, Skull and Brain accelerometers is completed along the two principal axes, both the plots confirm the timing distribution and order of the impact.

The higher and first peak is the helmet, then the skull receive the energy almost halved in magnitude, then the brain shows a wider and delayed acceleration value. The wider trend means a smoother distribution of the energy and a damped energy reception from the brain. This is helpful to confirm the usefulness of the CSF and intracranial layer, that work as energy inhibition.

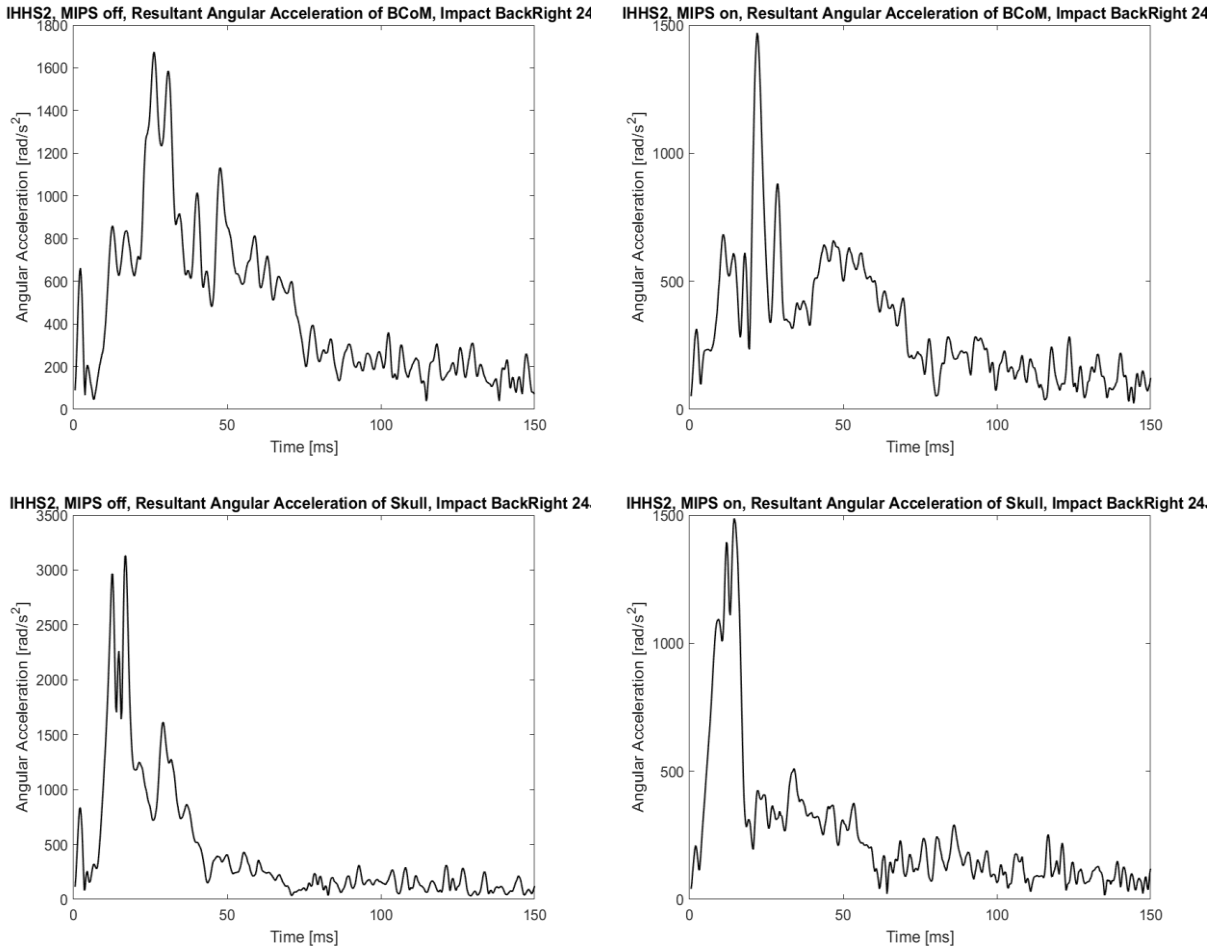

Figure 4.51 - Angular Acceleration resultant collected from sensors during 24J Back Right Impact a)Brain Centre of Mass angular acceleration MIPS off b) Brain Centre of Mass angular acceleration MIPS on c) Skull angular acceleration MIPS off d) Skull angular acceleration MIPS on

The rotational influence of a Back Right impact is more remarkable, this test is performed with activated (Figure 4.51 b and d) and not activate (Figure 4.51Figure 4.42 a and c) MIPS at the same energy level. The angular acceleration is lower if the MIPS system is activated into the skull, a reduction is noticeable in the brain acceleration and even a higher one on the skull. The peak value of angular acceleration is almost the same for brain and skull, this could be justified as an effect of the system of reduction of frictional force between the helmet and the skull.

Pressure Sensors

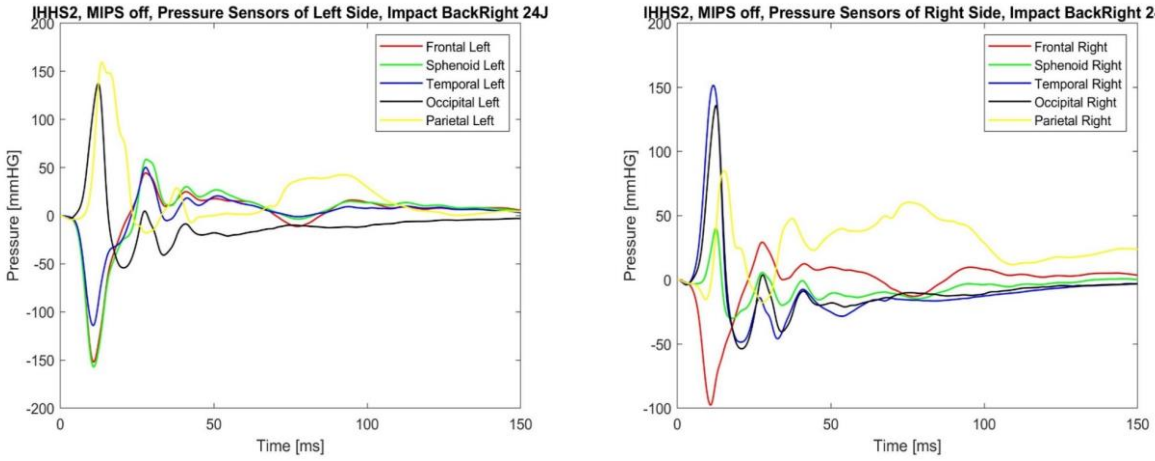

Figure 4.52 - Pression values collected from sensors during a 24J Back Right Impact a)Sensors on the Left Side of the skull b)Sensors on the right Side of the skull

IHHS2 has a distribution of pressure sensors located all around the brain, to comprehend the different activities of right and the left lobe during an impact two different plot are displayed. It's important to point out that the original not filtered signals collected during the test showed a saturation of the values for every signal bigger that 150 mmHg, so for each peak, was originally obtained a plateau region. This plateau region is not visible because of the 7th order low-pass filter at 200 Hz applied during the data analysis but the represented values are not trustable as number but useful to describe the pressure overall timing and distribution. The signal saturates not because of the sensors, but because of the board used to record the signals.

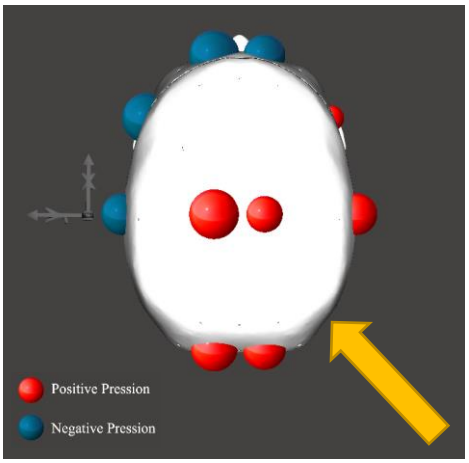

Figure 4.53 - Pression distribution representation around the skull for 24J Back Right impact; the diameter of the circle represents the scale, the colour represents the sign of the pression

The hammer is hitting the head from the Right Back and as first reaction is possible to observe a positive compression of the sensors located and the right side, in particular Temporal and Sphenoid , both the sensor on the Parietal and Occipital bones display a

compression. The Frontal sensors and both Temporal and sphenoid sensors on the left side display a depression. The impact is not symmetric, and the compression is in the part of the skull where the hit come from on the opposite side the brain moves away from the bones and generates a depression.

The global distribution of the pression helps to comprehend the behaviour of the inner head component and understand which impact more dangerous and which parts are more stressed.

After the first impact a global increase in the pressure is noticeable for every sensor, probably related with the deformation of the brain and global growth in volume.

1.14 Right Impact 24 J IHHS2

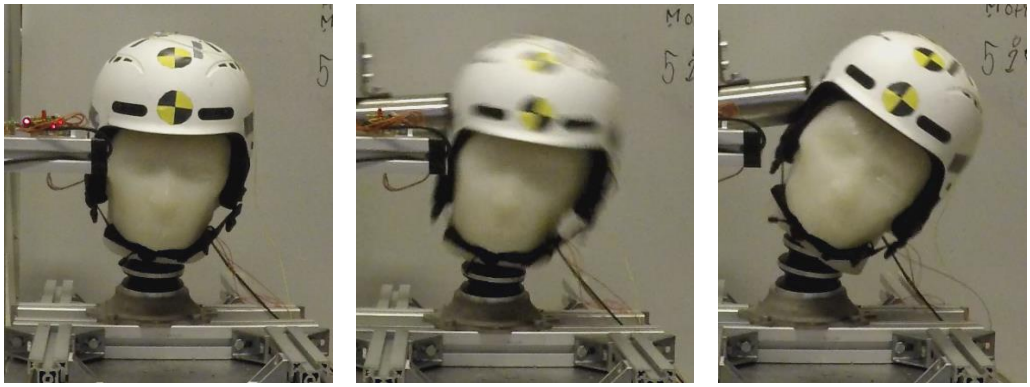

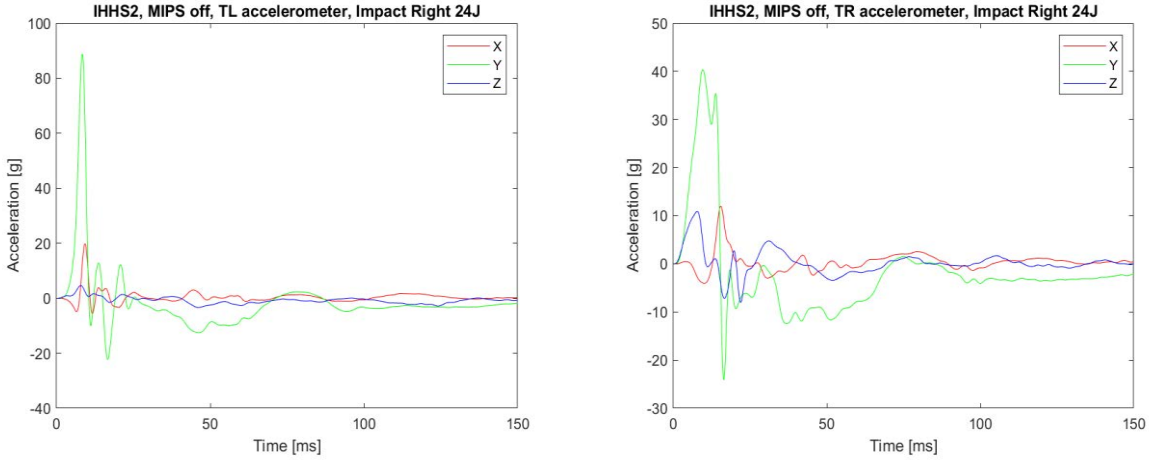

Figure 4.54 Acceleration collected from sensors during a 24J Right Impact a)TopLeft b)TopRight

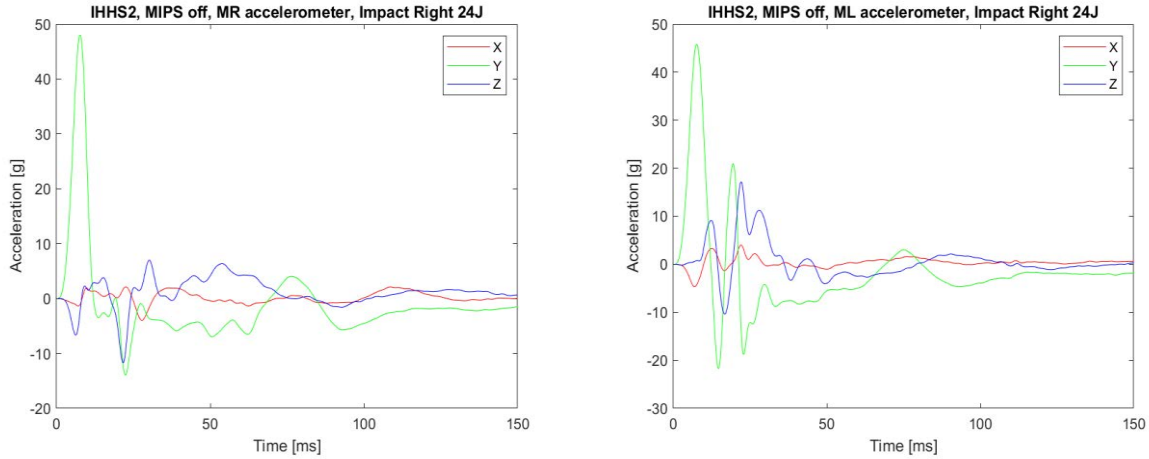

Figure 4.55 - Acceleration collected from sensors during a 24J Right Impact a) MidLeft b) MidRight

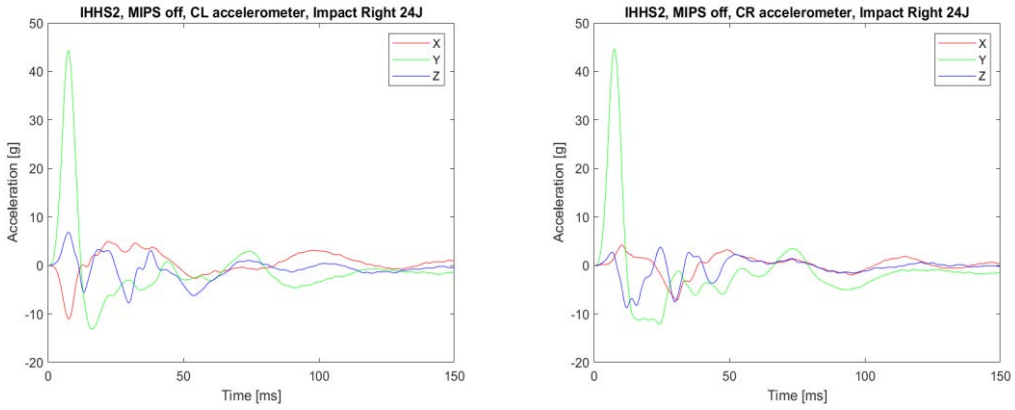

Figure 4.56 Acceleration collected from sensors during a 24J Right Impact a) CerebellumLeft b) CerebellumRight

The previous plots are related with a right impact performed at a 24J Energy Level and show the responses of respectively TopLeft, TopRight, MidLeft and MidRight accelerometers in all the 3 axes directions. Since the impact is from the right side the principal direction is along Y.

The main peak is along Y for each sensor, the sensors on the top layer TL is characterized by a higher peak with respect to the others but this problem is already noticed and discussed, probably acquisition problems pop up and create an out of range result, but the despite the value the conduct is comprehensible.

TR reaches a 40g acceleration, ML and MR reach a value of acceleration around 45g. After the peak values that correspond to the hit moment of the dummy head some oscillations describe the movement of the head until the complete stabilization.

The same overall trend is showed by the sensors of ML and MR, along the main principal direction and with a reached valued of the previous described accelerometers.

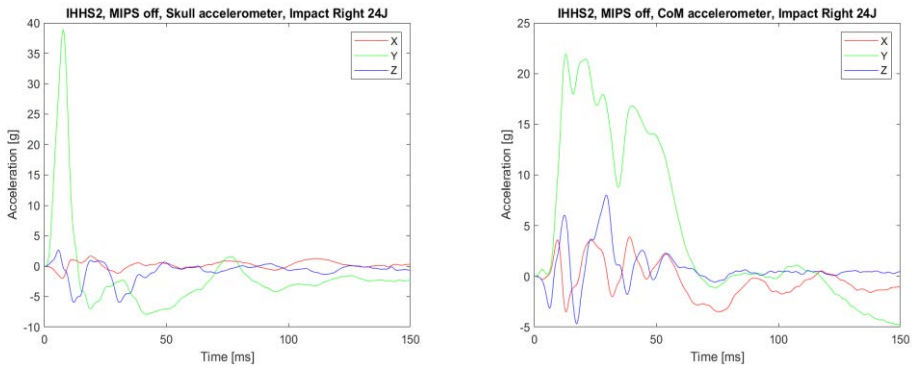

Figure 4.57 - Acceleration collected from sensors during a 24J Right Impact a) Skull b) Brain Centre of mass

As the previous impact the sensors located in the brain centre of mass and on the skull shows a trend equivalent to the other sensors embedded in the brain: main acceleration along the X; the skull accelerometer shows again itself as the first signal collected after the impact.

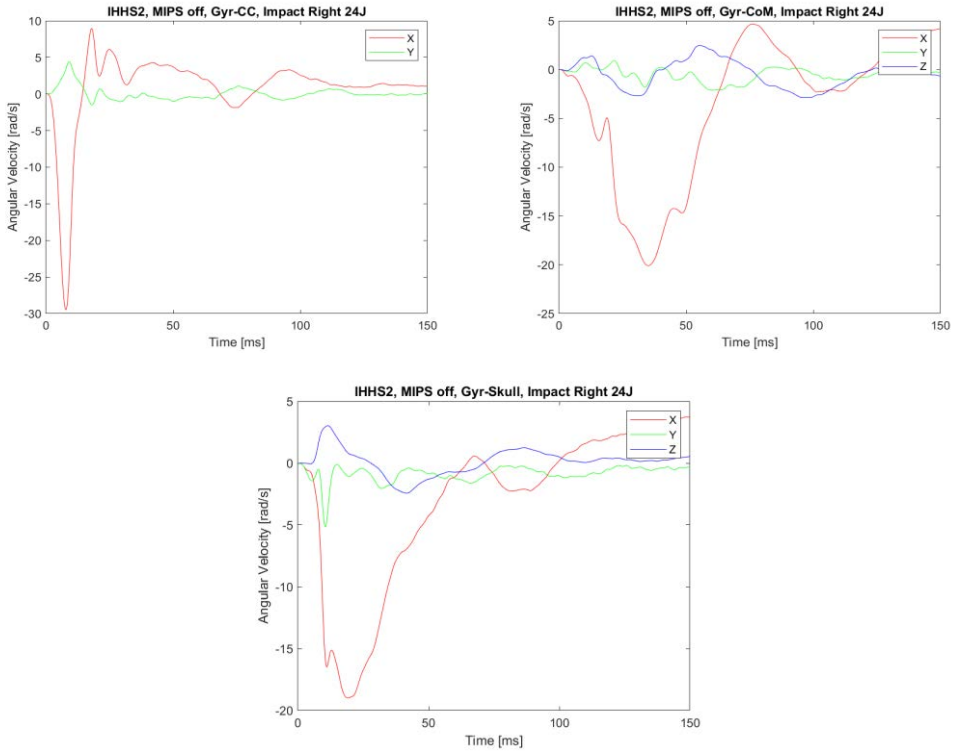

Figure 4.58 - Angular velocity collected from gyroscopes during a 24J Right Impact a) Cerebellum centre b) Brain Centre of mass c) Skull

The rotations are around the X direction, that represent a roll oscillation the rotational velocity is higher in the cerebellum sensors and happens before the other gyroscope, the peaks on the skull and brain plots are similar in value but wider in the distribution.
Since the impact direction is only along one axe the main rotation is only one as well.

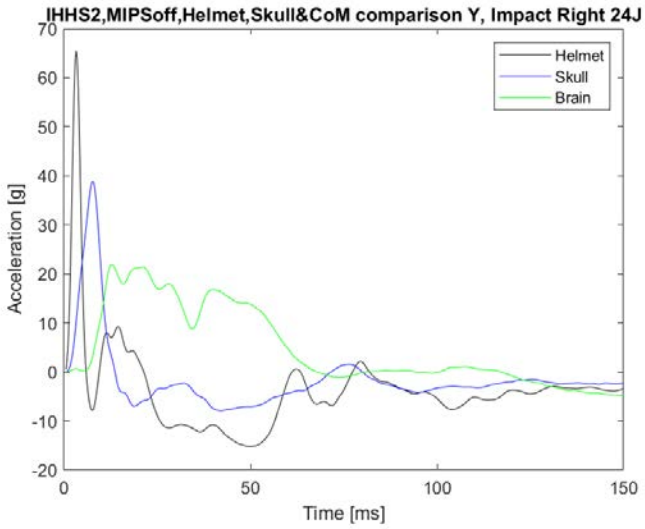

Figure 4.59 - Acceleration comparison between Helmet, Skull Brain; collected from sensors during a 24J Right Impact along Y

The acceleration comparison within the Helmet, Skull and Brain accelerometers is confirming one more time the order of impact energy transference.

The higher and first peak is the helmet, then the skull receive the energy almost halved in magnitude, then the brain shows a wider and delayed acceleration value. The wider trend means a smoother distribution of the energy and a damped energy reception from the brain.

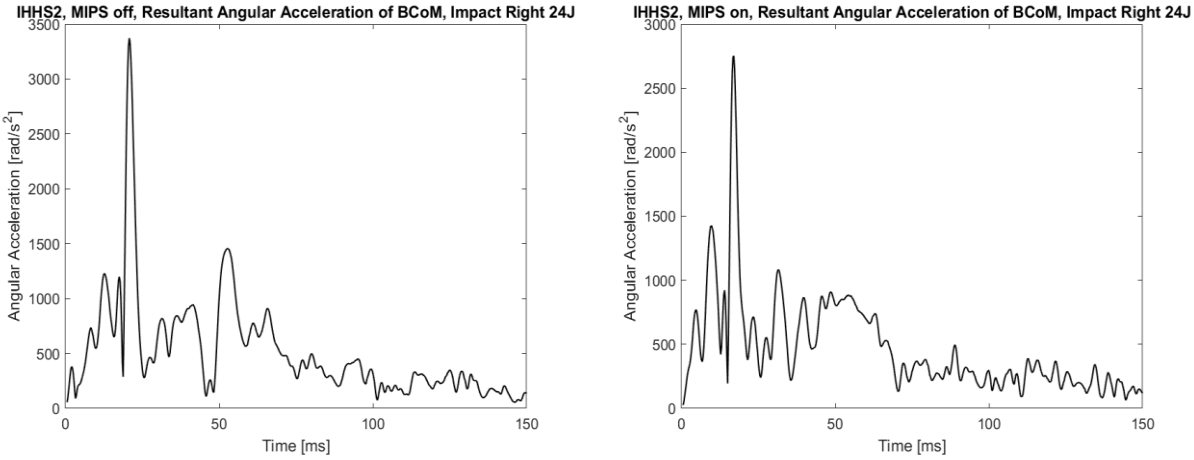

Figure 4.60 -- Angular Acceleration resultant collected from sensors during 24J Right Impact a) Brain Centre of Mass angular acceleration MIPS off b) Brain Centre of Mass angular acceleration MIPS on

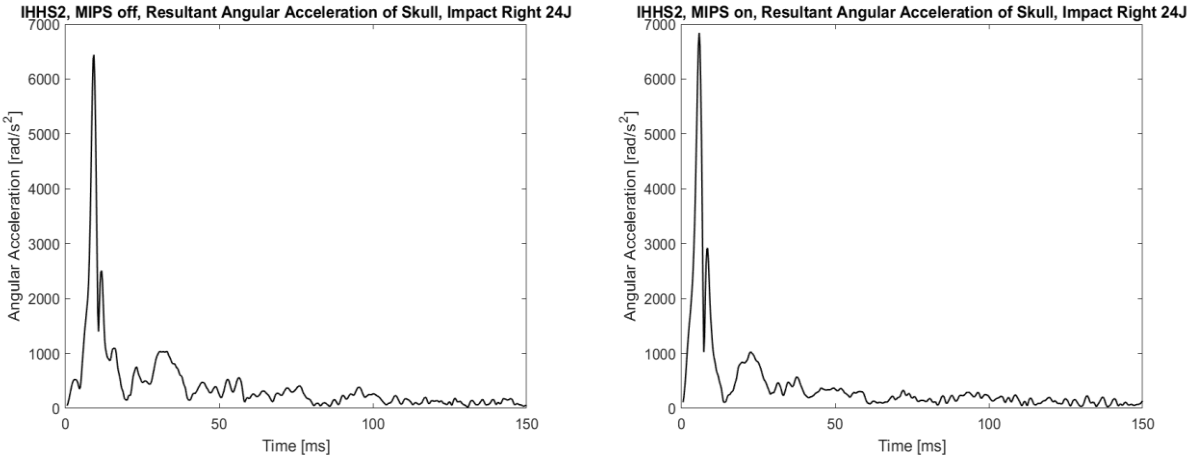

Figure 4.61 - Angular Acceleration resultant collected from sensors during 24J Right Impact a) Skull angular acceleration MIPS off b) Skull angular acceleration MIPS on

The previous plots show the angular acceleration collected during a Right impact performed with activated and not activate MIPS at the same energy level, both on the Brain (Figure 4.60) and the skull (Figure 4.61). The angular acceleration is higher on the skull then the value collected from the brain, the relative movement of the brain inside the skull helps to reduce rotational stress. The differences between the activated or not activated MIPS are however not interesting; very similarly to the back impact a little

rotational effect is impressed to the head and since the MIPS works during tangential component for the reduction of rotational stress, these results are coherent with what is expected.

Pressure Sensors

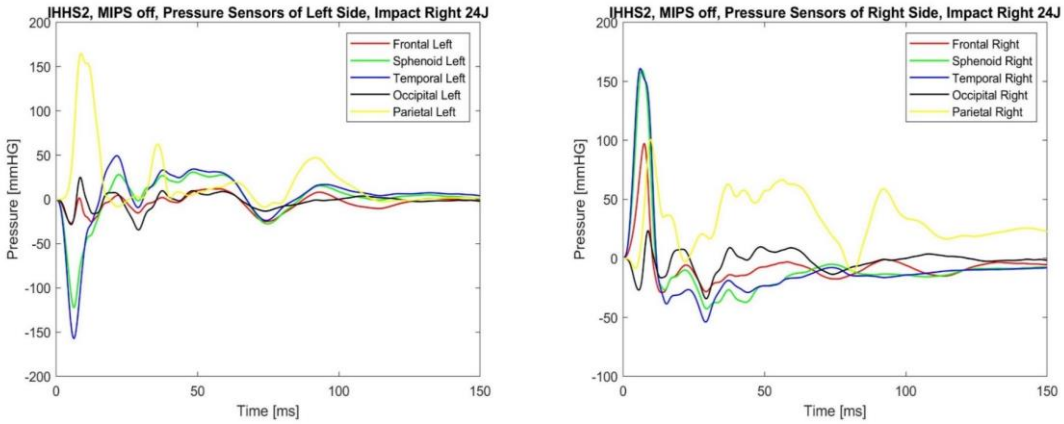

Figure 4.62 - Pression values collected from sensors during a 24J Right Impact a) Sensors on the Left Side of the head b) Sensors on the right Side of the head

The discussion of the pressions distribution in this type of impact is interesting because this type of test is not symmetric, and every sensor display an activity.

Analysing the plot of the left side sensors is noticeable that the only positive value is on the Parietal bone, and every other point of the left side is subject of depression of different magnitude; on the right side, where the impact is from, the fluid shows a compression of the brain skull volume.

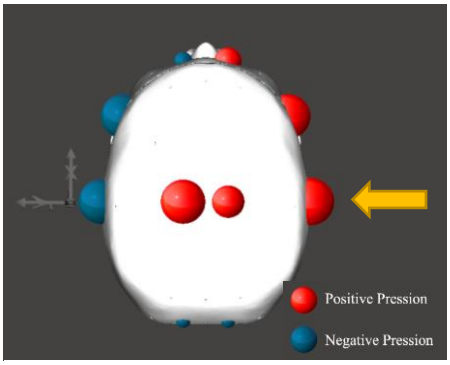

Figure 4.63 - Pression distribution representation around the skull; the diameter of the circle represents the scale; the colour represents the sign of the pression

1.15 Front Right 24J IHHS2

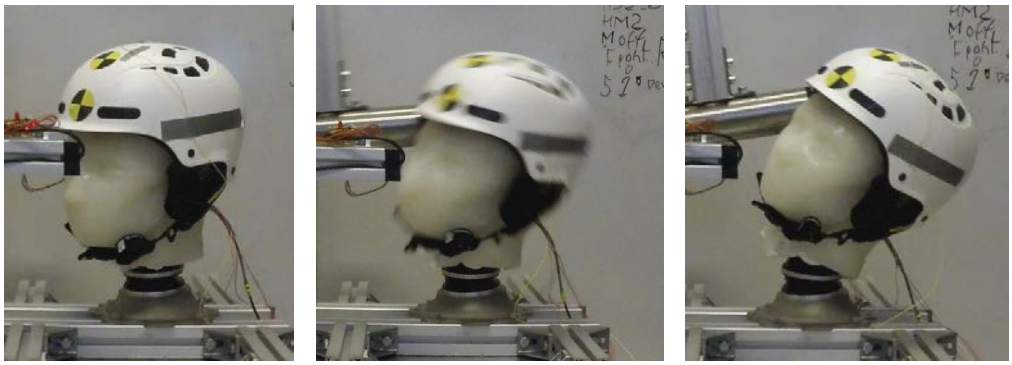

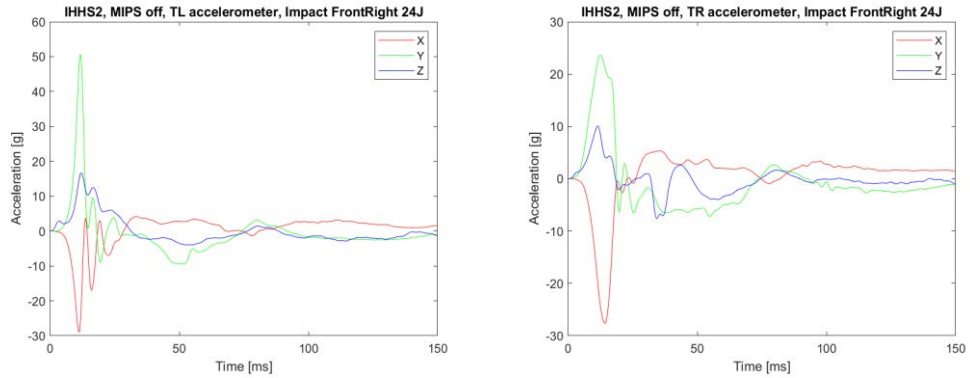

Figure 4.64 - Acceleration collected from sensors during a 24J Front Right Impact a) TopLeft b) TopRight

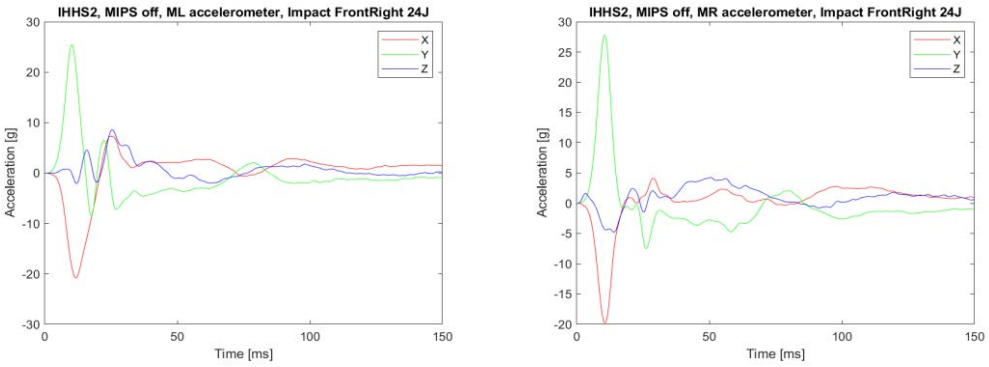

Figure 4.65 - Acceleration collected from sensors during a 24J Front Right Impact a) MidLeft b) MidRight

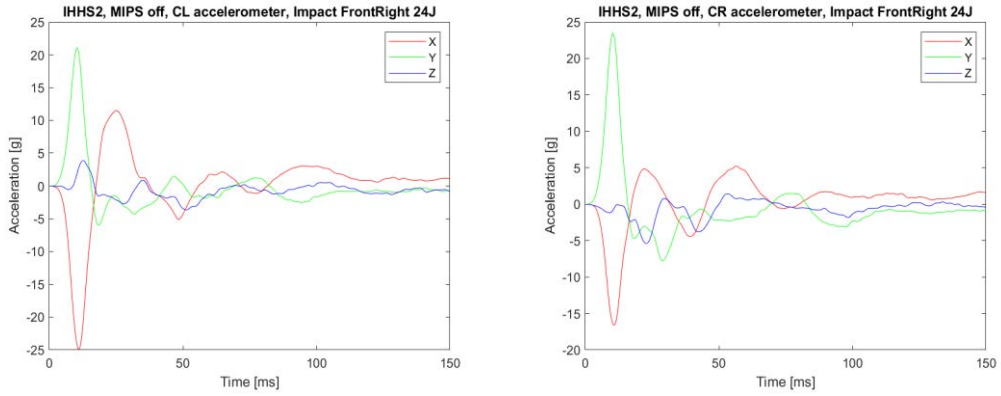

Figure 4.66 - Acceleration collected from sensors during a 24J Front Right Impact a) CerebellumLeft b) CerebellumRight

The Previous plots display the responses of respectively Top Left – TopRight (Figure 4.64) , MidLeft – MidRight (Figure 4.65) , Cerebellum Left Cerebellum Right ()accelerometers in all the 3 axes directions of a Front Right impact at a 24J energy level. The principal directions for this configuration are along both X and Y, this conduct is visible on each accelerometer, in fact the overall trend of sensors TL, TR, ML and MR is with a peak in X and Y direction. TL one shows a greater as discussed before. About the other sensors, the accelerometers on the right side show a greater value in Y direction respect the correspondent ones on the same plane, the values are slightly different but related with the priority of the impact on the right side and then transferred to the other. The opposite results are obtained on the X direction, with higher value before on the left then on the right.

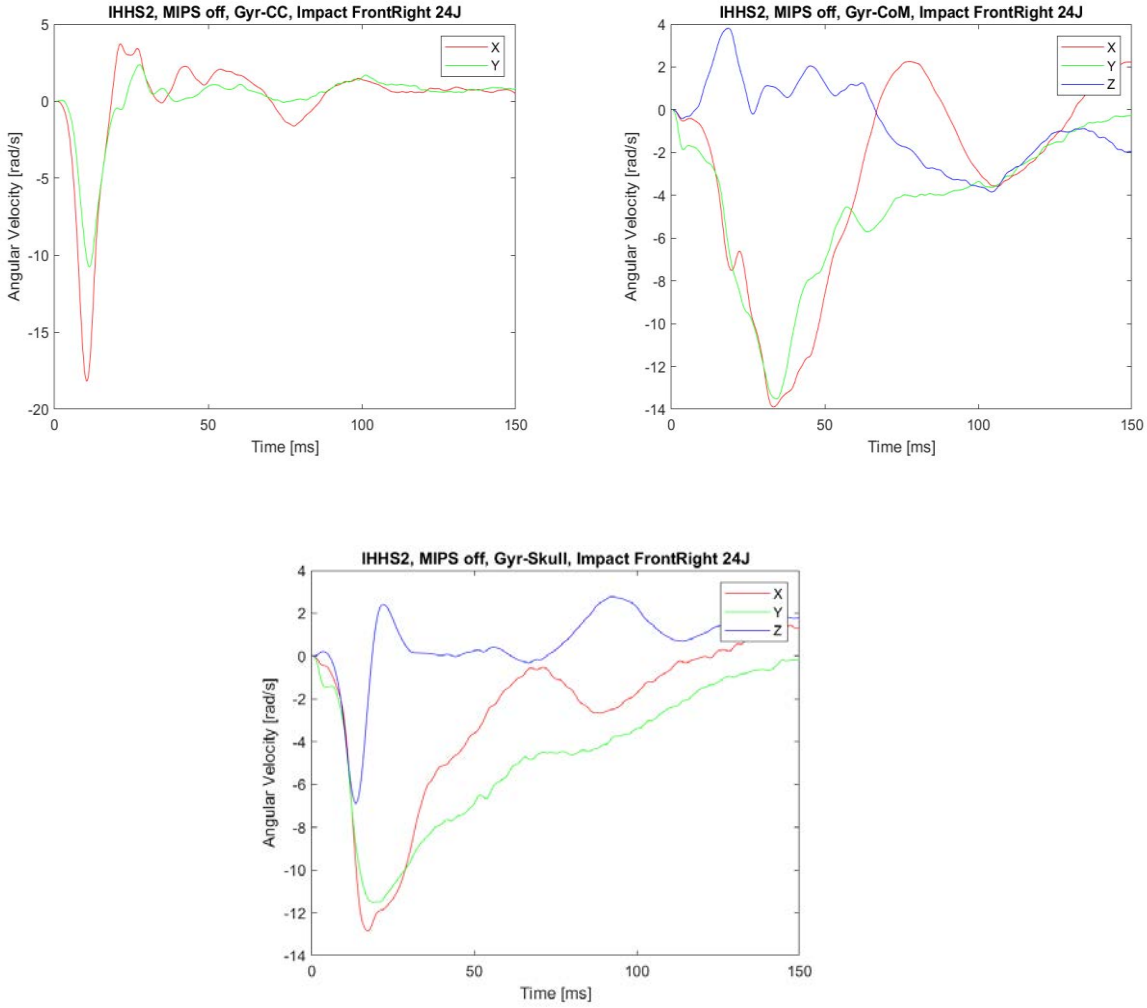

Figure 4.67 - Angular velocity collected from gyroscopes during a 24J Right Impact a) Cerebellum centre b) Brain Centre of mass c) Skull

The rotations happen around the Y axe, that represent a pitch oscillation and around the X which is a roll, the sign of the rotation is the other way around respect the back-right impact. The rotational velocity is higher in the cerebellum sensors and happen before the other gyroscope, the peaks on the skull and brain plots are similar in value but wider in the distribution.

A narrow peak around Z is displayed by the skull gyroscope, this value is representative of a fast-rotational movement impressed from the hammer and create a great acceleration around the neck axes.

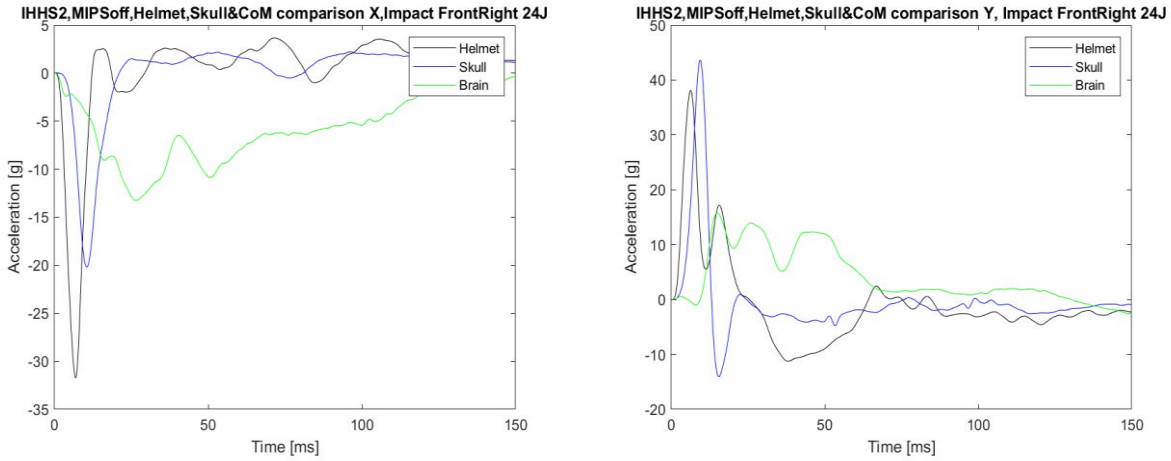

Figure 4.68 - Acceleration comparison between Helmet, Skull Brain; collected from sensors during a 24J Front Right Impact a) Acceleration along X direction b) Acceleration along Y direction

The acceleration comparison within the Helmet, Skull and Brain accelerometers is completed along the two principal axes, both the plots (Figure 4.68) confirm the timing distribution and order of the impact.

On the X direction a higher and first peak is on the helmet, then the skull receives the energy almost halved in magnitude, then the brain shows a wider and delayed acceleration value. About the plot characteristics of the Y direction is visible a double peak on the helmet signal and the highest peak is on the skull; this response could be related with the presence of a soft initial part of the helmet in the impact position, because this highly elastic point the impact is not properly damped, and this response is the result.

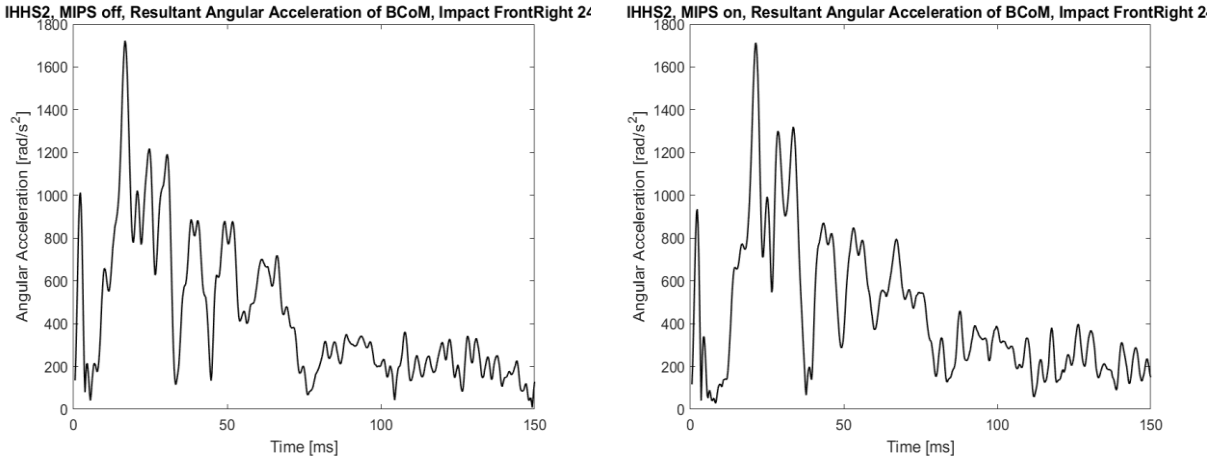

Figure 4.69 - Angular Acceleration resultant collected from sensors during a 24J Front Right Impact a) Brain Centre of Mass angular acceleration MIPS off b) Brain Centre of Mass angular acceleration MIPS on

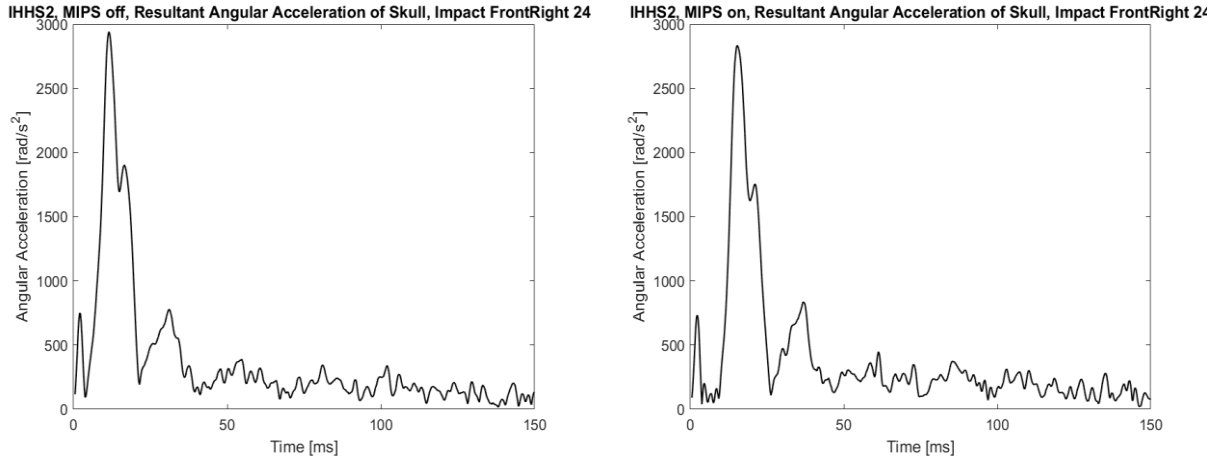

Figure 4.70 - Angular Acceleration resultant collected from sensors during a 24J Front Right Impact c) Skull angular acceleration MIPS off d) Skull angular acceleration MIPS on

The angular acceleration collected during a Front Right impact performed with activated and not activate MIPS at the same energy level, do no show interesting results. The Brain behaviour (Figure 4.69) and the skull's (Figure 4.70) are very similar with activated MIPS or not, despite this type of impact should generate higher rotational movement.

Pressure Sensor

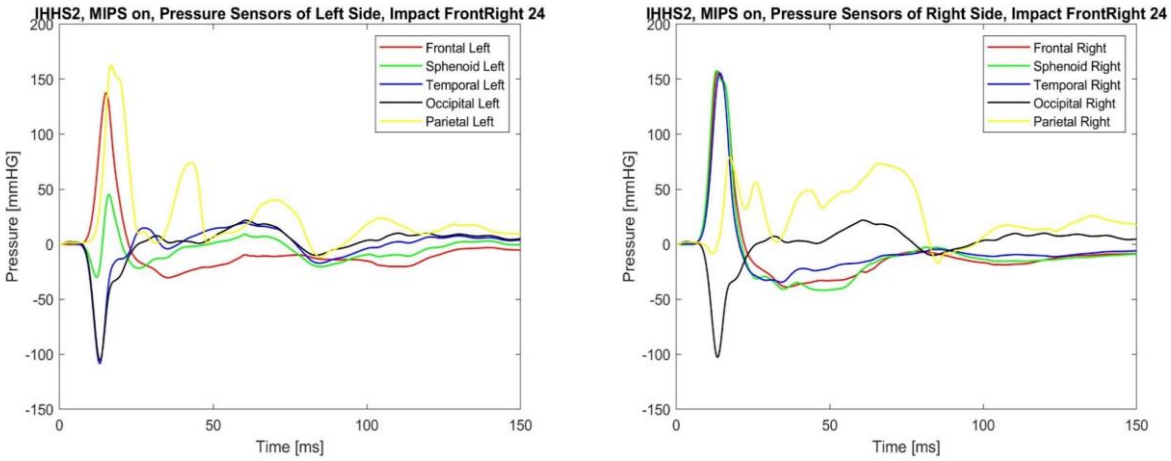

Figure 4.71 - Pression values collected from sensors during a 24J Front Right Impact a) Sensors on the Left Side of the head b) Sensors on the right Side of the head

The hammer is hitting the head from the Front Right and as first reaction is possible to observe a positive compression of the sensors located and the right side. Both frontal sensors, Temporal and Sphenoid on the right side, both the sensor on the Parietal bones display a compression. The two Occipital sensors, Temporal and sphenoid sensors on the left side display a depression. The impact is not symmetric, and the compression is in the part of the skull where the hit come from on the opposite side the brain moves away from the bones and generates a depression.

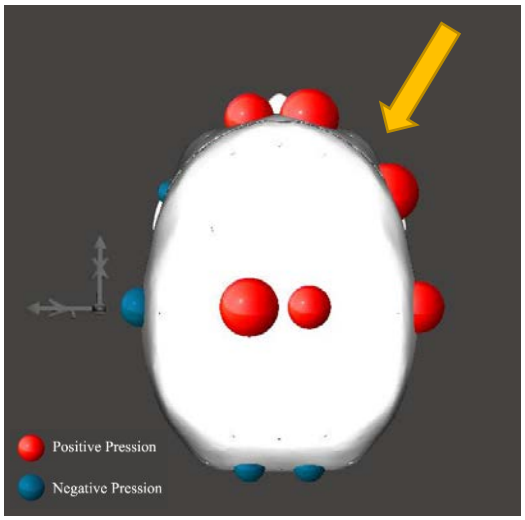

Figure 4.72 - Pression distribution representation around the skull for 24J Front Right Impact; the diameter of the circle represents the scale, the colour represents the sign of the pression

1.16 IHHS2 Histograms

Since only a part of all the results are displayed and discussed in the previous pages, to also explain and illustrate the trends of the tests, changing the type of impact and the energy level, some comparing graphs are reported to summarize the research study and present some more conclusions.

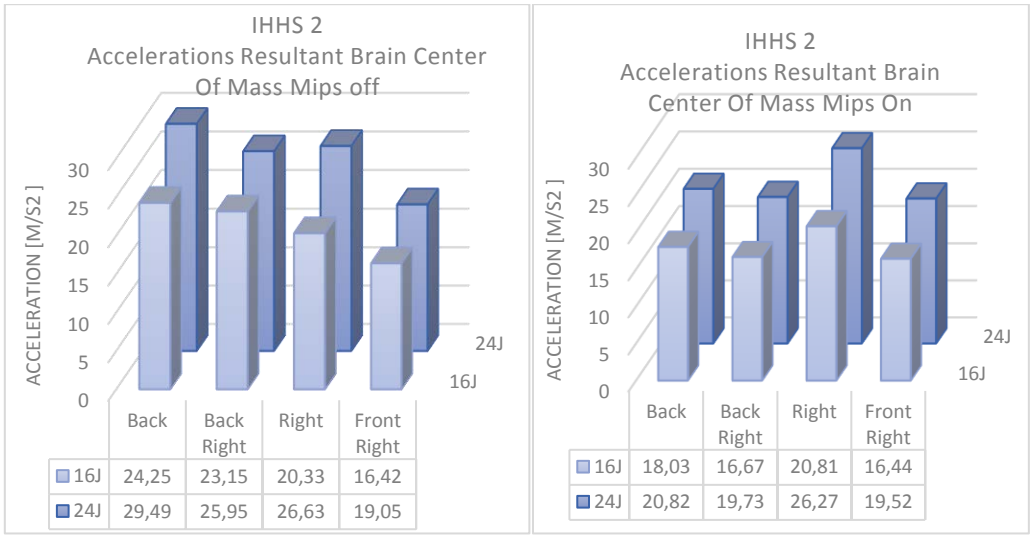

Figure 4.73 - Brain accelerations resultant from every energy level 16J, 24J on different type of impact, Back. Back-Right, Right, Front-Right. a) MIPS off b) MIPS on

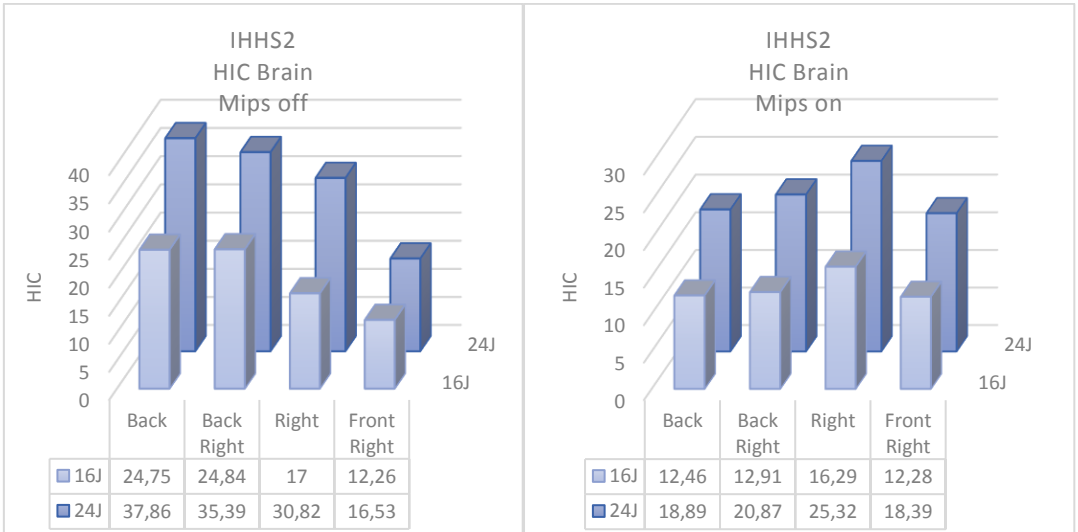

Figure 4.74 – HIC from every energy level 16J, 24J on different type of impact, Back. Back-Right, Right, Front-Right. a) MIPS off b) MIPS on

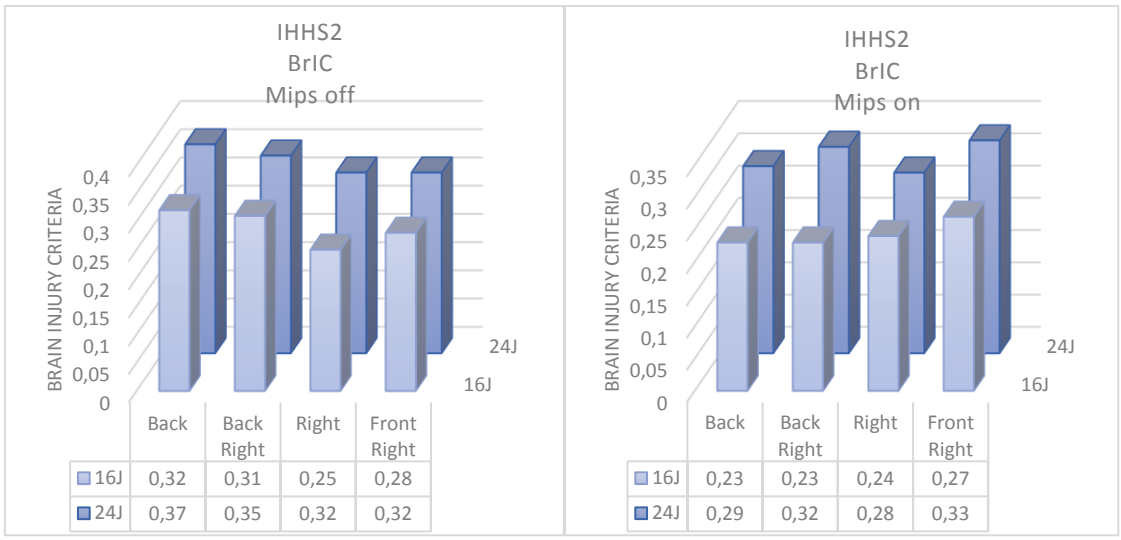

Figure 4.75 – Bric comparison from every energy level 16J, 24J on different type of impact, Back. Back-Right, Right, Front-Right. a) MIPS off b) MIPS on

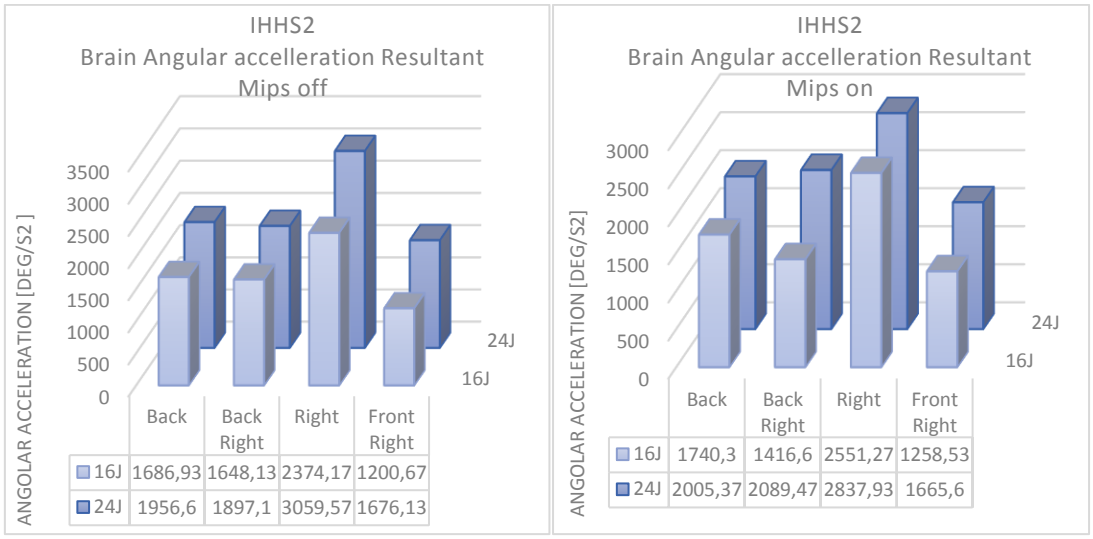

Figure 4.76 - Brain angular accelerations resultant from every energy level 16J, 24J on different type of impact, Back. Back-Right, Right, Front-Right. a) MIPS off b) MIPS on

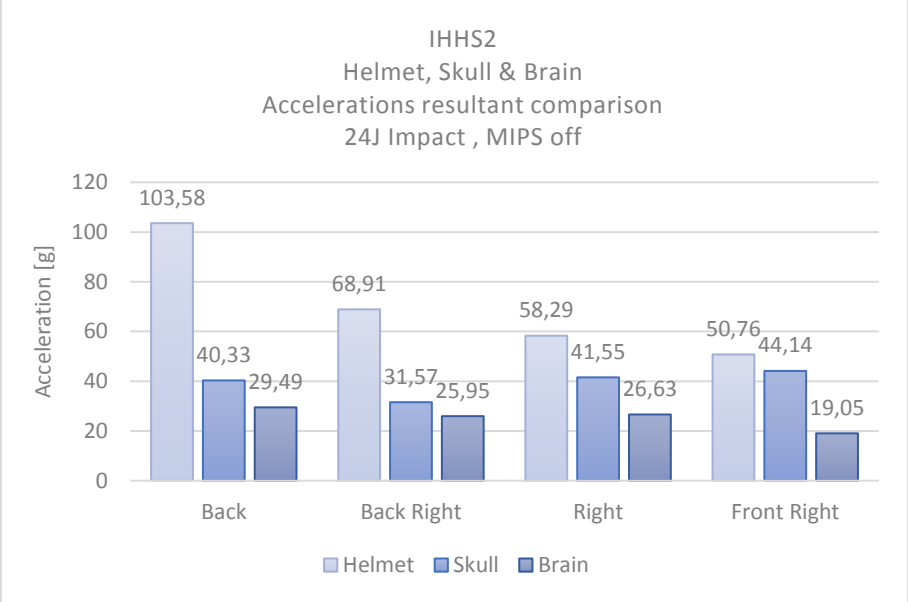

Figure 4.77 - Comparison of acceleration resultants for Helmet, Skull and Brain during 24J Test, on different type of impact, Back. Back-Right, Right, Front-Right

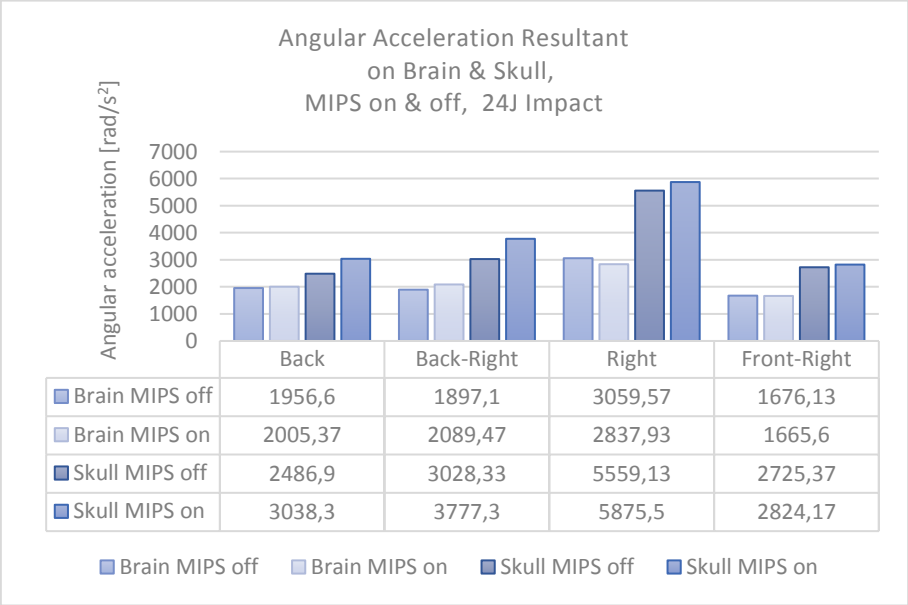

Figure 4.78 - Comparison of angular acceleration resultants on Skull and Brain during 24J Test, on different type of impact, Back. Back-Right, Right, Front-Right and comparing MIPS off and MIPS off

Table 17- IHHS1summary comparison table: 16J Impact; ,Mips Off, position and collected main data

IHHS2		BACK		BACKRIGHT		RIGHT		FRONTRIGHT	
MIPF OFF		Theta = 0 deg		Theta = 45 deg		Theta = 90 deg		Theta = 135 deg	
16J		Mean	STD Dev	Mean	STD Dev	Mean	STD Dev	Mean	STD Dev

Helmet	acc_x [g]	64.04	4.81	35.21	7.48	9.02	2.27	-29.59	6.07
	acc_y [g]	-3.91	15.75	28.10	5.76	38.06	3.17	38.64	9.52
	acc_z [g]	18.36	37.34	-17.50	8.41	-12.25	2.88	-11.41	1.30
	acc_R [g]	65.19	4.83	45.28	8.76	38.89	3.12	48.72	11.29
Skull	acc_x [g]	32.10	3.25	22.92	2.00	1.10	0.17	-17.26	4.54
	acc_y [g]	6.65	0.47	17.44	0.37	26.36	3.60	32.38	11.34
	acc_z [g]	35.25	4.50	3.99	12.34	-3.02	0.12	14.23	1.82
	acc_R [g]	35.69	4.06	26.17	1.12	26.38	3.59	38.09	12.26
	HIC*	31.23	4.29	14.55	0.19	7.73	0.65	21.84	7.93
	ω_x [rad/s]	-0.71	3.66	-9.00	11.89	-16.34	0.54	-11.06	0.53
	ω_y [rad/s]	18.27	0.84	10.14	0.08	-1.51	0.24	-9.56	0.71
	ω_z [rad/s]	0.47	1.98	8.42	0.07	4.48	0.97	-2.60	5.39
	ω_R [rad/s]	18.29	0.84	18.42	0.51	16.47	0.51	14.40	0.80
	ω_R [dps]	1048.06	48.13	1055.30	29.42	943.43	29.29	824.94	45.68
	BRiC*	0.33	0.01	0.36	0.00	0.26	0.01	0.27	0.02
	α_R [rad/s^2]	2223.20	111.93	3101.90	689.52	3229.27	690.45	2116.17	377.47
Brain	acc_x [g]	23.26	1.39	16.31	0.44	1.57	4.67	-10.34	0.65
	acc_y [g]	6.30	0.38	16.08	0.89	20.19	1.72	13.33	1.74
	acc_z [g]	963.24	1667.76	0.27	0.01	0.30	0.01	0.34	0.04
	acc_R [g]	24.25	0.57	23.15	0.88	20.33	1.67	16.42	1.40
	HIC	24.75	4.53	24.84	0.63	17.00	1.09	12.26	2.38
	ω_x [rad/s]	1.81	0.08	-12.76	0.55	-15.88	0.02	-12.61	1.16
	ω_y [rad/s]	17.70	0.67	11.73	0.36	-1.60	0.05	-10.74	0.47
	ω_z [rad/s]	1.95	0.28	-4.95	0.15	-3.35	0.24	0.93	4.08
	ω_R [rad/s]	17.71	0.67	17.34	0.11	16.07	0.05	16.58	0.84
	ω_R [dps]	1014.91	38.48	993.31	6.53	920.83	2.93	950.10	48.36
	BRiC	0.32	0.01	0.31	0.00	0.25	0.00	0.28	0.02
	α_R [rad/s^2]	1686.93	29.19	1648.13	108.26	2374.17	55.29	1200.67	161.35

Table 18 - IHHS1summary comparison table: 24J Impact,Mips Off, position and collected main data

IHHS2		BACK		BACKRIGHT		RIGHT		FRONTRIGHT	
MIPSOFF		Theta = 0 deg		Theta = 45 deg		Theta = 90 deg		Theta = 135 deg	
24J		Mean	STD Dev	Mean	STD Dev	Mean	STD Dev	Mean	STD Dev
Helmet	acc_x [g]	100.98	24.61	54.50	11.47	12.34	3.36	-33.41	2.11
	acc_y [g]	-8.53	27.92	42.03	7.45	57.06	7.39	38.16	0.19
	acc_z [g]	-42.66	12.92	-32.61	13.37	-29.81	10.37	-17.39	2.41
	acc_R [g]	103.58	25.94	68.91	12.84	58.29	8.35	50.76	0.46
Skull	acc_x [g]	38.87	6.18	26.90	5.38	0.31	2.00	-18.42	1.64
	acc_y [g]	0.54	8.18	20.48	3.85	41.53	2.44	37.86	5.62
	acc_z [g]	-6.47	33.37	-14.95	2.27	-5.43	0.48	18.15	0.57
	acc_R [g]	40.33	5.54	31.57	3.99	41.55	2.41	44.14	5.69
	HIC*	47.59	11.96	23.93	3.54	15.67	1.54	33.39	7.11
	ω_x [rad/s]	-0.48	3.24	-18.35	0.32	-20.63	1.42	-13.01	0.26
	ω_y [rad/s]	19.26	0.74	12.34	0.70	-3.21	1.70	-3.73	13.78
	ω_z [rad/s]	2.10	0.42	9.18	1.83	4.77	1.51	-2.52	6.11
	ω_R [rad/s]	19.30	0.72	21.73	0.67	20.68	1.42	17.48	0.19
	ω_R [dps]	1105.73	41.41	1245.07	38.56	1184.90	81.40	1001.81	10.62
	BRiC*	0.35	0.02	0.41	0.03	0.34	0.02	0.31	0.01
	α_R [rad/s^2]	2486.90	791.13	3028.33	367.25	5559.13	1257.63	2725.37	189.87
Brain	acc_x [g]	28.29	2.07	18.64	2.09	4.30	0.42	-13.50	0.23
	acc_y [g]	6.43	0.29	20.45	0.92	26.01	3.54	15.47	0.25
	acc_z [g]	0.10	0.35	0.44	0.06	0.41	0.02	0.46	0.02
	acc_R [g]	29.49	2.06	25.95	2.47	26.63	3.18	19.05	0.55
	HIC	37.86	3.73	35.39	6.58	30.82	2.72	16.53	1.04
	ω_x [rad/s]	0.67	2.37	-15.00	0.81	-20.00	0.10	-13.56	0.31
	ω_y [rad/s]	20.50	0.90	13.50	0.70	-2.21	0.10	-13.47	0.07
	ω_z [rad/s]	-0.30	2.70	-5.01	0.59	-3.69	0.74	1.00	4.19
	ω_R [rad/s]	20.55	0.89	20.24	0.82	20.31	0.07	19.11	0.25
	ω_R [dps]	1177.60	51.14	1164.67	42.51	1163.53	3.75	1095.00	14.23
	BRiC	0.37	0.02	0.35	0.01	0.32	0.01	0.32	0.01
	α_R [rad/s^2]	1956.60	352.54	1897.10	287.51	3059.57	274.60	1676.13	106.73

Table 19 - IHHS1summary comparison table: 16J Impact, Mips On, position and collected main data

IHHS2		BACK		BACKRIGHT		RIGHT		FRONTRIGHT	
MIPS ON		Theta = 0 deg		Theta = 45 deg		Theta = 90 deg		Theta = 135 deg	
16J		Mean	STD Dev	Mean	STD Dev	Mean	STD Dev	Mean	STD Dev

Helmet	acc_x [g]	77.28	2.35	53.36	2.33	-1.37	8.26	-30.33	2.19
	acc_y [g]	-2.13	6.09	37.12	0.57	39.01	2.18	27.58	1.04
	acc_z [g]	-14.68	52.10	-10.97	46.82	-14.00	1.73	2.26	20.94
	acc_R [g]	77.44	2.33	65.36	2.10	39.45	2.00	41.62	0.95
Skull	acc_x [g]	32.77	3.53	17.90	3.98	-2.87	0.06	-17.67	0.89
	acc_y [g]	1.63	4.62	17.93	2.75	37.93	0.83	34.37	4.52
	acc_z [g]	-26.92	1.25	-16.15	1.47	-3.65	0.06	11.76	0.44
	acc_R [g]	34.56	3.77	27.24	5.21	38.06	0.84	39.68	4.32
	HIC*	30.17	3.12	14.62	0.96	15.22	0.22	23.93	1.64
	ω_x [rad/s]	-2.63	1.87	-9.82	0.90	-15.77	0.48	-10.23	0.31
	ω_y [rad/s]	13.85	0.13	8.08	0.53	-3.24	2.00	-8.33	0.43
	ω_z [rad/s]	-1.74	0.08	1.42	2.90	0.55	2.12	-5.82	0.19
	ω_R [rad/s]	13.98	0.12	12.71	1.01	16.07	0.89	13.14	0.36
	ω_R [dps]	800.92	7.01	728.38	58.00	920.66	50.79	752.76	20.89
	BRiC*	0.25	0.01	0.22	0.02	0.25	0.02	0.25	0.00
	α_R [rad/s^2]	2218.20	170.61	2218.20	657.91	3958.43	1424.89	1962.50	159.79
Brain	acc_x [g]	17.77	0.18	12.69	1.01	-0.98	4.19	-9.47	0.27
	acc_y [g]	5.05	0.31	12.02	0.15	20.56	0.30	13.51	0.59
	acc_z [g]	0.37	0.04	0.09	0.44	0.36	0.03	0.31	0.03
	acc_R [g]	18.03	0.11	16.67	0.29	20.81	0.23	16.44	0.39
	HIC	12.46	0.43	12.91	1.19	16.29	0.11	12.28	0.33
	ω_x [rad/s]	-1.34	0.17	-2.08	13.42	-15.17	0.19	-12.11	0.27
	ω_y [rad/s]	6.92	10.11	4.70	8.04	-1.94	0.12	-10.49	1.38
	ω_z [rad/s]	0.54	1.29	2.24	0.03	2.41	0.06	-1.20	4.35
	ω_R [rad/s]	12.69	0.21	12.84	0.38	15.27	0.17	15.67	0.09
	ω_R [dps]	727.13	12.30	735.69	21.71	874.81	9.65	897.85	5.21
	BRiC	0.23	0.00	0.23	0.01	0.24	0.00	0.27	0.00
	α_R [rad/s^2]	1740.30	158.27	1416.60	51.72	2551.27	42.19	1258.53	68.24

Table 20 - IHHS1summary comparison table: 24J Impact, Mips on, position and collected main data

IHHS2		BACK		BACKRIGHT		RIGHT		FRONTRIGHT	
MIPS 0N		Theta = 0 deg		Theta = 45 deg		Theta = 90 deg		Theta = 135 deg	
24J		Mean	STD Dev	Mean	STD Dev	Mean	STD Dev	Mean	STD Dev
Helmet	acc_x [g]	101.03	0.07	48.80	4.37	8.71	1.98	-39.94	1.54
	acc_y [g]	-8.68	0.94	53.38	5.41	30.33	15.07	34.07	2.17
	acc_z [g]	-54.58	1.40	-34.91	4.94	-22.01	7.41	11.74	0.99
	acc_R [g]	101.42	0.02	72.33	6.84	36.75	9.62	52.89	2.82
Skull	acc_x [g]	50.50	0.81	31.01	1.78	-3.78	0.38	-21.66	1.28
	acc_y [g]	4.67	0.20	25.34	2.21	52.31	1.23	48.40	1.80
	acc_z [g]	-31.96	0.55	-15.54	0.19	-5.25	0.58	17.07	0.18
	acc_R [g]	51.99	0.73	36.03	2.41	52.47	1.25	54.48	2.10
	HIC*	61.63	1.30	32.83	1.96	22.08	4.97	43.11	0.94
	ω_x [rad/s]	-3.86	1.73	-15.85	0.51	-18.67	0.39	-12.86	0.14
	ω_y [rad/s]	16.44	0.26	10.81	0.41	-3.94	2.83	-11.20	0.20
	ω_z [rad/s]	-2.26	0.13	9.30	0.33	-2.28	0.10	-7.52	0.21
	ω_R [rad/s]	16.60	0.30	18.89	0.68	19.13	0.33	17.24	0.23
	ω_R [dps]	950.87	17.28	1082.40	38.96	1096.27	19.09	987.67	12.98
	BRiC*	0.30	0.01	0.38	0.01	0.30	0.01	0.33	0.01
	α_R [rad/s^2]	3038.30	136.83	3777.30	712.53	5875.50	880.06	2824.17	63.36
Brain	acc_x [g]	20.80	0.09	16.49	0.35	-4.58	0.27	-12.57	0.43
	acc_y [g]	5.40	0.07	16.50	0.43	25.72	1.22	16.56	0.10
	acc_z [g]	0.38	0.04	0.16	0.50	0.45	0.08	0.39	0.09
	acc_R [g]	20.82	0.10	19.73	0.84	26.27	1.10	19.52	0.14
	HIC	18.89	0.41	20.87	1.72	25.32	1.55	18.39	0.35
	ω_x [rad/s]	-1.01	0.01	-13.54	0.32	-17.75	0.52	-13.83	0.37
	ω_y [rad/s]	16.26	0.37	12.71	0.36	-2.55	0.46	-12.82	0.27
	ω_z [rad/s]	1.98	0.21	-4.35	0.28	2.69	0.13	-4.86	0.12
	ω_R [rad/s]	16.38	0.40	18.11	0.39	17.91	0.59	18.91	0.22
	ω_R [dps]	938.69	22.89	1037.43	22.56	1026.08	33.71	1083.67	12.49
	BRiC	0.29	0.01	0.32	0.01	0.28	0.01	0.33	0.00
	α_R [rad/s^2]	2005.37	1.15	2089.47	63.95	2837.93	322.42	1665.60	133.01

The first results obtained testing the new prototype are interesting and useful for the global evaluation of beahviour of the head during different impact conditions.

The comparison between the data collected from each sensor during the experiments, give a first helpful view of the values trend and head response with dissimilar helmet setup and working settings.

The general designing and construction procedure is deeply described and each step illustrated with justified choices and solutions.

The tables display all the most important data for the analysis of the traumatic response of the hits on the dummy surrogate.

In future additional and more accurate test are necessary for validating the system and in a further future being able of creater a standard procedure for head impact analysis and prevention.

In the following chapter the material characterization is illustrated for the better comprehension of the developed prototype.

Chapter 5
Characterization of IHHS 2.0 Materials

In this section the materials used for building the prototypes are discussed is always important to remember that the choice of the materials is mostly taken on the reliability side, is interesting to build a physical model not perfect from the bio fidelity point of view but robust for a FEM validation and reproduction.
The aim of the surrogate was studying the effects on the brain of blunt impacts, trying to collect data from the sensors integrated in it.

1.16.1 Skull Material

ABSplus-P430 IHHS 1.0 Skull

The first prototype dummy head developed as first project has been 3D printed with ABSplus-P430, using FDM technology. The material properties are showed in the material information but is necessary to investigate how the 3d printed material behaves under different load condition and in relation with the filament printing direction.

The material's characteristics are tested in earlier studies related with this project. [1], [73], [74].

Different specimens were prepared, both in horizontal and vertical direction, aim to obtain equal shaped specimens but investigating how the printing process affects the resistance of the final object.

Table 21 - Mechanical Properties of ABSplus-P430 used for IHHS1 skull

Tests at 5 mm/min	Specimen type	Ultimate Stress [MPa]	Ultimate Strain	Young Modulus [MPa]
Test 1	Horizontal	21.4	2,5 %	1052
	Vertical	19.6	1 %	1852
Test 2	Horizontal	20.4	2,6%	1057
	Vertical	21	1%	1931

The properties of this type of material printed with FDM technology is strong anisotropic, the structure of this kind of 3D printed material is not uniform and this could relate a different behaviour in different areas of the printed part itself.

Polyamide PA2200 IHHS2.0 Skull

The material used for the skull is the PA2200 (Polyamide polymer), it was chosen because the main necessity was to fix the leakage problem related with the oil, the 3D printing SLS technology allows to obtain a bulk structure without any cavity.

To have a better comprehension of the polymer behaviour a series of tensile tests were planned.

The interest was into the evaluation of the mechanical properties of some 3D printed specimens and investigate if the printing direction affects the material characteristics and compare the results with the bones mechanical properties and the plastic used for the first skull model.

Some specimens of the same plastic of the skull were created, in vertical and horizontal direction with respect to the printing base.

Tensile Test

The testing machine used for the tensile test is the Instron 5969.

Instron 5969 is a machine manufactured by Illinois Tool Works Inc. (Buckinghamshire, United Kingdom), and is one model of the 5960 Series of Testing Series.

This machine is a universal static testing system that perform tensile and compression testing and perform shear, flexure, peel, tear, cyclic, and bend tests. This instrument is engineered for precision and offer the possibility to change the gauge type and grip accuracy. This system are multi-purpose instruments commonly used for different types of mechanical tests on plastics, metals, rubber materials and other components.

Figure 5.1 - Instron 5969 Dual

The machine available in the Research Centre can achieve a 50 kN (11,250 lbf) load capacity and a vertical test space of 1212 mm (47.7 in).

The Tensile test follow the Standard BS EN ISO 527-1:1996 the specimens have the dog-bone shape and the dimension is the one listed in the standard protocol.

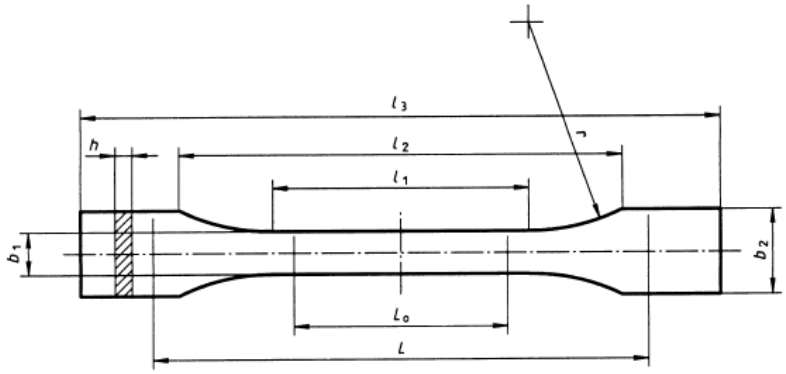

Dimensions in millimetres

	Specimen type	1A	1B
l_3	Overall length	⩾ 150[a]	
l_1	Length of narrow parallel-sided portion	80 ± 2	60,0 ± 0,5
r	Radius	20 to 25	⩾ 60[b]
l_2	Distance between broad parallel-sided portions	104 to 113[c]	106 to 120[c]
b_2	Width at ends	20,0 ± 0,2	
b_1	Width of narrow portion	10,0 ± 0,2	
h	Preferred thickness	4,0 ± 0,2	
L_0	Gauge length	50,0 ± 0,5	
L	Initial distance between grips	115 ± 1	$l_2 \, {}^{+5}_{0}$

Figure 5.2 - Standard BS EN ISO 527-1:1996

The Tensile test is Performed following the standard set up:

Table 22 - Specimen and test setup description following Standard BS EN ISO 527-1:1996

Specimen Type	1A
Test Rate	5 mm/min
Width	10mm
Thickness	4mm

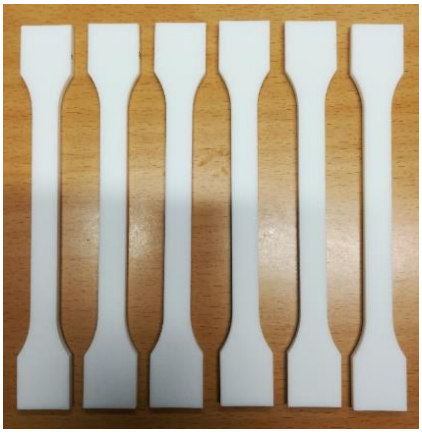

Figure 5.3 - Figure 6.3 -Polyamide PA2200 3DPrinted Dog bone Specimens for tensile test

The STL file designed following the standards is modelled and then printed with Formiga SLS machine, 6 Specimens were oriented in the Vertical and 6 In the Horizontal direction. The tensile tests results are displayed in the following plots:

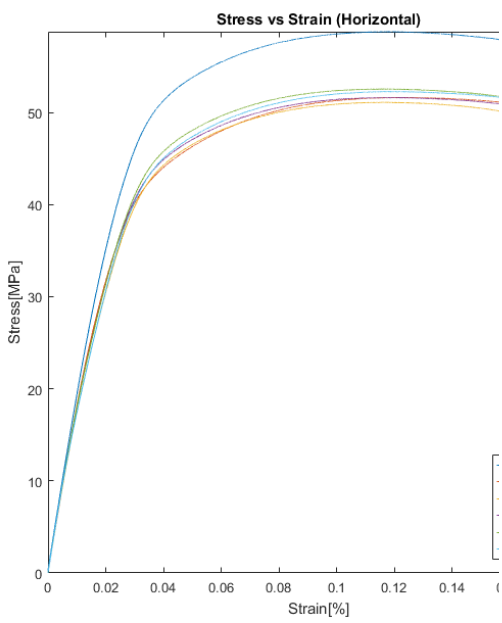

Figure 5.5 - Tensile Test of PA Specin printed in Horizontal direction

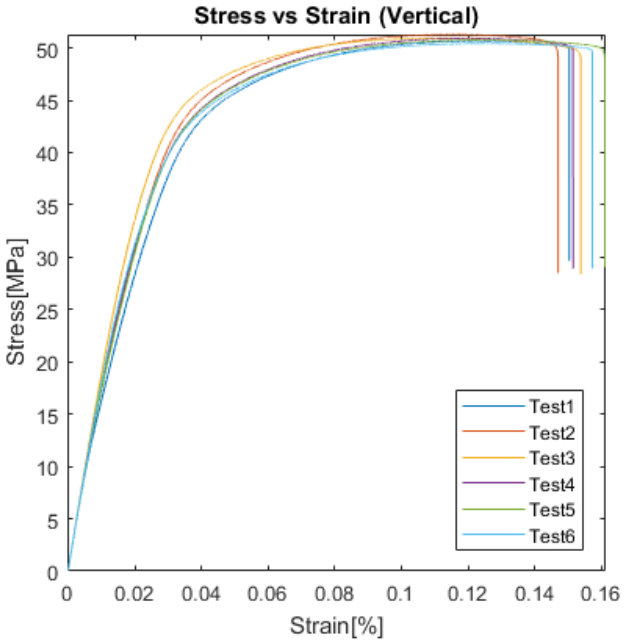

Figure 5.4 - Tensile Test of PA Specimens printed in Vertical direction

Table 23 - Specimens printed in Horizontal direction PA2200

	Tensile Strength [MPa]	Tensile strain at Yield [%]	Young Modulus [Mpa]
1	58.8	11.62	2134.90
2	51.6	12.08	1988.80
3	51.1	11.53	1942.30
4	51.6	11.66	1970.40
5	52.5	11.43	1981.90
6	52.3	11.67	1979.80
Mean	53	11.66	2009.41

Table 24 - Specimens printed in Vertical direction PA2200

	Tensile Strength [MPa]	Tensile strain at Yield [%]	Young Modulus [Mpa]
1	50.7	12.23	1936.50
2	51.3	11.42	1985.30
3	50.9	11.03	1990.90

4	50.9	11.81	1960.80
5	50.8	12.46	1949.10
6	50.4	12.29	1956.40
Mean	50.8	11.87	1963.17

From the obtained results is possible to observe that the mechanical behaviour of the material is mainly Isotropic, the Laser sintering technology guarantees this kind of characteristic and allows to design and produced complex 3D geometries without affecting the properties in relation with the direction of the forces applied to the structure.

1.16.2 Brain Material

Dummy Brain

The wide variability found in literature about brain properties, it was decided to use a material that was easy to obtain and easy to mould including the embedding of the sensors.

The material selected for the reproduction of the artificial brain is the silicon Rubber.

The choice for this material is because the use of silicone rubber is very common both in experimental tests, to simulate human tissues and in FEMs, using its properties as simulation inputs.

The choice for the head prototype brain was a silicone rubber manufactured by Polytek® Development Corp. Easton, PA,USA (Data Sheet pag.147).

This type of rubber is composed of two component A+B that must mixed for obtain the reaction and the curing of the material, different silicon rubber is available and distributed and some preliminary test are performed on specific specimen for analyse and select the material in relation of its own mechanical properties.

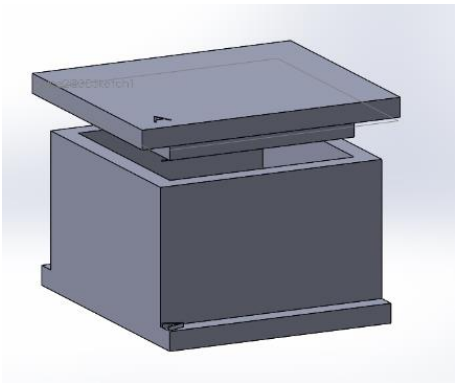

Figure 5.6 - 3D Model of the testing mould

For the comprehension of the silicon rubber behaviour some compression tests are planned and performed, to comparing the different characteristics.

Silicon Rubber Compression Test

The material of study is characterized by a nonlinear elastic behaviour, and comparison

The test is performed on a specimen with dimensions of 50x50x30 mm.

The test procedure is based on the compression of the prepared specimens and apply a constant shortening displacement.

The linear function of displacement in time: from 0 mm to 15 mm in 150 s, that is a strain rate of 0.067 mm/s. The compression test is performed using Instron Machine.

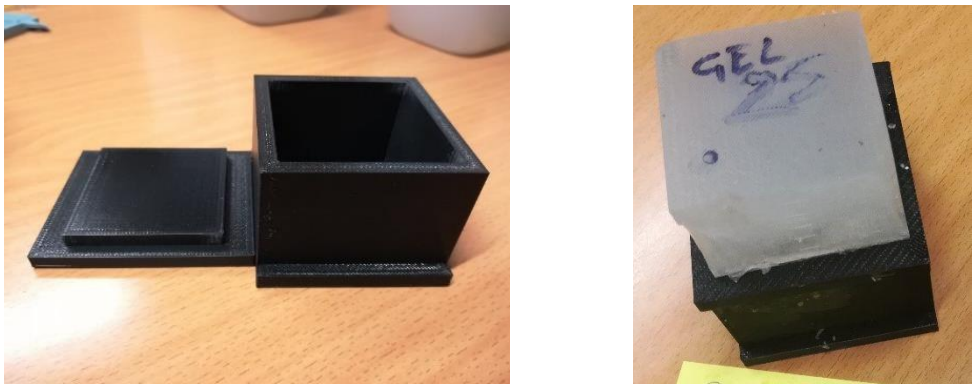

Figure 5.7 - Specimen Mould preparation, rubber sample demoulding and test setup

The stress – strain curve obtained is displayed in the following plots. The strain is calculated as $\frac{h_i - h_f}{h_i}$ where h_i is the initial thickness of the specimen (30 mm) and h_f the final thickness (15 mm). The stress is calculated as $\frac{F}{A}$ where F is the contact force between the surfaces of the top plate and of the specimen, and A is the area of the surface of the specimen (2500 mm2).

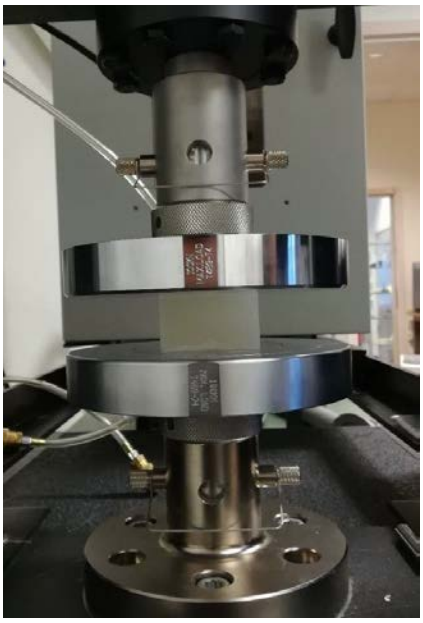

Figure 5.8 - Silicon Rubber sample compression test

Three different type of rubber that are tested:

- PlatSilGel 00-20 A+B
- PlatSilGel 25 A+B
- PlatSilGel 01-30 A+B

The properties of each rubber type are showed in the datasheet (page 148)

The results of the tests are aiming to compare the resultant load and stress acted from the material under the same compression condition, and after that it will be possible to identify and compare the different materials.

Only few tests are performed for each rubber, because of there was only few materials available and the interest of the test was only to recognize the differences between each other and not characterize the full material properties.

Table 25 - Rubber Samples dimension; equal for each rubber type

	Length [mm]	Height [mm]	Thickness [mm]	Volume[mm^3]
Specimen Size	50	50	30	75000

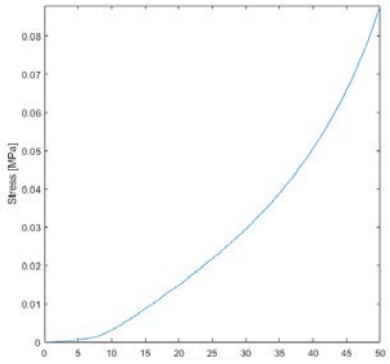

Figure 5.10- Plastigel 00-20 Stress vs Strain Compression Test

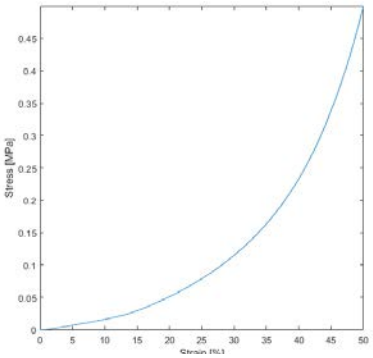

Figure 5.11 - Plastigel 00-25 Stress vs Strain Compression Test

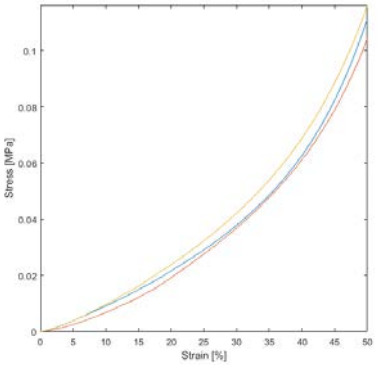

Figure 5.9- Plastigel 01-30 Stress vs Strain Compression Test

Plastigel 00-20

Test Figure 5.10	Stress [MPa]	Strain [%]	Load [N]
Plastigel 00-20	0.0878	50	219.56

Plastigel 00-25

Test Figure 5.11	Stress [MPa]	Strain [%]	Load [N]
Plastigel 00-25	0.4991	50	1247.8

Plastigel 01-30

Test Figure 5.9	Stress [MPa]	Strain [%]	Load [N]
Plastigel 01-30	0.1112	50	278.32
	0.1043	50	260.32
	0.1161	50	290.32

After those tests has been choose the Silicon Rubber with the softest properties, the one that has the lowest load and stress values at the same compression strain limit.

The material used for the moulding of the second Dummy Brain is the PlastiGel 00-20 A+B.

1.16.3 Subarachnoid Material

This anatomical part is a thick layer that allows the flooding of the CSF around the brain, in our model this part is substituted with a NONWOVEN fabric, the same already used in the first dummy head[1].

The material chosen for representing the web-like arachnoid trabeculae was a polyester like the ones used for air filters. This choice allows to simulate both the cushion effect of the material and the hydrodynamic role of the fibres in slowing down the CSF flow during a skull-brain relative rotation.

Figure 5.12 - Nonwoven Fabric used as Arachnoid substitute in the Dummy Head prototype a) Non-woven fabric coupled with silicone rubber b) Non-Woven Fabric testing sample thickness

In the second prototype, this material is arranged only in some spot in contact with the brain and below the Dura Mater. The aim of this layer is to create a first damping effect of impact on the brain and keep it in position allowing the flowing of the fluid around. The hollow part of the Arachnoid is called Arachnoid trabeculae, and it's the part where the CSF flows completely.

The theoretical reason of positioning the NW only in some spots is because it is supposed to be easier to model it from a mathematical point of view and analyse in a FEM system.

Some tests are performed on this material because there is a completely unknowledge of the properties of this fabric. It is used because it can be useful for reproduce the aim brain suspension and damping, but for the reproduction in the fem software is necessary to investigate it more deeply.

Tensile and compression test are performed with the Instron Machine and some mechanical data are collected.

Compression Test

Compression Test Performed on Squared Specimen of Area $50 * 50\ mm^2$ and $30\ mm$ thick.

The Test is run with the aim to evaluate the Load stress and shortening. The results of the tests are aiming to compare the resultant load and stress acted from the material under the same compression condition, and after that it will be possible to identify and compare the different materials.

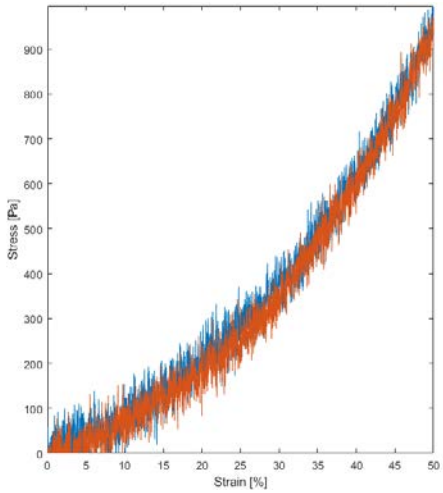

Figure 5.13- Nonwoven Fabric Stress vs Strain Compression Test

Table 26 - Compression test results non-Woven fabric

Figure 5.13	Stress [Pa]	Strain [%]	Load [N]
Nonwoven Fabric	996.23	50	2.49
	974.80	50	2.43

Tensile Test

Tension Test Performed on 3 Specimens with 50mm Widht and 9mm Thickness

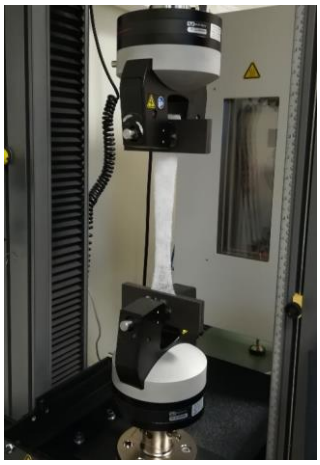

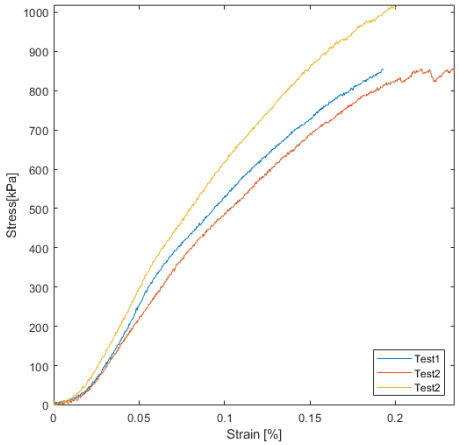

Figure 5.14 - Non Woven Fabric tension test a) Setup of the sample on Instron traction Machine b) Nonwoven Stress vs Strain tension test

Table 27 - Tension tests results Non-Woven Fabric

Figure 5.14	Stress [Pa]	Strain [% [	Load[N]
Non-Woven Fabric	855.93	0.1927	38,51
	857.32	0.2347	34.29
	1017	0.2008	45.79
Mean	910	0.2112	39.53

1.16.4 Dura Mater Material

After a discussion if the stakeholders have been decided to put only a very thin layer of Silicon Glues as a substitution of the Dura Mater connection directly on the skull.

This Material is very strong and very good for the coupling with other polymeric material.

A small specimen of this silicon glue will be prepared with the aim to test his mechanical behaviour.

No other layer will be put inside the head because is not possible to obtain the proper thickness and every other option is difficult to guarantee the real stability and keep the position inside the brain.

The precedent way for obtaining the shape of the wrap around the brain will be used for the cut of the Non-Woven Fabrics that will be used for the substitution of the Arachnoid material and the only coverage around the brain.
The Silicon Glue that is used is Contactive Adhesive S9 Super (datasheet page 154) it will be spread around the internal part of the Skull with the aim to reproduce the Dura Mater thin Layer and properties. The Silicon Glue Layer will reproduce the anatomical correspondence of the Dura Sticking directly on the Skull. The problem is that is not possible to obtain a very uniform layer of material because of the extremely high viscosity of it. It would be interesting perform some mechanical test on it, for evaluate properties as tensile strength or compression behaviour.
The only properties known from datasheet are viscosity and density.

The mechanical properties of the used material are very dissimilar to the biologic structure that characterize the human body. The reason is that is almost impossible to obtain and reproduce a complete reproduction of an anatomical structure also mimicking the mechanical characteristics.
The knowledge of the properties is however important for the possible implementation of a FEM model, and evaluate the physical model with a mathematical method.
The next improvement are related with the research and implementation of more reliable material substitute.

Conclusion

The initial goal of creating a dummy head prototype for the evaluation of head trauma and helmets testing has been reached. The first head surrogate has been restored and analysed to solve revealed problems and inaccuracies, some materials interaction ad sensors problems have been acknowledged and noted for the future improvement. The testing setup has been prepared, and the surrogate equipped with two more accelerometers and a proper helmet. A sequence of impact tests was performed, and the collected data analysed and commented.

From the knowledge of the first study the second human dummy head prototype has been designed and assembled. The head surrogate is rescaled to a 90% and created; the different parts are: a 3D printed polyamide skull with isotropic properties, two softer Silicon Rubber type for Brain and skin, and simplified reproduction of intracranial layers. The accelerometers are positioned carefully into the brain rubber, layer by layer, before the curing, taking care of respecting the chosen position and correspondent orientation. Seven accelerometers and two gyroscopes are embedded into the brain in different position with the purpose of compare the different response of each part; ten pression sensors are located as well into the head in contact with the inner skull wall, the chosen different positions are selected to being able of reconstruct the trend of the intracranial pression. After the closure the head is filled with synthetic oil to reproduce the cerebral fluid and recreate a more biofidelic condition. The Head surrogate is than coupled on a force platform through a standard dummy neck and equipped with a fitting helmet.

The collected speed and acceleration values are plotted and compared to figuring out the main parameters and constrictions that influence the global head behaviour.
The characterizations of each material used are performed to validate the model and with the upcoming purpose of designing an analogue FEM model of the dummy head and deeply investigate the reliability of the physical prototype.
The rotational behaviour of the brain and skull and their relative movement are analysed and commented, specific angular acceleration is evaluated comparing the results obtained with the energy level and the impact position and orientation.
The interest was to observe the differences on the helmet with MIPS system activated or not, and the first results displayed that the attended result in reduction of rotational acceleration are not obtained. The reliability of the prototype is still to guarantee but this research work reached a remarkable milestone for the realization of a functional and consistent dummy head prototype and an important step towards the validation of an advanced instrumented head in relation with the modern testing devices.
New studies are in progress for the continuous improvement of the physical model and implementation of other sensors for the acquisition of different type of data. From the literature study appeared that one of the problems correlated with head injury is related with brain material strain, due to the stress caused by acceleration and rotation.
The next stages are focused on the implementation of sensors for the analysis of the deformation and the correlation of this information with different type of impact and crash.
The improving of the bio fidelity of the prototype is another step reach, a better material selection and characterization is needed to obtain more realistic results and being able to produce realistic results and evaluation.
In conclusion this research work acquired a admirable step towards the realization of a truly useful tool for investigate and understand the increasing problem of traumatic brain injuries, and it would been a fundamental device for research group for the testing of head protective equipment.

Bibliography

[1] G. Carraro, “Development of a sensorized human head prototype for studying traumatic brain injury mechanisms prototype for studying traumatic brain injury,” Università degli Studi di Padova, MidSweden University, 2016.

[2] S. DalCastello, “New project of physical modeling of the anatomically correct multi sensors human head,” Università degli study di Padova, Mid Sweden University, 2016.

[3] L. Broggio, “Development of a sensorized human head prototype,” Università degli Studi di Padova, MidSweden University, 2017.

[4] L. M. Gessel, S. K. Fields, C. L. Collins, R. W. Dick, and R. D. Comstock, “Concussions among United States high school and collegiate athletes,” *J. Athl. Train.*, vol. 42, no. 4, pp. 495–503, 2007.

[5] K. G. Harmon *et al.*, “American Medical Society for Sports Medicine position statement: concussion in sport.,” *Br. J. Sports Med.*, vol. 47, no. 1, pp. 15–26, 2013.

[6] M. Faul, L. Xu, M. M. Wald, and V. G. Coronado, “Traumatic brain injury in the United States,” 2010.

[7] C. D. Weber, K. Horst, R. Lefering, M. Hofman, T. Dienstknecht, and H. C. Pape, “Major trauma in winter sports: an international trauma database analysis,” *Eur. J. Trauma Emerg. Surg.*, vol. 42, no. 6, pp. 741–747, 2016.

[8] M. R. Bambach, R. J. Mitchell, R. H. Grzebieta, and J. Olivier, “The effectiveness of helmets in bicycle collisions with motor vehicles: A case-control study,” *Accid. Anal. Prev.*, vol. 53, pp. 78–88, 2013.

[9] R. S. Thompson, F. P. Rivara, and D. C. Thompson, “A case-control study of the effectiveness of bicycle safety helmets,” *N. Engl. J. Med.*, vol. 320, no. 21,

pp. 1361–1367, 1989.

[10] J. G. Beckwith, R. M. Greenwald, and J. J. Chu, “Measuring head kinematics in football: Correlation between the head impact telemetry system and hybrid III headform,” *Ann. Biomed. Eng.*, vol. 40, no. 1, pp. 237–248, 2012.

[11] T. J. Dickson, G. Waddington, S. Trathen, D. Baltis, and R. Adams, “Technology applications to enhance understanding of realtime snowsport head accelerations,” in *Procedia Engineering*, 2013, vol. 60, pp. 220–225.

[12] M. A. Allison, Y. S. Kang, J. H. Bolte IV, M. R. Maltese, and K. B. Arbogast, “Validation of a Helmet-based system to measure head impact biomechanics in ice hockey,” *Med. Sci. Sports Exerc.*, vol. 46, no. 1, pp. 115–123, 2014.

[13] H. T. Hurst, S. Atkins, and B. D. Dickinson, “The magnitude of translational and rotational head accelerations experienced by riders during downhill mountain biking,” *Journal of Science and Medicine in Sport*, vol. 0, no. 0, Elsevier, Mar-2018.

[14] S. Kleiven, “Influence of Direction and Duration of Impacts to the Human Head Evaluated Using the Finite Element Method,” *Proc. Int. Res. Counc. Biomech. Inj. Conf.*, no. September, pp. 41–57, 2005.

[15] R. Jadischke, D. C. Viano, J. McCarthy, and A. I. King, “The Effects of Helmet Weight on Hybrid III Head and Neck Responses by Comparing Unhelmeted and Helmeted Impacts,” *J. Biomech. Eng.*, vol. 138, no. 10, p. 101008, 2016.

[16] R. Makkar, “Tackling Concussion in Football: A different approach to football Helmet Design,” *STEM Res. Proj.*

[17] Humanetics Innovative Solutions, “Humanetics Innovative Solutions - Crash Test Dummies,” *Hybrid III 5th Female, [verkkodokumentti]*, vol. 2012, no. June 11th, 2010.

[18] D. Kallieris, A. Rizzetti, and R. Mattern, “The biofidelity of Hybrid III Dummies,” *Int. Res. Counc. Biomechancs Inj.*, 1995.

[19] A. Bartsch, E. Benzel, V. Miele, D. Morr, and V. Prakash, “Hybrid III anthropomorphic test device (ATD) response to head impacts and potential

implications for athletic headgear testing," *Accid. Anal. Prev.*, vol. 48, pp. 285–291, 2012.

[20] E. Park, J. J. Gottlieb, B. Cheung, P. N. Shek, and A. J. Baker, "A Model of Low-Level Primary Blast Brain Trauma Results in Cytoskeletal Proteolysis and Chronic Functional Impairment in the Absence of Lung Barotrauma," *J. Neurotrauma*, vol. 28, no. 3, pp. 343–357, 2011.

[21] F. Zhu *et al.*, "Using a gel/plastic surrogate to study the biomechanical response of the head under air shock loading: A combined experimental and numerical investigation," *Biomech. Model. Mechanobiol.*, vol. 11, no. 3–4, pp. 341–353, 2012.

[22] Z. Taha, M. H. Arif Hassan, I. Hasanuddin, M. A. Aris, and A. P. P. Abdul Majeed, "Impact-absorbing materials in reducing brain vibration caused by ball-to-head impact in soccer," *Procedia Eng.*, vol. 72, no. 72, pp. 515–520, 2014.

[23] N. Awad and W. El-Dakhakhni, "A Physical Head and Neck Surrogate Model to Investigate Blast-Induced Mild Traumatic Brain Injury.," *Arab. J.*, no. 40, pp. 945–958, 2015.

[24] C. J. Freitas, J. T. Mathis, N. Scott, R. P. Bigger, and J. MacKiewicz, "Dynamic response due to behind helmet blunt trauma measured with a human head surrogate," *Int. J. Med. Sci.*, vol. 11, no. 5, pp. 409–425, 2014.

[25] T. J. Horgan and M. D. Gilchrist, "The creation of three-dimensional finite element models for simulating head impact biomechanics," *Int. J. Crashworthiness*, vol. 8, no. 4, pp. 353–366, 2003.

[26] B. Yang *et al.*, "Development of a finite element head model for the study of impact head injury.," *Biomed Res. Int.*, vol. 2014, p. 408278, 2014.

[27] H. Mao *et al.*, "Development of a Finite Element Human Head Model Partially Validated With Thirty Five Experimental Cases," *J. Biomech. Eng.*, vol. 135, no. 11, p. 111002, 2013.

[28] Y. Chen and M. Ostoja-Starzewski, "MRI-based finite element modeling of head trauma: Spherically focusing shear waves," *Acta Mech.*, vol. 213, no. 1–2,

pp. 155–167, 2010.

[29] S. Kleiven and W. N. Hardy, “Correlation of an FE Model of the Human Head with Local Brain Motion--Consequences for Injury Prediction,” *Stapp Car Crash J.*, vol. 46, pp. 123–144, 2002.

[30] Y. Chen, B. Sutton, and C. Conway, “Brain Deformation Under Mild Impact: Magnetic Resonance Imaging-Based Assessment and Finite Element Study,” *Mechanical.Illinois.Edu*, vol. 3, no. 1, pp. 20–35, 2012.

[31] Y. Feng, T. M. Abney, R. J. Okamoto, R. B. Pless, G. M. Genin, and P. V. Bayly, “Relative brain displacement and deformation during constrained mild frontal head impact,” *J. R. Soc. Interface*, vol. 7, no. 53, pp. 1677–1688, 2010.

[32] S. Song, N. S. Race, A. Kim, T. Zhang, R. Shi, and B. Ziaie, “A Wireless Intracranial Brain Deformation Sensing System for Blast-Induced Traumatic Brain Injury,” *Sci. Rep.*, vol. 5, no. May, pp. 1–10, 2015.

[33] V. Hodgson and L. Thomas, “Acceleration Induced Shear Strains in a Monkey Brain Hemisection,” *Stapp Car Crash Conf.*, pp. 589–611, 1979.

[34] A. A. Sabet, E. Christoforou, B. Zatlin, G. M. Genin, and P. V. Bayly, “Deformation of the human brain induced by mild angular head acceleration,” *J. Biomech.*, vol. 41, no. 2, pp. 307–315, 2008.

[35] V. H. Aaron M. Drake, Erik G. Takhounts, “Investigation of Parameters Affecting Brain Model Validation and Brain Strains Using the SIMon Finite Element Head Model,” *IRCOBI Conf. 2017*, vol. c, pp. 674–676, 2017.

[36] S. Rowson *et al.*, “Rotational head kinematics in football impacts: An injury risk function for concussion,” *Ann. Biomed. Eng.*, vol. 40, no. 1, pp. 1–13, 2012.

[37] H. W. Henn, “Crash tests and the head injury criterion,” *Teach. Math. its Appl.*, vol. 17, no. 4, pp. 162–170, 1998.

[38] P. Prasad and H. J. Mertz, “The Position of the United States Delegation to the ISO Working Group 6 on the Use of HIC in the Automotive Environment,” no. January 1985, 1985.

[39] D. Li, C. Ma, M. Shen, P. Li, and J. Zhang, “Brain Injury Differences in Frontal Impact Crash Using Different Simulation Strategies,” *Comput. Math.*

Methods Med., vol. 2015, pp. 1–8, 2015.

[40] E. Hertz, "A note on the head injury criterion (HIC) as a predictor of the risk of skull fracture," *Proc. Assoc. Adv. Automot. Med. Annu. Conf.*, vol. 37, pp. 303–312, 1993.

[41] E. J. Pellman *et al.*, "Concussion in professional football: Reconstruction of game impacts and injuries," *Neurosurgery*, vol. 53, no. 4, pp. 799–814, 2003.

[42] J. R. Funk, S. Rowson, R. W. Daniel, and S. M. Duma, "Validation of concussion risk curves for collegiate football players derived from HITS data," *Ann. Biomed. Eng.*, vol. 40, no. 1, pp. 79–89, 2012.

[43] S. Ji *et al.*, "Parametric comparisons of intracranial mechanical responses from three validated finite element models of the human head," *Ann. Biomed. Eng.*, vol. 42, no. 1, pp. 11–24, 2014.

[44] E. G. Takhounts, M. J. Craig, K. Moorhouse, J. McFadden, and V. Hasija, "Development of brain injury criteria (BrIC)," *Stapp Car Crash J.*, vol. 57, no. November, p. 243, 2013.

[45] D. Marjoux, D. Baumgartner, C. Deck, and R. Willinger, "Head injury prediction capability of the HIC, HIP, SIMon and ULP criteria," *Accid. Anal. Prev.*, vol. 40, no. 3, pp. 1135–1148, 2008.

[46] N. Petrone, E. Marzella, F. Uriati, A. Koptyug, M. Backstrom, and G. Carraro, "Experimental measurement of helmet, head & brain kinematics during multidirectional impact tests on a novel Instrumented Human Head Surrogate."

[47] N. Petrone, G. Carraro, S. D. Castello, L. Broggio, A. Koptyug, and M. Bäckström, "A Novel Instrumented Human Head Surrogate for the Impact Evaluation of Helmets," *Proceedings*, vol. 2, no. 6, p. 269, 2018.

[48] A. H. S. Holbourn, "Mechanics of Head Injuries," *Lancet*, vol. 242, no. 6267, pp. 438–441, 1943.

[49] R. Willinger, H. S. Kang, and B. Diaw, "Three-dimensional human head finite-element model validation against two experimental impacts," *Ann. Biomed. Eng.*, vol. 27, no. 3, pp. 403–410, 1999.

[50] R. J.S., K. T., and K. A.I., “Dynamic response of the human head to impact by three-dimensional finite element analysis,” *J. Biomech. Eng.*, vol. 116, no. 1, pp. 44–50, 1994.

[51] M. Claessens, “Finite Element Modeling of the Human Head under Impact Conditions,” pp. 2–6, 1997.

[52] Y. Hong, “Routledge handbook of ergonomics in sport and exercise,” p. 591.

[53] A. Rezaei, M. Salimi Jazi, and G. Karami, “Computational modeling of human head under blast in confined and open spaces: Primary blast injury,” *Int. j. numer. method. biomed. eng.*, vol. 30, no. 1, pp. 69–82, 2014.

[54] F. Zhu, P. Skelton, C. C. Chou, H. Mao, K. H. Yang, and A. I. King, “Biomechanical responses of a pig head under blast loading: A computational simulation,” *Int. j. numer. method. biomed. eng.*, vol. 29, no. 3, pp. 392–407, 2013.

[55] D. Singh, D. Cronin, P. A. Lockhart, T. N. Haladuick, A. Bouamoul, and J.-P. Dionne, “Evaluation of head response to blast using sagittal and transverse Finite Element Head Model,” *Pers. Armour Syst. Symp.*, pp. 68–77, 2012.

[56] H. Ipek, C. Mayer, H. Luce, and D. E. G. P, “Coupling of Strasbourg University Head Model To Thums Human Body Fe Model : Validation and Application To Automotive Safety Finite,” pp. 1–13, 2002.

[57] E. G. Takhounts *et al.*, “Investigation of traumatic brain injuries using the next generation of simulated injury monitor (SIMon) finite element head model,” *Stapp Car Crash J.*, vol. 52, pp. 1–31, 2008.

[58] M. H. A. Hassan and Z. Taha, “Finite element analysis of soccer heading,” *Procedia Eng.*, vol. 112, pp. 46–51, 2015.

[59] M. Lashkari, F. Frahmand, and K. Kangarlou, “Finite element modeling of the human Brain Under impact conditions,” vol. 6, no. 6, pp. 875–881, 2014.

[60] M. Claessens, “Finite element modeling of the human head under impact conditions,” 1997.

[61] P. Saboori and A. Sadegh, “Histology and Morphology of the Brain Subarachnoid Trabeculae,” *Anat. Res. Int.*, vol. 2015, pp. 1–9, 2015.

[62] A. N. Bashkatov, E. A. Genina, Y. P. Sinichkin, V. I. Kochubey, N. A.

Lakodina, and V. V. Tuchin, “Glucose and Mannitol Diffusion in Human Dura Mater,” *Biophys. J.*, vol. 85, no. 5, pp. 3310–3318, 2003.

[63] R. Van Noort, T. R. P. Martin, M. M. Black, A. T. Barker, and C. G. Montero, “The mechanical properties of human dura mater and the effects of storage media,” *Clin. Phys. Physiol. Meas.*, vol. 2, no. 3, pp. 197–203, 1981.

[64] A. C. P. Lui, T. Z. Polis, and N. J. Cicutti, “Densities of cerebrospinal fluid and spinal anaesthetic solutions in surgical patients at body temperature,” *Can. J. Anaesth.*, vol. 45, no. 4, pp. 297–303, 1998.

[65] “MIPS.” [Online]. Available: http://mipsprotection.com/.

[66] W. Hardy, M. Mason, and C. Foster, “A study of the response of the human cadaver head to impact,” *Stapp car crash …*, vol. 51, pp. 17–80, 2007.

[67] C. N. Stephan and E. K. Simpson, “Facial soft tissue depths in craniofacial identification (Part I): An analytical review of the published adult data,” *J. Forensic Sci.*, vol. 53, no. 6, pp. 1257–1272, 2008.

[68] P. Halldin, A. Gilchrist, and N. J. Mills, “A new oblique impacttest for motorcycle helmets,” *Int. J. Crashworthiness*, vol. 6, no. 1, pp. 53–64, 2001.

[69] D. Sahoo, C. Deck, and R. Willinger, “Brain injury tolerance limit based on computation of axonal strain,” *Accid. Anal. Prev.*, vol. 92, pp. 53–70, 2016.

[70] E. (Università di P. Marzella, “Comparative analysis of two biofidelic instrumented human head surrogates for sport helmets evaluation,” University of Padova.

[71] P. Saboori and A. Sadegh, “Material modeling of the head’s subarachnoid space,” *Sci. Iran.*, vol. 18, no. 6, pp. 1492–1499, 2011.

[72] P. Saboori and A. Sadegh, “Brain subarachnoid space architecture: Histological approach,” *ASME 2011 Int. Mech. Eng. Congr. Expo. IMECE 2011*, vol. 2, no. 2007, pp. 89–94, 2011.

[73] S. Prosdocimo, “Finite Element Modelling and Materials Characterization of an Innovative Dummy Head for Impact Studies Finite Element Modelling and Materials Characterization of an Innovative Dummy Head for Impact Studies,”

Università degli studi di padova, 2016.
[74] M. Scarpari, “Sviluppo di modelli virtuali per l’analisi numerica e sperimentale del comportamento ad impatto di prototipi fisici della testa umana,” Università degli studi di Padova, 2011.

Chapter 6 Appendix

1.17 Force Platform

Force

KISTLER
measure. analyze. innovate.

Multicomponent Force Plate

Type 9281E...

for Dynamic Applications in Biomechanics, F_z –10 ... 20 kN

Multicomponent force plate with wide range for measuring ground reaction forces, moments and the center of pressure in biomechanics.

- Extremely wide measuring range
- Excellent measuring accuracy
- High natural frequency
- Versatile
- Threshold F_z <250 mN

Description
The multicomponent force plate Type 9281E... consists of a 600x400 mm aluminum sandwich top plate of advanced, lightweight construction and four built-in piezoelectric 3-component force sensors. Thus it is extremely rigid overall, and allows measurements over a very wide useful frequency range.

Thanks to the special properties of the piezoelectric sensors, the plate is highly sensitive and can simultaneously measure very dynamic phenomena involved in a wide range of applications.

Application
This force plate is designed specifically for use in basic research and sport. Its extensive range and high rigidity allow it to be employed across a very wide spectrum of measuring tasks and application sectors. Despite the very generous measuring range of –10 ... 20 kN, it offers excellent accuracy and linearity, and even under a large preload allows precise measurement of minute forces. In all these situations the plate can be mounted in any position without affecting the measurement result in any way.

The Type 9281EA has an built-in charge amplifier compatible with all of the common motion analysis systems.

Technical Data

Dimensions		mm	600x400x100
Measuring range	F_x, F_y	kN	–10 ... 10
	F_z	kN	–10 ... 20
Overload	F_x, F_y	kN	–15/15
	F_z	kN	–10/25
Linearity	%FSO		<±0,2
Hysteresis	%FSO		<0,3
Crosstalk	F_x <–> F_y	%	<±1,5
	F_x, F_y –> F_z	%	<±1,5
	F_z –> F_x, F_y	%	<±0,5[1]
Rigidity	x-axis (a_y = 0)	N/µm	≈250
	y-axis (a_x = 0)	N/µm	≈400
	z-axis (a_x = a_y = 0)	N/µm	≈30
Natural frequency	f_n (x, y)	Hz	≈1 000
	f_n (z)	Hz	≈1 000
Operating temperature range		°C	0 ... 60
Weight		kg	16
Degree of protection	EN 60529:1992		IP65

[1] inside sensor rectangle

9281E_000-711e-09.08

Page 1/4

Polytek Development Corp.

Physical Properties Bulletin

PlatSil® 71-Series, 73-Series & PlatSil® Gel Series Silicone Rubber Products

Product	Mix Ratio	Part A Color	Part B Color	Pour Time (min)	Demold Time (hr)	Total Cure Time (hr)	Specific Gravity	Mix Viscosity (cP)	Shore Hardness	Tensile Strength psi (mPa)	% Elongation	Linear Shrinkage	Die B Tear Strength pli (kN/m)	Die T Tear Strength pli (kN/m)
PlatSil 71-Series														
PlatSil® 71-10	1A:10B	Clear	Pink[1]	5	0.5	24	1.06	3,500	A10	173 (1.19)	311	Nil	42 (7.35)	ND
PlatSil® 71-11	1A:1B	Blue[1]	Green[1]	20	4	24	1.12	6,000	A10	281 (1.93)	751	Nil	117 (20.48)	36 (6.31)
PlatSil® 71-20	1A:1B	Blue[1]	Pink[1]	25	4	24	1.12	12,000	A20	368 (2.54)	530	Nil	117 (20.48)	33 (5.78)
PlatSil® 71-30	1A:10B	Green[1]	White	60	24	48	1.12	25,000	A30	561 (3.87)	419	Nil	140 (24.51)	ND
PlatSil® 71-35	1A:10B	Blue[1]	White	60	24	48	1.12	25,000	A35	635 (4.38)	413	Nil	145 (25.39)	37 (6.48)
PlatSil® 71-40	1A:5B	Clear	White	60	24	48	1.10	25,000	A40	366 (2.52)	386	Nil	60 (10.51)	17.1 (3.00)
PlatSil 73-Series														
PlatSil® 73-15	1A:1B	White	White	20	4 to 5	48	1.10	2,500	A15	265 (1.82)	640	Nil	55 (9.63)	17 (2.98)
PlatSil® 73-20	1A:1B	Blue	Blue	5	5	24	1.10	3000	A22	230 (1.58)	460	Nil	45 (7.87)	17 (2.98)
PlatSil® 73-25	1A:1B	Yellow	Green	15	4 to 5	48	1.14	6,000	A25	380 (2.61)	405	Nil	120 (21.02)	30 (5.25)
PlatSil® 73-29	1A:10B	Clear	White	45	16	48	1.10	15,000	A30	542 (3.74)	531	Nil	90 (15.76)	39 (6.83)
PlatSil® 73-40	1A:10B	Yellow	White	45	16	48	1.10	15,000	A40	465 (3.21)	355	Nil	52 (9.11)	7 (1.23)
PlatSil® 73-45	1A:10B	Green[1]	Tan	40	16	48	1.27	35,000	A45	631 (4.35)	707	Nil	145 (25.39)	62.9 (11.01)
PlatSil® 73-60	1A:10B	Blue[1]	Tan	45	16	48	1.29	40,000	A60	537 (3.70)	202	Nil	113 (19.79)	45 (7.88)
PlatSil® SilGlass	1A:1B	Clear	Clear	7	0.5	24	0.97	200	A40	NA	NA	NA	NA	NA
PlatSil® SilFoam	1A:1B	Clear	Milky White	45 sec	0.5	24	15 lb/ft3	7,500	NA	NA	NA	NA	NA	NA
PlatSil Gel														
PlatSil® Gel-OO20	1A:1B	Milky White	Milky White	40	2	24	1.05	3,900	OO20	122 (0.84)	964	Nil	24.8 (4.34)	1.3 (0.52)
PlatSil® Gel-OO30	1A:1B	Milky White	Milky White	45	4	24	1.05	6,200	OO30	118 (0.81)	848	Nil	36.6 (6.41)	10.7 (1.87)
PlatSil® Gel-OO	1A:1B	Milky White	Milky White	6	0.5	24	1.10	22,000	OO30	154 (1.06)	1275	Nil	56 (9.81)	19 (3.33)
PlatSil® Gel-10	1A :1B	Milky White	Milky White	6	0.5	24	1.10	15,000	A10	228 (1.57)	970	Nil	80 (14.01)	27 (4.73)
PlatSil® Gel-25	1A:1B	Milky White	Milky White	5	1	24	1.12	3,500	A25	434 (2.99)	385	Nil	148 (25.56)	28 (4.90)

[1] Component requires stirring before use.

Conventions: psi/145 = MPa (megaPascals)
pli x .1751 = kN/m (kiloNewtons per meter)
ND = Not Determined

1.19 PA2200 Polyamide

Material Data Sheet

Fine Polyamide PA 2200 for EOSINT P

Application:

PA 2200 is suitable for use in all EOSINT P systems with fine polyamide option.
The recommended layer thickness is 0.15 mm. Unexposed powder can be reused. Depending on building time it has to be mixed with fresh powder by a ratio of 2:1 to 1:1 (old : new) in order to guarantee constant process parameters and persisting part quality.

Typical applications of the material are fully functional prototypes with high end finish right from the process. They easily withstand high mechanical and thermal load.

Material Properties:

Average grain size	Laser diffraction	60	µm
Bulk density	DIN 53466	0,435 - 0,445	g/cm³
Density of laser-sintered part	EOS-Method	0,9 - 0,95	g/cm³

Mechanical Properties:*

Tensile Modulus	DIN EN ISO 527	1700 ± 150	N/mm²
Tensile strength	DIN EN ISO 527	45 ± 3	N/mm²
Elongation at break	DIN EN ISO 527	20 ± 5	%
Flexural Modulus	DIN EN ISO 178	1240 ± 130	N/mm²
Charpy - Impact strength	DIN EN ISO 179	53 ± 3,8	kJ/m²
Charpy - Notched impact	DIN EN ISO 179	4,8 ± 0,3	kJ/m²
Izod – Impact Strength	DIN EN ISO 180	32,8 ± 3,4	kJ/m²
Izod – Notched Impact Strength	DIN EN ISO 180	4,4 ± 0,4	kJ/m²
Ball indentation hardness	DIN EN ISO 2039	77,6 ± 2	
Shore D - hardness	DIN 53505	75 ± 2	

EOS GmbH Electro Optical Systems
Patinger Straße 2
D-82152 Planegg/München
Telefon ++49 (0)89/856 85 - 0
Telefax ++49 (0)89/859 84 02
Internet: www.eos-gmbh.de

1.20 Pressure Sensor MS54XX

RoHS

MS54XX

Miniature SMD Pressure Sensor

SPECIFICATIONS

- **1, 7, 12, and 70 bar absolute pressure range**
- **Uncompensated**
- **Piezoresistive silicon micromachined sensor**
- **Miniature surface mount**
- **Ceramic carrier**
- **Low noise, high sensitivity, high linearity**

The MS54XX SMD pressure sensor series is designed for pressure sensor systems with highest demands on resolution and accuracy. The device consists of a silicon micromachined pressure sensor die mounted on a 6.2 x 6.4 mm ceramic carrier. The MS54XX can be delivered in a high sensitivity version giving a maximal output voltage or in a high linearity version. Both versions provide an output voltage directly proportional to the applied pressure

Carrier	Full scale pressure	High Sensitivity Versions			High Linearity Versions		
		Product code	Full scale span	Linearity	Product code	Full scale span	Linearity
Ceramic	1 bar	MS5401-AM	240 mV	±0.20 % FS	MS5401-BM	150 mV	±0.05 % FS
	7 bar	MS5407-AM	392 mV	±0.20 % FS			
	12 bar				MS5412-BM	150 mV	±0.05 % FS
	70 bar	MS5470-AM	310 mV	±0.25 % FS			

1.21 Accelererometer

ANALOG DEVICES

Small, Low Power, 3-Axis ±200 *g* Accelerometer

Data Sheet **ADXL377**

FEATURES

- 3-axis sensing
- Small, low profile package
  - 3 mm × 3 mm × 1.45 mm LFCSP
- Low power: 300 µA (typical)
- Single-supply operation: 1.8 V to 3.6 V
- 10,000 *g* shock survival
- Excellent temperature stability
- Bandwidth adjustment with a single capacitor per axis
- RoHS/WEEE and lead-free compliant

APPLICATIONS

- Concussion and head trauma detection
- High force event detection

GENERAL DESCRIPTION

The ADXL377 is a small, thin, low power, complete 3-axis accelerometer with signal conditioned voltage outputs. The ADXL377 measures acceleration resulting from motion, shock, or vibration with a typical full-scale range of ±200 *g*.

The user selects the bandwidth of the accelerometer using the C_X, C_Y, and C_Z capacitors at the X_{OUT}, Y_{OUT}, and Z_{OUT} pins. Bandwidths can be selected to suit the application, with a range of 0.5 Hz to 1300 Hz for the x-axis and y-axis and a range of 0.5 Hz to 1000 Hz for the z-axis.

The ADXL377 is available in a small, low profile, 3 mm × 3 mm × 1.45 mm, 16-lead lead frame chip scale package (LFCSP_LQ).

FUNCTIONAL BLOCK DIAGRAM

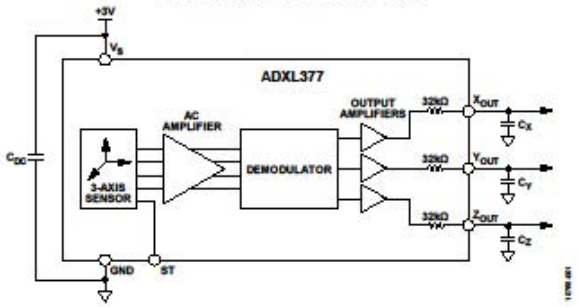

Figure 1.

Rev. 0 Document Feedback

One Technology Way, P.O. Box 9106, Norwood, MA 02062-9106, U.S.A.
Tel: 781.329.4700
Technical Support www.analog.com

1.22 Gyroscopes

LPR4150AL

MEMS motion sensor: dual-axis pitch and roll ±1500 dps analog gyroscope

Features

- 2.7 V to 3.6 V single-supply operation
- Wide operating temperature range (-40 °C to +85 °C)
- High stability over temperature
- Analog absolute angular-rate outputs
- Two separate outputs for each axis (1x and 4x amplified)
- Integrated low-pass filters
- Low power consumption
- Embedded power-down
- Embedded self-test
- Sleep mode
- High shock and vibration survivability
- ECOPACK® RoHS and "Green" compliant (see *Section 6*)

Applications

- Gaming applications
- Pointing devices, remote and game controllers
- Motion tracking with user interface
- Industial and robotics

Description

The LPR4150AL is a low-power dual-axis micromachined gyroscope capable of measuring angular rate along pitch and roll axes.

It provides excellent temperature stability and high resolution over an extended operating temperature range (-40 °C to +85 °C).

LGA-28 (4x5x1 mm)

The LPR4150AL has a full scale of ±1500 dps and is capable of detecting rates with a -3 dB bandwidth up to 140 Hz.

The device includes a sensing element composed of a single driving mass, kept in continuous oscillation and capable of reacting, based on the Coriolis principle, when an angular rate is applied.

A CMOS IC provides the measured angular rate to the external world through an analog output voltage, allowing high levels of integration and production trimming to better match sensing element characteristics.

ST's family of gyroscopes leverages on the mature and robust manufacturing process already used for the production of micro-machined accelerometers.

ST is already in the field with several hundred million sensors which have received excellent acceptance from the market in terms of quality, reliability and performance.

The LPR4150AL is available in a plastic land grid array (LGA) package, which ST successfully pioneered for accelerometers.Today ST has the widest manufacturing capability and strongest expertise in the world for production of sensors in plastic LGA packages.

Table 1. Device summary

Order code	Temperature range (°C)	Package	Packing
LPR4150AL	-40 to +85	LGA-28 (4x5x1)	Tray
LPR4150ALTR	-40 to +85	LGA-28 (4x5x1)	Tape and reel

LPY4150AL

MEMS motion sensor: dual-axis pitch and yaw ±1500 dps analog gyroscope

Features

- 2.7 V to 3.6 V single-supply operation
- Wide operating temperature range (-40 °C to +85 °C)
- High stability over temperature
- Analog absolute angular-rate outputs
- Two separate outputs for each axis (1x and 4x amplified)
- Integrated low-pass filters
- Low power consumption
- Embedded power-down
- Embedded self-test
- Sleep mode
- High shock and vibration survivability
- ECOPACK® RoHS and "Green" compliant (see *Section 6*)

Applications

- Gaming applications
- Pointing devices, remote and game controllers
- Motion control with user interface
- Industrial and robotics

Description

The LPY4150AL is a low-power dual-axis micromachined gyroscope capable of measuring angular rate along pitch and yaw axes.

It provides excellent temperature stability and high resolution over an extended operating temperature range (-40 °C to +85 °C).

LGA-28 (4x5x1 mm)

The LPY4150AL has a full scale of ±1500 dps and is capable of detecting rates with a -3 dB bandwidth up to 140 Hz.

The device includes a sensing element composed of a single driving mass, kept in continuous oscillation and capable of reacting, based on the Coriolis principle, when an angular rate is applied.

A CMOS IC provides the measured angular rate to the external world through an analog output voltage, allowing high levels of integration and production trimming to better match sensing element characteristics.

ST's family of gyroscopes leverages on the mature and robust manufacturing process already used for the production of micro-machined accelerometers.

ST is already in the field with several hundred million sensors which have received excellent acceptance from the market in terms of quality, reliability and performance.

The LPY4150AL is available in a plastic land grid array (LGA) package, which ST successfully pioneered for accelerometers.Today ST has the widest manufacturing capability and strongest expertise in the world for production of sensors in plastic LGA packages.

Table 1. Device summary

Order code	Temperature range (°C)	Package	Packing
LPY4150AL	-40 to +85	LGA-28 (4x5x1)	Tray
LPY4150ALTR	-40 to +85	LGA-28 (4x5x1)	Tape and reel

October 2009 Doc ID 16581 Rev 1 1/14

www.st.com

1.23 Silicon Glue

TECHNICAL DATA SHEET

New Date: 2017-05-29

RubberFix

+ Repair set

Repairing paste for repairing, protecting and waterproofing.

Ideal for gluing, filling and sealing of rubber, leather, textile, neoprene, various synthetics (such as Hypalon®), wood, metal or ceramics.

- Contains no solvents
- Water resistance repair product with very strong bonding properties
- High flexibility
- Temperature resistant from - 40°C to + 120°C
- Gives a transparent joint
- Good adhesion to many materials

TECHNICAL DATA

Basis: MS-Polymer
Appearance: Transparent
Viscosity: approx. 125 mPa.s.
Moisture resistance: Very good
Water resistance: Good
Temperature resistance: from -40°C to +120°C
UV resistance: Good
Chemicals resistance: Good
Elasticity: Very good
Filling capacity: Very good

APPLICATION DATA

Application temperature: Do not use at temperatures below +5 °C or at an extremely low relative air humidity
Drying:
Skin over time: approx. 15-30 minutes
Dry/Cure time: approx. 48 hours.
Curing time may vary depending on a.o. surface, product quantity used, humidity level and ambient temperature.
Storage life: At least 12 months after date of manufacture Limited shelf life after opening. Store in a dry cool place.

Tools: Sand paper and spatula (enclosed for free).

FIELD OF APPLICATION

Ideal for gluing, filling and sealing of rubber, leather, textile, neoprene, various synthetics (such as Hypalon®), wood, metal or ceramics.

Also suitable for repairing (sports) shoes, (soles and heels), boots, gloves, slippers, (hockey) sticks, inflatable objects (such as boats, or multi-layered mats of rubber or soft PVC, rainwear, travel bags, wetsuits, diving gear, tents, (horse) saddles, decorative materials, headlights and to reinforce stitched seams and for filling joints and gaps.

DIRECTIONS FOR USE

Surface requirements: Materials to be repaired should be dry through and through.
Preliminary surface treatment: All parts should be perfectly clean and free of grease. Always roughen with enclosed sand paper.

Use spatula to apply paste in an even layer of at least 2 mm well around area to be repaired (preferably on entire surface).
Smoothen paste with spatula.
Repairing shoe soles and rubber boats: materials should be perfectly clean and dry through and through. Always sandpaper well.
Apply a thin layer of paste (less than 1 mm).
Press the enclosed polyester gauze (min. width of 2.5 cm) into paste using enclosed spatula.
Apply a thin layer of paste on and around gauze.
Smoothen with spatula and a little washing up liquid. Let cure for at least 48 hours.

Stains/residue: Remove fresh stains immediately with acetone. Dried adhesion residue can only be removed mechanically.

1.24 Titanium

Arcam EBM system

CHEMICAL SPECIFICATION

	Arcam Ti6Al4V, Typical	Ti6Al4V, Required*	Ti6Al4V, Required**
Aluminium, Al	6%	5,5–6,75%	5,5–6,75%
Vanadium, V	4%	3,5–4,5%	3,5–4,5%
Carbon, C	0,03%	< 0,1%	< 0,08%
Iron, Fe	0,1%	< 0,3%	< 0,3%
Oxygen, O	0,15%	< 0,2%	< 0,2%
Nitrogen, N	0,01%	< 0,05%	< 0,05%
Hydrogen, H	0,003%	< 0,015%	< 0,015%
Titanium, Ti	Balance	Balance	Balance

*ASTM F1108 (cast material) **ASTM F1472 (wrought material)

MECHANICAL PROPERTIES

	Arcam Ti6Al4V, Typical	Ti6Al4V, Required**	Ti6Al4V, Required***
Yield Strength (Rp 0,2)	950 MPa	758 MPa	860 MPa
Ultimate Tensile Strength (Rm)	1020 MPa	860 MPa	930 MPa
Elongation	14%	>8%	>10%
Reduction of Area	40%	>14%	>25%
Fatigue strength* @ 600 MPa	>10,000,000 cycles		
Rockwell Hardness	33 HRC		
Modulus of Elasticity	120 GPa		

*After Hot Isostatic Pressing **ASTM F1108 (cast material) ***ASTM F1472 (wrought material)

The mechanical properties of materials produced in the EBM process are comparable to wrought annealed materials and are better than cast materials.

POST PROCESSING

Heat treatment

Hot Isostatic Pressing (HIP) is recommended for fatigue-loaded components. The following HIP parameters are recommended:

- 920° C
- 100 MPa
- 120 minutes

Machining

Ti6Al4V parts manufactured in the EBM process feature good machinability and can be machined as stock parts.

The following factors contribute to efficient machining of Ti6Al4V parts:

- Low cutting speeds
- High feed rate
- Generous quantities of cutting fluid
- Sharp tools
- Rigid setup

Welding

Ti6Al4V may be welded by a wide variety of conventional fusion and solid-state processes, although its chemical reactivity typically requires special measures and procedures.

Arcam Ti6Al4V High Cycle Fatigue Test

HCF S/N diagram in MPa units